UNIVERSITY OF OKLAHOMA

GRADUATE COLLEGE

A STUDY ON MOBILE AD HOC NETWORKS EQUIPPED WITH FREE-SPACE OPTICAL CAPABILITIES

A Dissertation

SUBMITTED TO THE GRADUATE FACULTY

in partial fulfillment of the requirements for the

degree of

Doctor of Philosophy

By

PENG YAN

Norman, Oklahoma

2006

UMI Number: 3239053

UMI Microform 3239053

ProQuest Information and Learning Company
300 North Zeeb Road
P.O. Box 1346
Ann Arbor, MI 48106-1346

A STUDY ON MOBILE AD HOC NETWORKS
EQUIPPED WITH FREE-SPACE OPTICAL CAPABILITIES

A DISSERTATION APPROVED FOR THE
SCHOOL OF ELECTRICAL AND COMPUTER ENGINEERING

BY

_____
Dr. James J. Sluss, Jr. (Chair)

_____
Dr. Joseph P. Havlicek

_____
Dr. William O. Ray

_____
Dr. Hazem H. Refai

_____
Dr. Pramode K. Verma

TABLE OF CONTENTS

LIST OF TABLES

LIST OF FIGURES

ABSTRACT

A mobile ad hoc network (MANET) offers a cost-effective solution for communications in areas where infrastructure is unavailable, e.g. emergency response, disaster recovery, and battlefield scenarios. Traditional MANETs operate in the radio frequency (RF) spectrum, where the available bandwidth is facing the challenge of the rapidly increasing demands. Free-space optics (FSO) provides an attractive complement to RF wireless MANETs because of its high bandwidth and interference-free operation. An effort to combine the main advantages of MANET and FSO technologies by equipping the network nodes with hybrid communications capabilities will be presented. Computer models of such a network were created using the network simulator OPNET Modeler. Various indicators of network performance, including packet loss ratio, end-to-end delay, throughput, etc. were obtained through simulation and examined. The analysis will be of significant assistance in the design and implementation of such next-generation MANETs.

CHAPTER 1 – INTRODUCTION

Free-space optics (FSO) and mobile ad hoc networks (MANETs) are two areas in telecommunications research that have seen rapid development over the last several years.

The modern FSO technology was initially developed in the 1960s for military applications. It was not until the late 1990s to the beginning of the 21st century that FSO communications started to see significant advancement in research and considerable shares of the commercial telecommunications market. The major driving force behind it has been the universal and exponentially increasing demand for high-bandwidth connectivity. FSO provides us with high-bandwidth connections at relatively low costs.

In the mean time, the demand for portable and/or pervasive computing has been boosting the development of the MANET technology. The infrastructure-free and mobile characteristics of a MANET give rise to great flexibility and cost efficiency.

The vast majority of FSO research and development efforts have, until now, been focused on fixed transceiver units mounted on rooftops, which form stationary point-to-point links and networks with relatively simple topologies. Data exchange between two mobile nodes, on the other hand, has yet to take advantage of the high data rate offered by means of optical communications.

Today's existing MANETs operate solely in the domain of radio frequency (RF) wireless transmissions.

This dissertation will make an effort to combine the main advantages of broad bandwidth and support for transceiver mobility offered by FSO and MANET technologies, respectively, by studying the integration of FSO capabilities into MANETs. It will be demonstrated that:

- The currently available hardware equipment makes it possible to introduce optical communication capabilities into a mobile network;
- The RF and FSO modules residing in the same node are able to co-operate seamlessly, resulting in a stable network;
- The throughput of the network is greatly improved with the introduction of FSO capabilities, while its support for node mobility is maintained.

Because of the high bandwidth, interference immunity and intrinsically excellent security offered by the FSO technology, such an enhanced-MANET can better facilitate communications needs of a wide range of scenarios where infrastructure is unavailable, communicating terminals are mobile, and/or cost efficiency is critical. Such scenarios may include emergency response, disaster recovery, environment monitoring, healthcare, home automation, geographical exploration, distributed gaming, military surveillance, etc.

Original contributions made by this dissertation include the following:

- An approach to simulate a network where FSO is employed as a communications means was proposed, discussed in detail, and validated. This was done with a lack of computer tools designed to handle simulation of FSO networks.
- Simulation models for different types of MANETs enhanced with FSO capabilities were developed. Specifically, models for modules that handle FSO operations were designed from scratch, existing models for RF MANETs modified, and interfacing mechanisms between the FSO and RF modules constructed.
- The performance of such networks was analyzed and evaluated by performing perturbation study on the simulation models. The simulation results validated the proposed network design.

The rest of the dissertation is organized as follows:

Chapter 2 presents the results of the literature survey conducted for the research project of this dissertation, including brief introductions to the involved FSO and MANET technologies, and a review of published peer research on relevant topics.

Chapter 3 reports an investigation on certain hardware equipment required by a MANET with FSO capabilities and demonstrates that physical implementation of such a network is feasible.

Chapter 4 introduces the methodology employed by the research project of this dissertation, using a simple simulation model as a test project.

Chapter 5 presents preliminary research efforts that are focused on the modeling of the proposed FSO module.

Chapter 6 discusses in detail simulation models developed to study FSO-enhanced ad hoc Wi-Fi networks (the ad hoc mode of a Wi-Fi network can be considered a special case for MANET).

Chapter 7 extends the scope of the RF ad hoc network to the general MANET and presents simulation studies on FSO enhancement to such networks.

Chapter 8 closes this dissertation providing conclusions and suggestions on future work.

References are listed in the end as an appendix.

CHAPTER 2 - LITERATURE SURVEY

This chapter provides an introduction to the technical background of the dissertation. It will be organized into four sections: Section 2.1 deals with the fundamentals of how FSO operates; Section 2.2 focuses on basic characteristics of MANETs; Section 2.3 presents a review on the current status of FSO communications research; and Section 2.4 investigates published peer research in the related area of the dissertation.

2.1 FUNDAMENTALS OF FREE-SPACE OPTICAL COMMUNICATIONS

2.1.1 Overview

Free-space optics (FSO) is a technology for transmitting data using optical signals propagating through the air. FSO employs infrared (IR) laser beams as the signal carrier [1, 2], as does fiber optics. Therefore, each FSO link is "point to point" in nature, which is different from the "broadcasting" characteristic of radio frequency (RF) wireless communications. The typical wavelength at which commercial FSO systems operate is usually either 850 nm or 1550 nm [3].

FSO is capable of offering high-bandwidth services over a relatively short distance at attractive costs. A cumulative bandwidth as high as 80 GHz over a single FSO link has been reported in the literature [4]. Although FSO provides data rates comparable to those offered by conventional fiber optics, the time and cost required to set up an FSO link are significantly less than a fiber cable. In urban

areas, it takes several months and hundreds of thousands of dollars to dig a trench and lay a fiber inside; in contrast, the setup cost of an FSO link is in the range of a few thousand to tens of thousands of dollars, and the link can be established in days [3].

2.1.2 Basic Configuration of an FSO Communication System

An FSO communications link is composed of an optical transmitter at one end and an optical receiver at the other end. A transmitter/receiver pair, or a transceiver, is usually installed on each terminal to accommodate bi-directional connectivity. Figure 2.1 is a schematic drawing of an FSO transceiver.

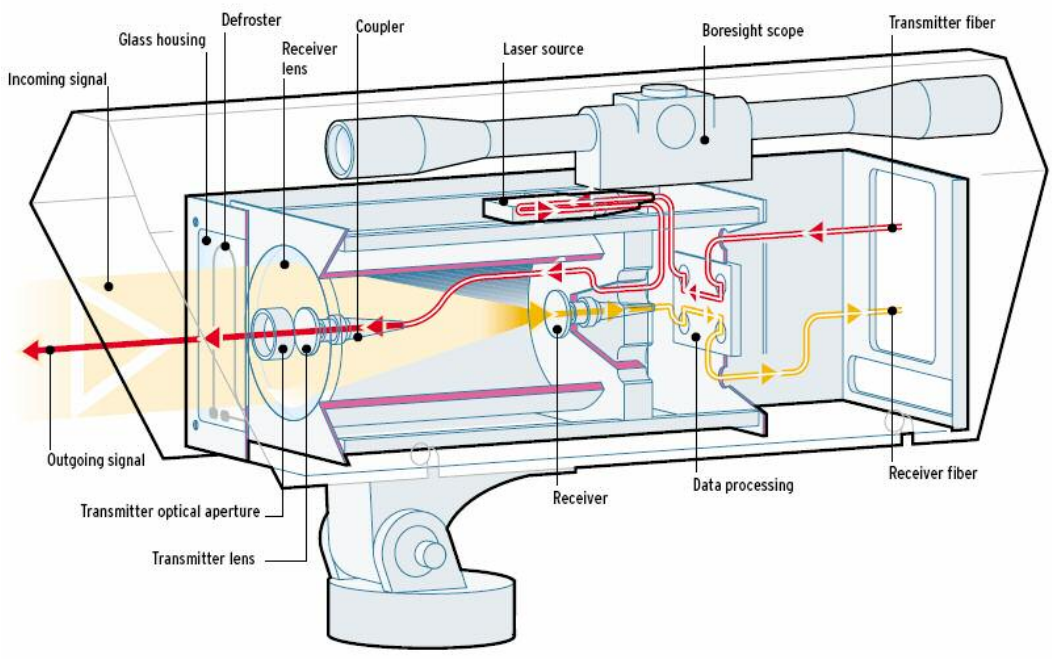

Figure 2.1 Schematic of an FSO transceiver. [2]

An FSO link consisting of a pair of such transceivers operates as follows:

The data to be transmitted over the FSO link enters the link head through the transmitter fiber (or wire) and modulates the laser source. The modulated signals then traverse through a set of lenses that are used to adjust the divergence of the laser beam. Next, the signal-carrying laser beam exits the optical aperture and continues to propagate through the air, and is projected upon the optical aperture of the transceiver at the other end of the link. The light enters the receiver, also through a series of lenses, which focus the received light onto a photodetector, or, in some cases, couple the signals directly into a fiber. More advanced systems may employ an optical amplifier, such as an erbium-doped fiber amplifier (EDFA), in front of the photodetector. They may also be equipped with certain devices for active tracking, in addition to more commonplace auxiliary devices such as a defroster and a boresight telescope.

It is worth noting that the transmitted laser beam is often intentionally made to have a certain amount of divergence so that the cross-sectional area of the beam at the receiver end is much larger than the optical aperture of the link head, as shown in Figure 2.2. The purpose of such a measure is to compensate for small terminal movements due to environmental factors such as building sway.

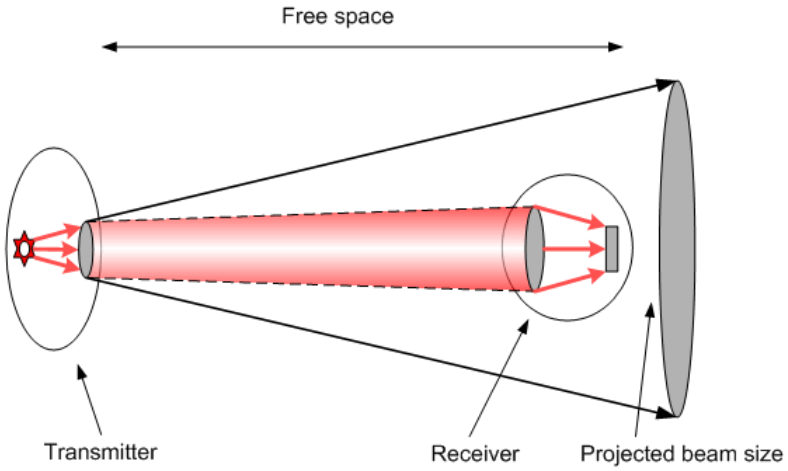

Figure 2.2 Illustration of an FSO communications link. [5]

2.1.3 Link Margin Analysis [5]

As in all communications systems, a link margin analysis is an important task in designing an FSO link. In an FSO system, causes for signal degradation include imperfect optical elements, imprecise pointing, divergence, and atmospheric factors [5]. The goal of the link margin analysis is to ensure that the launched optical power minus the losses caused by those factors stays above the sensitivity of the receiver photodetector. The larger the link margin, the higher the availability of the link. However, for an FSO system with a particular laser source, allocating more signal power to the link margin means taking away power that would otherwise be used to increase the link distance. This is a trade-off between reliability and link distance.

Before the link equation is presented in Section 2.1.3.5, the degradation factors mentioned above will be discussed in detail first, in Sections 2.1.3.1-4.

2.1.3.1 Optical Loss

The term "optical loss" refers to the FSO signal degradation due to imperfect optical elements, such as lenses and couplers. The amount of optical loss depends on the characteristics of the equipment, and needs to be derived from the product specifications or measured. Typically, the optical elements in an FSO link impose a few decibels (dB) of reduction in signal power.

2.1.3.2 Geometrical Loss

Geometrical loss is caused by the laser beam's divergence, which is often intentionally set to a certain amount such that some portion of the beam will always be cast upon the receiver aperture even if the beam wobbles. The result of the divergence is that the projected beam size at the receiver end is much larger than the optical aperture of the receiver (illustrated in Figure 2.2), and much of the optical power cannot be collected by the receiver.

The ratio of the effectively collected power, P_r, to the total optical power arriving at the receiver end, P_1, is equal to the ratio of the area of the receiver, A_r, to the area of the beam at the receiver, A_1, and can be expressed as follows:

$$\frac{P_r}{P_1} = \frac{A_r}{A_1} = \frac{d_r^2}{(d_t + \Theta \cdot x)^2} \approx \frac{d_r^2}{(\Theta \cdot x)^2} \tag{2.1}$$

where d_r and d_t are the diameters, in meters, of the receiver and transmitter, respectively; Θ is the divergence, in radians, of the laser beam; and x is the link distance, in meters.

Using the frequently used dB scale, the geometrical loss, L_g, can be expressed as:

$$L_g = P_1(dB) - P_r(dB) = 20 \times [\log(\Theta x) - \log(d_r)] \tag{2.2}$$

2.1.3.3 Pointing Loss

If the transmitter is not pointed accurately enough at the receiver, pointing loss will be produced. Essentially, pointing loss is of the same nature as geometrical loss, in the sense that the receiver is not collecting all the optical power arriving at its photodetector. In practice, the use of divergence and/or active tracking can limit the value of pointing loss to effectively zero dB.

2.1.3.4 Atmospheric Loss

The physics of the atmosphere plays a critical role in determining most of the limitations of an FSO system. Laser transmission in the air suffers from detrimental factors including absorption, scattering, and scintillation. The overall

effects of these factors are reflected in the attenuation of the laser beam and the degradation of the received signals.

Absorption of laser beams traveling through the air is by molecules of water, ozone, carbon dioxide, oxygen, etc. The absorption is strongly dependent on the laser wavelength [3, 5, 6].

Scattering is another phenomenon that attenuates the laser beam. Scattering can be classified as Rayleigh scattering and Mie scattering. For today's FSO systems, which all employ IR lasers with relatively long wavelengths, the latter is the dominant scattering effect. Mie scattering becomes a serious problem for FSO links when there is fog, haze, or heavy dust in the air. It is well documented that dense fog can cause an attenuation of more than 200 dB per kilometer [3, 5].

Scintillation is reflected in intensity fluctuations of the received signal due to thermally induced changes in the refractive index of the air. Commercial FSO links operating horizontally and close to the earth surface face much stronger scintillation compared to vertical earth-satellite links. However, the signal degradation due to scintillation is much less than attenuation caused by foggy/rainy conditions, and is easily compensated [7, 8]. And it is worth noting that the air is always clear when the maximum scintillation takes place. Therefore, an appropriately designed FSO system capable of operating under ordinarily bad weather conditions can automatically account for scintillation.

In general, the Beer-Lambert law, which governs the attenuation of an optical beam through the air, can be expressed as [3]

$$\frac{I_1}{I_0} = e^{-\alpha x} \tag{2.3}$$

where I_0 is the initial optical intensity in W/m^2, I_1 is the intensity in W/m^2 after the beam passes through a distance of x kilometers, and α is the attenuation coefficient of the air in km^{-1}. Since the total received power is of interest in the research of FSO, Equation (2.3) can be written as

$$\frac{P_1}{P_t} = \frac{A_1}{A_t} e^{-\alpha x} \tag{2.4}$$

where P_t is the optical power out of the transmitter optics, A_t is the area of the transmitter aperture, P_1 is the optical power of the beam at the receiver end, and A_1 is the cross-sectional area of the projected beam (not the receiver aperture). Using the dB scale, the atmospheric loss, L_a, can be expressed as

$$L_a = P_t(dB) - P_1(dB) = 10 \cdot \alpha \cdot x(\log \frac{A_t}{A_1} + 0.4343) \tag{2.5}$$

In practice, one can directly measure the atmospheric attenuation coefficient, β (dB/km), under different weather conditions. Therefore, the atmospheric loss is simply

$$L_a = \beta \cdot x \tag{2.6}$$

MODTRAN, a software program developed by the U.S. Air Force and commercially marketed by Ontar Corporation under the name PcModWin, is the standard computer tool for calculating atmospheric transmission of lightwaves of which the spectrum ranges from ultraviolet (UV) to microwave [9]. Figure 2.3 shows the total transmission of a laser as a function of its wavelength, over a distance of 1 kilometer under fair weather conditions. Based on the graph, several transmission windows can be clearly identified: regions around 0.78, 0.85, 1.05, 1.3, and 1.55 μm. It is worth noting that portions of the FSO transmission windows overlap with the transmission windows of fiber optics currently in use (0.85 and 1.55 μm). Therefore, FSO systems can directly make use of the currently available optical components, such as laser sources and receivers. This

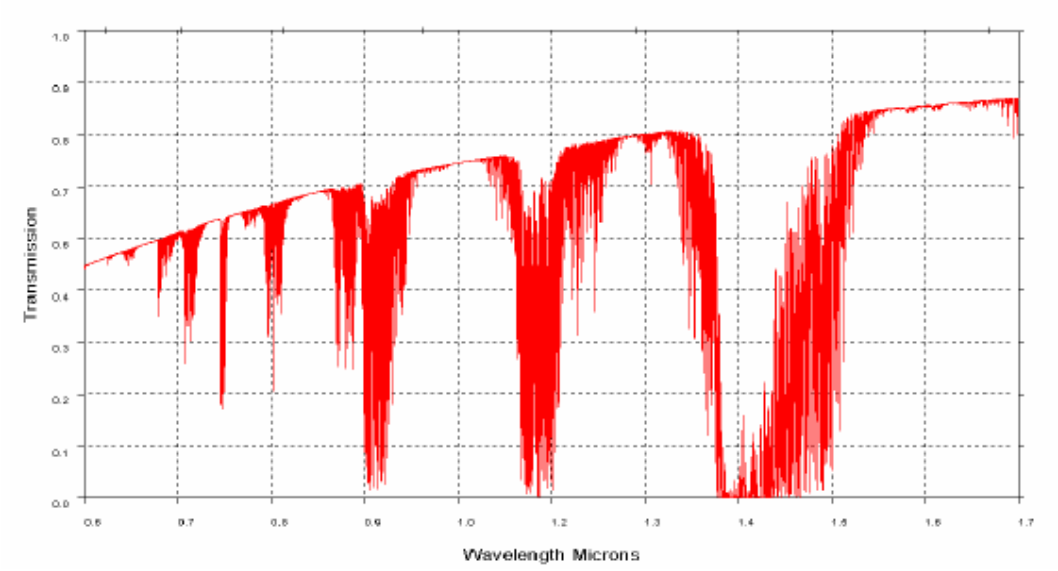

Figure 2.3 Transmission spectrum generated by MODTRAN.

provides the design and manufacture of FSO systems with great cost efficiency, and is an important factor to account for the growth of the commercial FSO market.

2.1.3.5 Link Equation

The link equation for an FSO system can be expressed as follows:

$$P_r = P_{ls} - L_o - L_g - L_p - L_a = R_s + C_{lm} \tag{2.7}$$

where P_r is the optical power collected by the receiver optics in dBm; P_{ls} is the optical power emitted by the transmitter laser source in dBm; L_o, L_g, L_p, and L_a are the optical, geometrical, pointing, and atmospheric losses, all in dB; R_s is the receiver sensitivity in dBm; and C_{lm} is the link margin in dB.

In general, the atmospheric loss dominates the performance of an FSO link due to the exponential term with respect to the link distance [see Equations (2.3) through (2.6)]. For example, consider a 1-km FSO system operating at a certain link margin M, for a typical atmospheric attenuation coefficient of β = 100 dB/km (moderate to heavy fog), even if the transmitted power is increased to 10 times the original value, the link distance at which the same link margin M can be achieved is only increased to 1.09 km.

It can be concluded that, for fixed commercial FSO systems where high availability, i.e., low downtime is desired, one should not extend the link distance beyond a realistic value (500 – 1000 m). The upper limit of FSO link distance

depends on the atmospheric conditions of a specific area and customer requirements of availability. Some examples of practical values of maximum link distance can be found in various publications [1, 10, 11, 12]. There have also been some efforts into predicting the availability of FSO links using historical weather data collected at airports [13]. The prediction results, in turn, can provide assistance in determining the link distance limitations according to specific availability requirements.

In MANET applications, which are the main focus of this dissertation, where the volumes of data exchange are not as heavy as in fixed-line carrier systems, and where flexibility instead of availability is the priority, one can circumvent the occasional link-down problem, to some degree, by utilizing the inherent multi-hop routing feature, and by buffering and transmitting data in high-bandwidth pulses when the weather condition is good.

2.1.4 Laser Safety

A laser beam with too high an intensity may damage the eye. The amount of power the eye can safely tolerate varies with the laser's wavelength [3, 5]. The latest laser safety regulation is developed by the American National Standards Institute (ANSI), which tabulates the maximum permissible exposure level (MPE) as a function of wavelength [14]. Most FSO communication systems are designed to be eye safe.

2.1.5 Current Status of FSO Research

The current research on FSO is mainly focused on the following aspects: environmental adversities on system operation [6, 15-26]; improvements in system capacity [4, 27], availability [10, 11, 13, 23, 28, 29], and link distance [4, 27, 30, 31]; hardware design [32-34]; transmission security [35-37]; and networking [38-40]. From an application point of view, a number of researchers and commercial vendors are looking into the prospect of using FSO for enterprise connectivity [41-43], metro area networks [29, 41-45], optical fiber backbone extension [41-43, 46], and deep space communications [47-49], etc.

2.2 FUNDAMENTALS OF MOBILE AD HOC NETWORKS

2.2.1 Overview

A mobile ad hoc network (MANET) is a collection of dynamically communicating mobile nodes. It requires no infrastructure or system administration. The control over a MANET is distributed among its mobile nodes. Each node is autonomous and can serve as the source, destination, or relay of a data transmission.

Mobile devices participating in a MANET can exist in many forms [50], such as palmtops, laptops, mobile phones, etc. They differ in size, computational power, storage capacity, and battery life. Some devices are more powerful than

others in terms of computational capabilities, and some can serve as "servers" while others can only be "clients".

There are two types of communication taking place in a MANET. One is peer-to-peer, or single-hop, communication, which is the direct communication between two nodes within each other's transmission range, without involving a third "relay" node. The other is remote-to-remote, or multi-hop, communication, which is the communication between two nodes with the "forwarding" or "relaying" assistance from one or more other nodes.

The two major challenges facing MANET research are media access control (MAC) protocols and routing protocols [50]. Sections 2.2.2 and 2.2.3, respectively, will discuss the two challenges in some detail.

A working group within the Internet Engineering Task Force (IETF) is dedicated to MANET research by drafting and standardizing various protocols involved in MANET operations [51].

It should be noted that the popular wireless local area networks (WLANs) also include an ad hoc operational mode. An ad hoc-mode WLAN can be considered a special case for MANETs in the sense that such a network also requires no infrastructure and supports node mobility. However, it does not support multi-hop routing as a general MANET does. A separate introduction to ad hoc WLANs will be presented in Chapter 6.

2.2.2 Media Access Control Protocols

Since the same media are shared by multiple nodes in a MANET, access to the common channel must be made in a distributed fashion. Therefore, media control access (MAC) protocols that require centralized control, such as TDMA, FDMA and CDMA, are not suitable. Various issues, including mobility, hidden terminals, and exposed nodes, should be considered when designing a MAC protocol for MANETs.

There are a number of existing MAC protocols that can be used by MANETs. They include: Multiple Access with Collision Avoidance (MACA) [52], MACA by Invitation (MACA-BI) [53], Power-Aware Multi-Access Protocol with Signaling (PAMAS) [54], Dual Busy Tone Multiple Access (DBTMA) [55], Floor Acquisition Multiple Access (FAMA) [56], etc.

Since the proposed project will employ a point-to-point laser-based FSO link instead of broadcasting radio waves as the transmission carrier, it can be expected that media access will not impose a problem. Therefore, besides listing a reference that compares the performance of some of the MAC protocols mentioned above [57], this section will not go into further details in discussing MAC protocols designed for MANETs in the radio frequency (RF) domain.

2.2.3 Routing Protocols

Routing is the most commonly studied topic in MANET research. Since nodes in a MANET move frequently, which forms and breaks data links often, the topology of a MANET changes dynamically, which gives rise to the necessity of a suitable routing protocol.

There exist a rather large number of MANET routing protocols. Some of them are merely extensions of previously existing ones. Literature review reveals that the following two are most widely studied, implemented, and accepted as effective routing protocols: Ad Hoc On-Demand Distance Vector Routing (AODV), and Dynamic Source Routing (DSR).

2.2.3.1 AODV

The specifications of AODV are currently published by the IETF as a Request for Comments (RFC) [52].

In AODV, when a source node desires to send data to a destination node to which it does not have a valid route yet, it initiates a "route discovery" process. It broadcasts a "route request" (RREQ) packet to its neighbors, which then forward the RREQ to their neighbors, and so on, until either the destination node or an intermediate node with a "fresh enough" route to the destination is reached. During the forwarding, each intermediate node records in its routing table the IP address of its neighbor from which the first copy of the RREQ was received,

thereby establishing a reverse route. Once the destination node or an intermediate node with a "fresh enough" route to the destination is located, this node responds by unicasting a route reply (RREP) packet back to the neighbor from which it first received the RREQ. Because the RREP is forwarded along the path established by the RREQ, AODV only supports symmetric, or bidirectional, links. Figure 2.4 illustrates the AODV route discovery process [50].

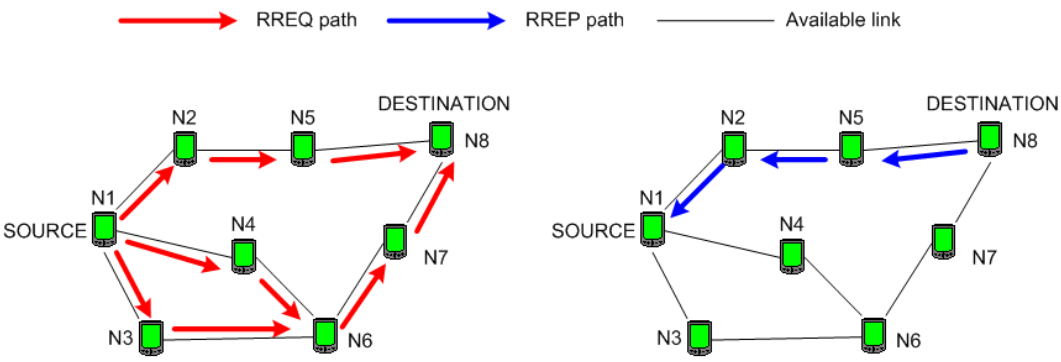

Figure 2.4 AODV route discovery.

2.2.3.2 DSR

The DSR specifications are listed in the IETF DSR Internet Draft [59]. In DSR, mobile nodes are required to maintain and continually update route caches that contain the source routes of which the node is aware. When a source node desires to send data to a destination, it first checks its route cache to determine whether or not it contains a route to the destination. If not, it initiates a route discovery process by broadcasting a RREQ packet, which contains the IP addresses of the source and destination, and a unique RREQ identification number.

Each node receiving the RREQ examines whether it stores a route to the destination. If not, it adds its own address to the route record of the RREQ packet and passes it along. If the RREQ reaches the destination or an intermediate node that knows of an unexpired route to the destination, a RREP is generated. In most cases, the RREP is relayed back to the source node along the reverse route in the route record of the RREQ. But the destination node may also initiate its own route discovery for the source node and piggyback the RREP on a new RREQ. Figure 2.5 illustrates the DSR route discovery process [50].

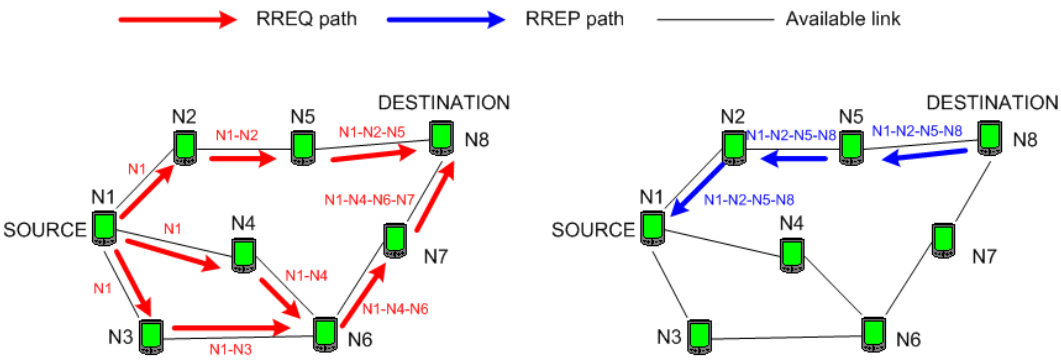

Figure 2.5 DSR route discovery.

For link maintenance purposes, RERR packets are generated at a node when the data link layer encounters a fatal transmission problem. When a RERR is received, the hop in error is removed from the node's route cache, and all routes containing the hop are truncated at that point.

2.3 PEER RESEARCH ON FSO MOBILE NETWORKS

No published work has been located that focuses on the network-layer operation of an FSO-equipped MANET, which is the emphasis of this dissertation. There have been, however, research efforts in closely related areas. Three groups of researchers working in those areas have been identified. They are located at the University of Maryland [60], Rensselaer Polytechnic Institute [61], and Lehigh University [62].

Works published by the Maryland group [8, 63] presented algorithms of topology reconfiguration in FSO networks based on link-state monitoring. However, the FSO networks studied by this group did not involve any mobility issues. The topology change was necessitated by physical obscuration of the LOS between two static nodes.

The RPI group specifically lists "FSO MANET" as its research focus. It has published works on topics including optical transceiver design [64], automatic alignment circuit design [65], and mobility analysis [65]. However, there is no evidence that this group's research has yielded any significant results with respect to a fully functioning FSO MANET. The node mobility analyzed in [65] was based on a simple setup in which one mobile node follows a circular trajectory and a few static nodes are located within the circle. Evidently, such movements cannot closely mimic the typical node movements in an actual MANET.

The Lehigh group has focused its research on the design and deployment of hardware platforms for mobile FSO communications. Prototypes of mobile FSO terminals capable of automatic link acquisition over a relatively short distance (45 – 100 meters) have been presented [66, 67]. In [67], a routing scheme, namely Hierarchical State Routing (HSR), was proposed to be implemented in the hybrid FSO/RF networks studied by this group. However, besides giving a brief introduction to the HSR scheme, no actual implementation, simulation or evaluation of routing protocols was reported in the group's publications.

CHAPTER 3 - FEASIBILITY STUDY

The existing MANET technologies were developed strictly in the RF domain to take advantage of the broadcast nature of RF wireless transmission. The wireless nature of FSO gives rise to the possibility that MANETs employ optical means of communications to provide high bandwidths. From a networking point of view, however, a big disadvantage of FSO communications is that it is a point-to-point technology that always requires line of sight (LOS). In order to implement any ad hoc routing algorithm in a mobile FSO network, the nodes in the network need to be equipped with devices able to perform a number of essential tasks including fast steering of laser beams, self-detection of geographical position, automatic link acquisition, target tracking, etc. This chapter will report on investigations of hardware that can be used to provide such capabilities.

3.1 LASER BEAM STEERING

By definition, laser beam steering means the control of the direction of the laser beam by mechanical, optical and/or electrical means. In a MANET, each FSO transmitter needs to have the ability to dynamically steer its laser beam to facilitate the search for a receiver before a link is established and to track the movements of the receiver during active data transmission. Theoretically, any device that can be controlled to change the direction of an optical beam is a

candidate. Such devices include gimbals, electro-optic devices, acousto-optic devices, and fast steering mirrors.

3.1.1 Gimbals

Commonly, a gimbal refers to a device consisting of several rings mounted on axes at right angles to each other so that an object, such as a ship's compass, will remain suspended in a horizontal plane between them regardless of any motion of its support. A diagram of a gimbal is shown in Figure 3.1 [68]. Note that sometimes, such as in the figure, the rings in the gimbal device are also referred to as "gimbals"; but the standard practice is to name the whole set of rings a gimbal. Figure 3.2 shows two commercial gimbal products [69, 70].

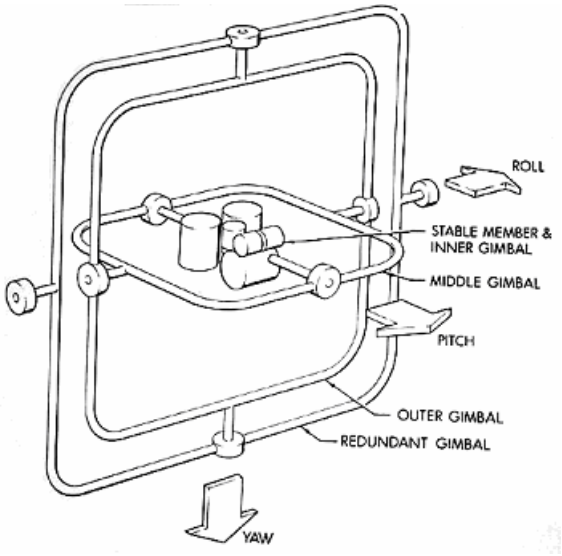

Figure 3.1 An example of a gimbal. [68]

Figure 3.2 Commercial gimbal products. [69, 70]

For applications in optical beam steering, the three rings with respect to the three degrees of freedom (pitch, roll, and yaw) are usually maneuvered by stepper or servo motors so that the laser transmitter mounted on the inner ring can point to any direction within a specified angular range. Important specifications of a gimbal include: travel range (both azimuth and elevation), travel rate, and positional resolution. Table 3.1 lists such parameters for two commercially available gimbal devices [69, 70].

	Travel range (°)		Travel rate (°/s)	Resolution (°)
	Azimuth	Elevation		
Model 1	360	-35 ~ +95	120	0.004
Model 2	-90 ~ +90	-90 ~ +90	10	0.01

Table 3.1 Gimbal parameters.

From the data listed in Table 3.1, one can draw the conclusion that Model 1 fits the application of FSO MANET better as its azimuthal travel range covers the entire perimeter while its elevational travel range is expected to be sufficient, and it has a much faster travel rate and finer resolution than Model 2.

Compared with other devices for laser beam steering (discussed later), gimbals have the advantages of fast speed for coarse pointing and wide range. Their disadvantages include low resolution and slow response time (typical values of the control bandwidth of a gimbal are in the ~10Hz range [71]). The former can be compensated either by intentionally making the laser beam diverge such that the gimbal does not leave "blind" spots when it steps, or by using a fine-pointing device with higher resolution in combination with the coarse-pointing gimbal. The latter means that gimbals alone cannot offset high-frequency motion of the mobile node, such as mechanical vibrations. This problem can be addressed either by the "hybrid" approach mentioned above, i.e., by using a pointing device with faster response time in combination with the gimbal, or by using some mechanical stabilization equipment.

3.1.2 Electro-optic Devices

Electro-optic laser beam steering, by name, takes advantage of the electro-optic effects, where the indices of refraction of certain waveguiding materials are altered proportionally to the strength of the electric field applied to the material.

The mechanism is well known and there are a great variety of materials that are subject to such effects. Since the 1970s, a large amount of research effort has been put into new materials and device structures that are capable of electro-optic deflection. Studies have been published on electro-optic beam steering using materials such as aluminum gallium arsenide [72], lithium tantalate [73], liquid crystal [74], lanthanum-modified lead zirconate titanate [75], etc., and device designs including single prism, prism arrays, channel waveguide arrays [76], and photonic crystal horns [77]. The performance of the published designs varies widely. The most important parameter, the maximum steering angle, ranges between 0.04 [75] to 30 degrees [77]. By applying the electric field appropriately, continuous steering within range can be achieved. The control bandwidths of different systems are similar, however, typically in the range of tens of MHz, because the electric field can be altered at very high speeds.

For applications in FSO MANETs, considerations should be given to steering angle, modulation frequency, and wavelength selectivity. Obviously, an electro-optic beam steering device operating at a wavelength that is used by the FSO units, with a large maximum steering angle and high modulation frequency, is desirable. Due to its relatively narrow steering angle, it is not viable to use an electro-optic device as the stand-alone steering equipment. A gimbal and an electro-optic device should be used in combination in order to complement each other's performance. In such a hybrid system, the gimbal subsystem would serve

as the coarse pointing device, and the electro-optic subsystem would do the fine pointing.

3.1.3 Acousto-optic Devices

Acousto-optic beam steering makes use of Bragg diffraction. When an ultrasonic wave propagates through a Bragg grating, causing changes in its density, the index of refraction of the grating is modulated. If a laser beam is incident on the grating, its direction can be controlled by adjusting the periodicity of the grating through the application of acoustic waves. A diagram of the operation is shown in Figure 3.3 [78].

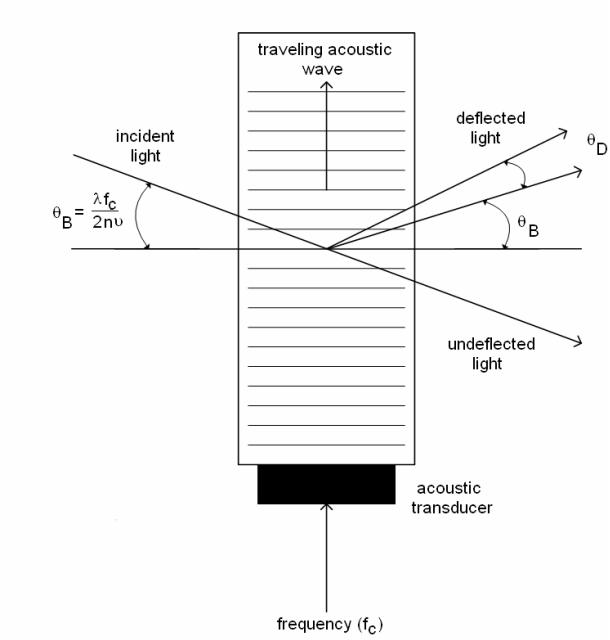

Figure 3.3 Acousto-optic beam steering using a Bragg grating. [78]

The deflection angle is found to be:

$$\Theta_D = \lambda f / nv - 2\Theta_B \tag{3.1}$$

where λ is the optical wavelength, f is the acoustic frequency, n is the index of refraction, v is the acoustic velocity, and Θ_B is the Bragg angle. Therefore, by rapidly changing the frequency of the acoustic wave, one can achieve fast steering of the optical beam.

Again, since a Bragg grating can only offer a much smaller steering angle than a gimbal, a hybrid steering system consisting of a Bragg grating mounted on a gimbal is desirable to achieve wide-range fast coarse pointing followed by fine tuning.

Compared with electro-optic devices, acousto-optic devices offer the advantages of low operating voltage, low drive power, high extinction ratio, simple design, rugged construction, insensitivity to temperature changes, and high safety factors. Electro-optic devices are more attractive when the desired control bandwidth is 100 MHz or up [79]. However, mechanical vibrations that affect FSO transceiver units are most likely below 1 MHz. Therefore, acousto-optic devices provide sufficient compensation for such vibrations.

3.1.4 Fast Steering Mirrors

A fast steering mirror (FSM) is a mirror that can be accurately maneuvered on a pivot by servo motors, magnetics or piezoelectrics. It offers two-axis, high-bandwidth tip/tilt mirror motion that can be used to steer a laser beam. Two commercial FSMs are shown in Figure 3.4. The model shown in Figure 3.4(A) is driven by voice coils, while the one shown in Figure 3.4(B) is driven by piezoelectrics [80, 81].

(A)

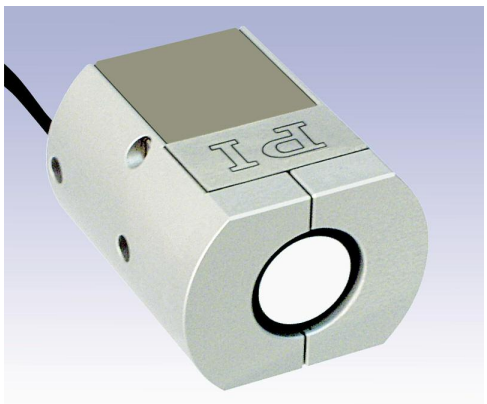

(B)

Figure 3.4 Fast steering mirrors. [80, 81]

The steering angle offered by FSMs is in the range of several degrees. The control bandwidth of FSMs is typically a few hundred Hz to several kHz. The resolution is related to the control mechanism. Typically, piezoelectric drivers offer higher resolution than other types; closed-loop control circuits achieve better results than open-loop ones. The two products shown in Figure 3.4 both offer an angular range of +/- 3^{o}. However, the resolution of the one shown in (A) is 2 μrads (0.0001^{o}), while the one in (B) has a 1-μrad resolution. Both products employ sensor-based feedback circuits, i.e., closed-loop control, to achieve high resolution.

3.2 LINK ACQUISITION AND TRACKING

Link acquisition refers to the operation in which the FSO transmitter and receiver recognize and lock on to each other during the course of searching for their counterpart via beam steering. Tracking is defined as the continuous adjustment to the angular positions of the transmitter and receiver to keep the optical link active in the presence of node movement. Both incorporate a mechanism that detects the presence and/or position of the beam at the receiver side and a control measure that keeps the beam on the receiver's photon detector. Beam steering devices have been discussed in the previous section. This section will be devoted to types of equipment that are capable of detecting the presence

and position of the laser beam on the receiver. Photodiode arrays and CCD arrays are the most commonly used devices in such applications.

3.2.1 Photodiode Arrays

Photodiodes arranged in a matrix are used to monitor the position of the centroid of the laser beam. They can be made from different materials, thus cover various spectral ranges. The simplest form of a photodiode array is the quadrant detector.

A quadrant detector consists of four separate photodiodes mounted together, as shown in part (A) of Figure 3.5 [82]. The gray spot represents the laser point on the detector.

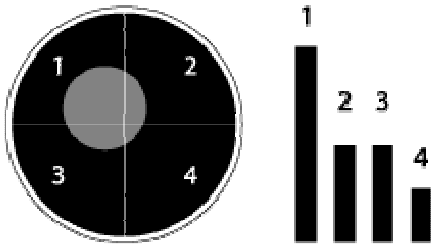

Figure 3.5 Diagram of a quadrant detector.

If the spot is located exactly in the center of the array, the signal output from all four photodiodes will be equal. If the spot moves, the amount of light collected by each photodiode will be different, resulting in a different level of the

output signal, as shown in Figure 3.5(B). The position of the spot can be determined by analyzing the output from all four photodiodes. Subsequently, the position information is put into an algorithm to control the beam steering device to correct deviations of the received beam.

Since quadrant detectors usually have relatively small configurations, their field of view (FOV) is only large enough for small angle deviations. In order to achieve a larger FOV, a fish-eye lens is sometimes placed in front of the detector. The resolution of quadrant detectors can be very high. Light spot movements of 10 μm can be detected.

More complex arrays consisting of more than four photodiodes have been proposed [83]. Nevertheless, they follow the same principle as quadrant detectors.

3.2.2 CCD Arrays

Charge-coupled device (CCD) arrays are commonly used in cameras and camcorders. A CCD array is a light-sensitive detector made up of many small metal oxide semiconductor (MOS) capacitors, each of them representing one pixel. The light applied onto a pixel is converted into a charge that is proportional to the light energy. The charge is stored in the capacitor until released by a gate signal. In a CCD array, the charge in each capacitor is measured sequentially by a serial shift register approach. Consider a one-dimensional array of pixels. When a gate (clock) signal releases the charge in the first pixel to the charge-measuring

mechanism, the charge from the second pixel is transferred to the first pixel, the charge from the third to the second, etc. The process is then repeated until the charges from all of the pixels are measured. Because the order of the transfer is known, each measurement is associated with its exact position in the array. In a two-dimensional array, the first row (or column) is completely measured, then the charges from the second row (or column) is transferred to the first row, etc., as shown in Figure 3.6 [84]. Once the CCD array has been read out, the position of the light spot on the array can be determined and used for steering purposes.

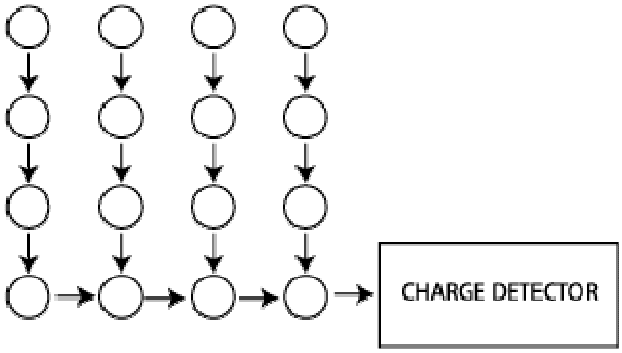

Figure 3.6 A simple CCD diagram.

CCDs are sensitive to the visible and infrared spectrums. Since FSO usually operates in the infrared domain, CCD arrays would satisfy the wavelength selectivity requirement.

The CCD pixel size can be very small (~10 μm), with an even much smaller gap between them. A large number of CCD pixels can be integrated into

an array (2048×2048 CCD arrays have been commercially available). Therefore, the total detection area is large compared to quadrant detectors. This is a major advantage for acquisition/tracking applications.

The biggest problem associated with a CCD array is its slow read-out time due to the sequential measurement, especially when the array is large. The control mechanism for the steering device must await the information for the complete array to be obtained, even if the actual region of interest covers only a small portion of the receiving aperture. The typical read-out time of a 2048×2048 CCD array is on the order of seconds, which is obviously too slow for FSO MANET applications.

To mitigate the read-out time problem, direct-readout CCD arrays offering the capability to read individual pixels separately are in development. As of this time, no commercial product or detailed information regarding such devices is available.

3.3 LOCATION DETECTION

As aforementioned, information is carried by narrow laser beams in FSO communications. A link can only be acquired when two FSO terminals point directly at each other in the presence of LOS. Such a pointing process requires each terminal in a two-terminal FSO hop to have (approximate) information on the geographical location of its counterpart, so that it can steer its linkhead to the

vicinity of the counterpart in search of its optical aperture. If each terminal is able to obtain its own geographical coordinates and such data can be disseminated throughout the network via RF means, either continuously or on an on-demand basis, then the target-search process for link acquisition purposes can be facilitated. Today's ubiquitous device for self-location detection is a Global Positioning System (GPS) receiver.

The GPS is a satellite-based navigation system developed by the U.S. Department of Defense (DoD) [85]. The fully operational GPS includes six circular orbits with four or more satellites approximately uniformly distributed on each of them. The orbits have the same radius of 26,560 km, and the angle between any two adjacent orbit planes is 60^{o}. A diagram of the GPS orbits is shown in Figure 3.7 [86].

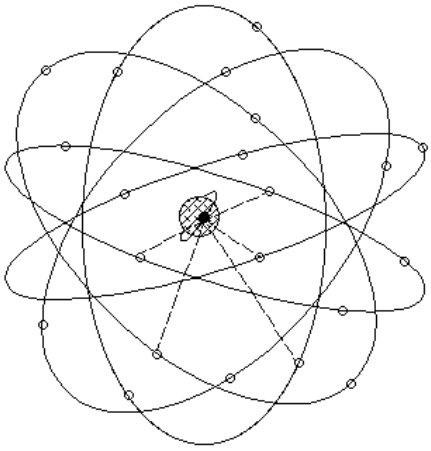

Figure 3.7 GPS orbits. [86]

If four or more GPS satellites are visible, a GPS receiver can determine its earth-centered, earth-fixed (ECEF) position (X, Y, Z) by solving the following equations (in matrix form) [87]:

$$\begin{pmatrix} \rho_{r1}^2 - (x_1^2 + y_1^2 + z_1^2) - r^2 \\ \rho_{r2}^2 - (x_2^2 + y_2^2 + z_2^2) - r^2 \\ \rho_{r3}^2 - (x_3^2 + y_3^2 + z_3^2) - r^2 \\ \rho_{r4}^2 - (x_4^2 + y_4^2 + z_4^2) - r^2 \end{pmatrix} = \begin{pmatrix} 2x_1 - 2y_1 - 2z_1 & 1 \\ 2x_2 - 2y_2 - 2z_2 & 1 \\ 2x_3 - 2y_3 - 2z_3 & 1 \\ 2x_4 - 2y_4 - 2z_4 & 1 \end{pmatrix} \begin{pmatrix} X \\ Y \\ Z \\ C_{rr} \end{pmatrix} \tag{3.2}$$

where C_{rr} is the clock bias correction; r is the radius of earth; x, y, and z are the satellite position coordinates calculated from ephemeris data; and ρ_r is the pseudorange, i.e., the apparent range to a GPS satellite from the receiver antenna, calculated from the time of signal transmission, time of signal reception, and speed of light. The index 1, 2, 3, or 4 for x, y, z and ρ_r denotes a parameter relevant to a specific GPS satellite.

Note that aside from the clock bias correction C_{rr}, the calculations in Equation 3.2 do not involve additional errors such as ionospheric errors, ephemeris data errors, multipath errors, receiver noise, etc. It is beyond the scope of this dissertation to go into the details of GPS error analysis. Thus, it suffices to know that, by advances in receiver technology in recent years, the user-equivalent range error (UERE) can be limited to about 6 meters; if additional techniques such as differential and augmented GPS are used, measurement accuracies in the millimeter range can be achieved [87].

Today's GPS receiver units are usually fairly compact in size (a few inches each in length, width, and thickness) and weight (less than a few kilograms). Since the DoD removed Selective Availability (SA), an intentional degradation of GPS signals available to the public, in May 2000, the performance of military and commercial GPS receivers has become indistinguishable in terms of precision. GPS receivers can be readily integrated into other hardware platforms, such as navigational systems for airplanes and automobiles, and steering systems for antennas and lasers. Figure 3.8 shows two GPS receiver units, of which Part (A) is a stand-alone handheld unit [88], and Part (B) is a unit integrated into the cockpit of an airplane [89].

(A) (B)

Figure 3.8 Examples of GPS receivers. [88, 89]

Competing systems for location detection include Russia's GLONASS and Europe's GALILEO. They work on the same principles as the GPS.

3.4 CONCLUSIONS

This section has reported an investigation on hardware required by an FSO-equipped MANET to provide essential functions such as fast optical beam steering, link acquisition, target tracking, and location detection. The currently available hardware would not pose fundamental obstacles for the implementation of ad hoc routing protocols in an FSO MANET. The actual construction of such a network would require further, more detailed studies on such topics as optimum hardware configuration, interactions and complementing performance of integrated equipment, etc. New technical developments in hardware renovation will make the construction and operation of FSO MANETs more effective and economical.

CHAPTER 4 - METHODOLOGY

The overall goal of the work reported in this dissertation is to study the performance of a MANET equipped with FSO communication capabilities, by means of computer modeling and simulation. This chapter will discuss the methodology employed in the modeling process.

4.1 COMPUTER TOOL SELECTION

The most commonly used software packages for discrete-event network simulation include NS-2 [92], GloMoSim [93], and OPNET Modeler [94]. Among them, NS-2 is an open-source package available to everyone free of charge, while GloMoSim and OPNET Modeler are commercial products with free licensing options for academic users. Each package has its pros and cons. OPNET Modeler was chosen as the modeling and simulation software tool for its powerful modeling capabilities, easy-to-use graphical interface, comprehensive library of open-source models, and commercial-quality documentation and support. (For simplicity, OPNET Modeler will be called Modeler from this point on.)

4.2 THE MODELER ENVIRONMENT

Modeler employs a hierarchical, project-and-scenario approach to modeling networks. A scenario is a single instance of a network, typically representing a unique network configuration, which can include aspects such as

topology, protocols, applications, traffic settings, etc. A project is a collection of scenarios, with each scenario exploring a different aspect of network design.

On the top hierarchical level of a scenario is a network model, on which simulations are run. A network model is essentially comprised of nodes, which may be connected to each other by links. Nodes are represented by icons, and links are represented by lines (wireless links are invisible). An example network model is shown in Figure 4.1. It consists of twelve workstations, one hub and one switch, which are interconnected by 10BaseT cables.

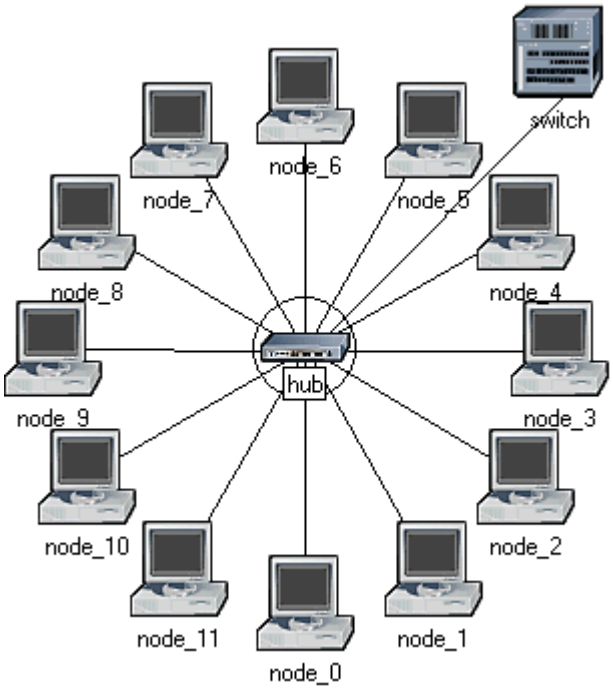

Figure 4.1 A sample network model in Modeler.

On the next level, each node model is made up of its basic building blocks – modules. Modules include processors, queues, transceivers, and generators. Different modules within a node model are connected by packet wires (solid lines) and statistic wires (dashed lines), as shown in Figure 4.2.

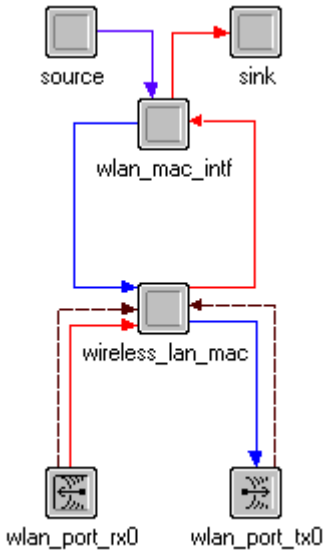

Figure 4.2 A sample node model in Modeler.

The functions of each module are described by a process model, taking the form of a finite state machine (FSM). The states in an FSM are represented by red and green plates, connected to each other by transition lines. A red plate indicates that it is an unforced state, which allows a pause during the execution; while a green one indicates a forced state not allowing a pause. An FSM is shown in Figure 4.3.

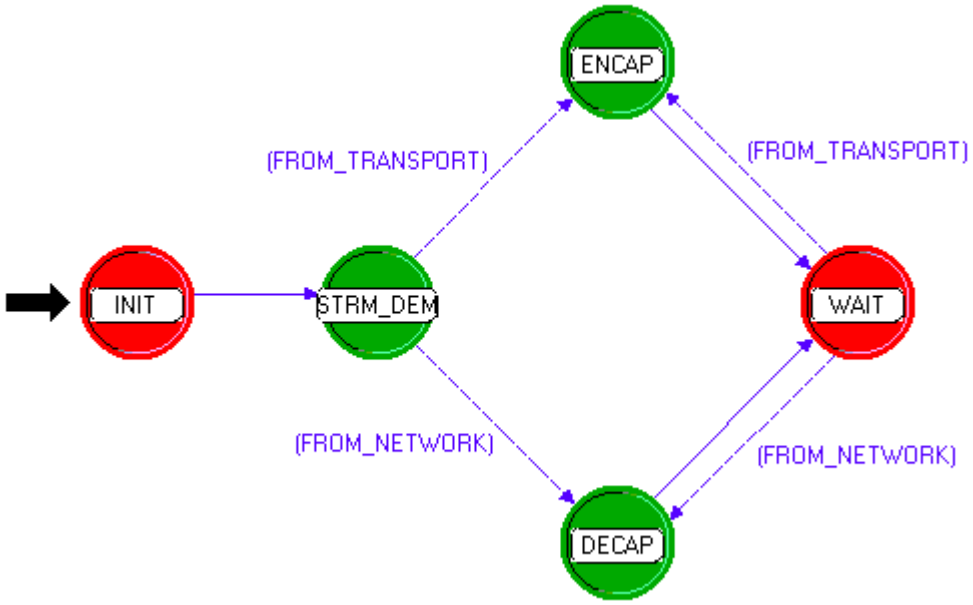

Figure 4.3 A sample process model in Modeler.

On the bottom level of the Modeler hierarchy lies the C/C++ code that describes the behavior of each state. The C/C++ statements are either Enter Executives or Exit Executives. Enter Executives are invoked on entering a state, while Exit Executives are invoked before exiting a state. Figure 4.4 shows a snapshot of the editor window for an example Enter Executives block.

Modeler is released with an extensive built-in library of models for common networks, equipment and protocols. In addition, processors and queues are set to be fully programmable to accommodate the creation of custom models.

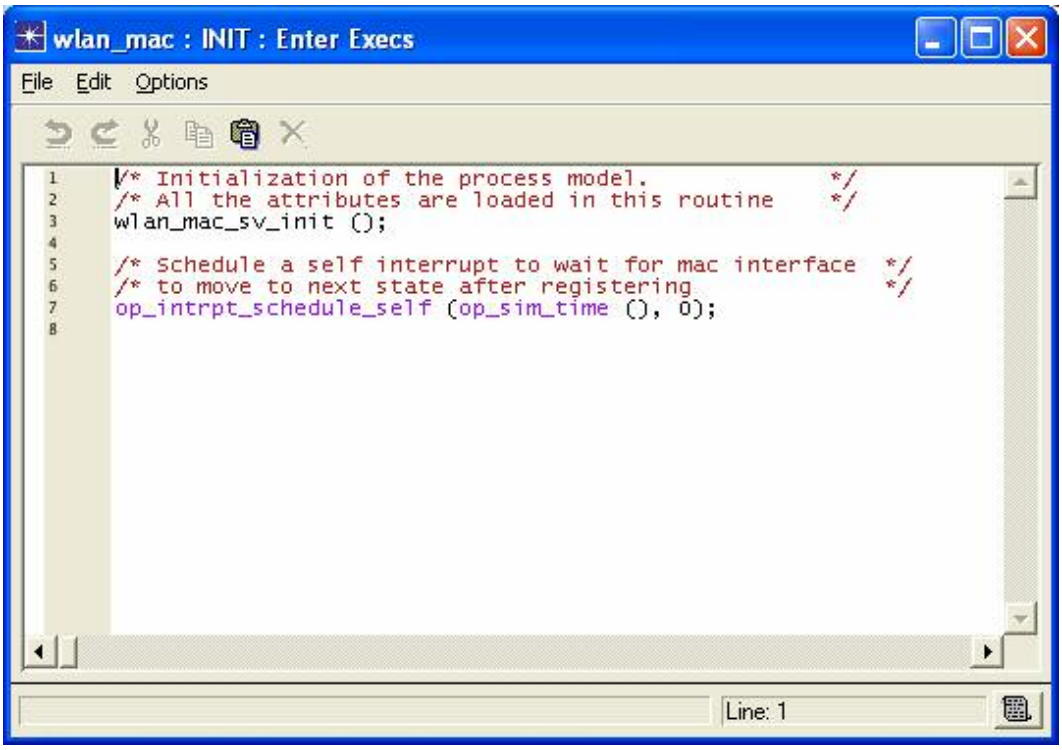

Figure 4.4 Modeler's C/C++ code editor.

4.3 MODELING FSO LINKS

The primary obstacle faced during the modeling process is explained below:

FSO links are, by nature, point to point. However, Modeler does not allow mobile nodes to be connected by point-to-point links. (In fact, none of the software packages mentioned in Section 4.1 allows this functionality.) Point-to-point links, which represent wires and optical fibers in the physical world, only support stationary nodes, while mobile nodes are only supported in the wireless

propagation environment, in which communication links are inherently broadcasting. This means that the physical layer of the proposed FSO MANET cannot be properly represented if such limitations are not lifted or circumvented.

To get around this problem, a concept of using a combination of the wireless propagation environment and directional antennas was proposed. Theoretically, such a concept can be justified, as laser beams and RF signals are both electromagnetic waves with the same propagation velocity in air. The Modeler wireless propagation model defaults to the LOS model, which is suitable for FSO applications. Directional antennas can be programmed to be dynamically steerable, which will be used to simulate the movements of FSO transceivers.

In order to verify the validity of this concept, a simple test project is designed.

4.3.1 Network Model

The network model in the test project is made up of two transmitter nodes (tx and tx2) and one receiver node (rx), as shown in Figure 4.5.

The initial positions of rx, tx, and tx2 are (4.0, 3.0), (3.0, 3.0), and (2.5, 3.0) (unit: km), respectively. All three nodes are mobile, and each follows its own trajectory. The trajectory parameters for rx, tx, and tx2 are listed in Table 4.1 (A), (B), and (C), respectively.

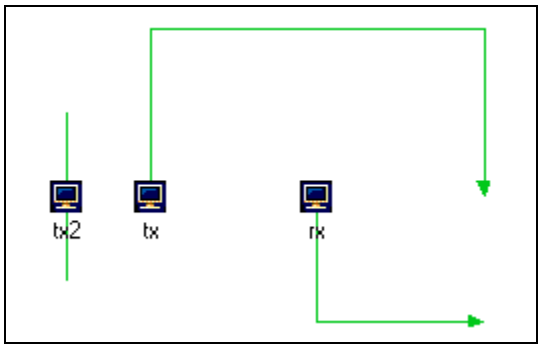

Figure 4.5 A simple test network.

Seg-ment	X Pos (km)	Y Pos (km)	Distance (m)	Traverse Time (s)	Speed (km/hr)	Wait Time (s)	Accum. Time (s)
1	4.0	3.0	0	n/a	n/a	60	60
2	4.0	3.75	750	60	45	0	120
3	5.0	3.75	1000	120	30	0	240

(A)

Seg-ment	X Pos (km)	Y Pos (km)	Distance (m)	Traverse Time (s)	Speed (km/hr)	Wait Time (s)	Accum. Time (s)
1	3.0	3.0	0	n/a	n/a	20	20
2	3.0	2.0	1000	60	60	0	80
3	5.0	2.0	2000	100	72	0	180
4	5.0	3.0	1000	60	30	0	240

(B)

Seg-ment	X Pos (km)	Y Pos (km)	Distance (m)	Traverse Time (s)	Speed (km/hr)	Wait Time (s)	Accum. Time (s)
1	2.5	3.0	0	n/a	n/a	60	60
2	2.5	2.5	500	60	30	0	120
3	2.5	3.5	1000	60	60	0	180
4	2.5	3.0	500	60	30	0	240

(C)

Table 4.1 Trajectory parameters (A: rx; B: tx; C: tx2) for the network of Fig. 4.5.

At the start of the simulation, all three nodes wait at their respective initial positions (rx for 20 seconds, tx for 60 seconds, and tx2 for 60 seconds) before they start moving along their respective trajectory. The receiver node, rx, has an L-shaped trajectory; the first transmitter node, tx, has an n-shaped trajectory and is intended to transmit useful data; and the second transmitter node, tx2, just moves back and forth along a straight line, providing interference.

4.3.2 Node Models

Each of the transmitter nodes (tx and tx2 in Figure 4.5) consists of a packet generator module "tx_gen", a radio transmitter module "radio_tx" (which simulates a modulated laser source in an actual FSO transmitter), a directional antenna module "ant_tx", and an antenna steering module "ant_point". The transmitter node architecture is shown in Figure 4.6.

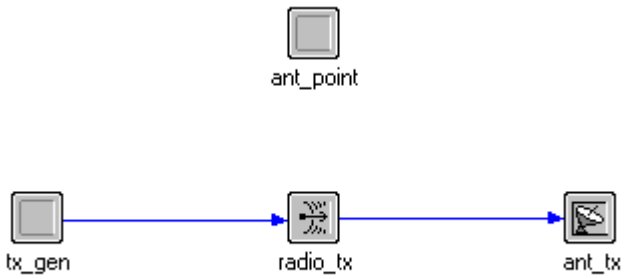

Figure 4.6 The architecture of the transmitter nodes.

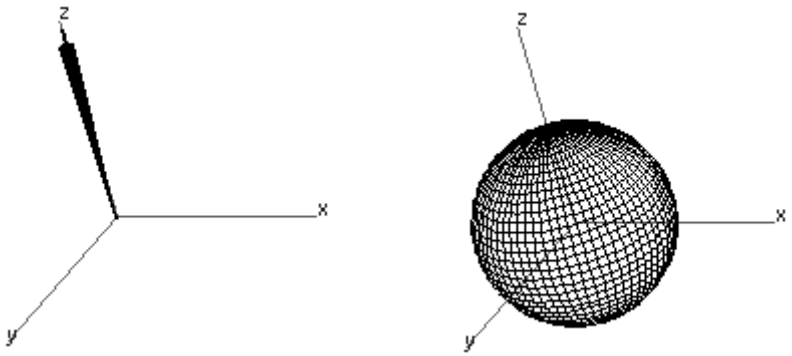

(A) (B)

Figure 4.7 Antenna patterns (A – directional; B – omnidirectional).

The packet generator for both tx and tx2 generates one packet of 100 megabits every 30 seconds. The data rate of the radio transmitter module for both tx and tx2 is set at 100 Mbit/s. The antenna used in both tx and tx2 is directional, with a gain of about 200 dB in one direction (a 1-degree field of view, or FOV) and 0 dB in all other directions. The antenna pattern is illustrated in Figure 4.7(A). Figure 4.7(B) shows the omnidirectional antenna pattern for comparison purposes.

In the case of tx, its antenna will have to be dynamically pointed to follow rx; in the case of tx2, its antenna will be pointed at rx at the start of the simulation, and will retain its absolute direction during the course of the simulation.

The receiver node (rx in Figure 4.5) measures the quality of the signal it receives. It consists of an antenna module “ant_rx”, a radio receiver module “radio_rx” (which simulates the photodetector in an actual FSO receiver), a data sink module “rx_sink”, and an antenna pointing module “rx_point”, as shown in

Figure 4.8. The receiver antenna is the same as the ones used on both transmitters (see Figure 4.7(A)).

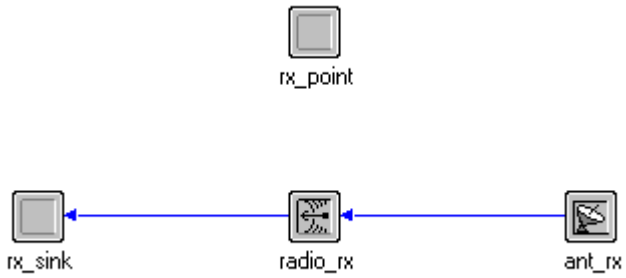

Figure 4.8 The architecture of the receiver node.

The communications channel in this test setup is set at 50 GHz, which is in the infrared spectral range. Therefore, each data link established in the simulation can properly represent a point-to-point optical link.

The antenna pointing module of rx has to provide continuous adjustments to the direction of its antenna, as does the pointing module of tx.

The function of the antenna pointing modules is explained below:

First, it acquires the local position of its target (from the point of view of rx, it is tx, and vice versa), converts the position information into global coordinates, and sets the antenna to the direction of the target; then, after a time period of t seconds, it needs to repeat the actions of acquiring, converting and

directing to ensure that the antenna does not lose track of its target. The calculation of a suitable value for t is illustrated in Figure 4.9.

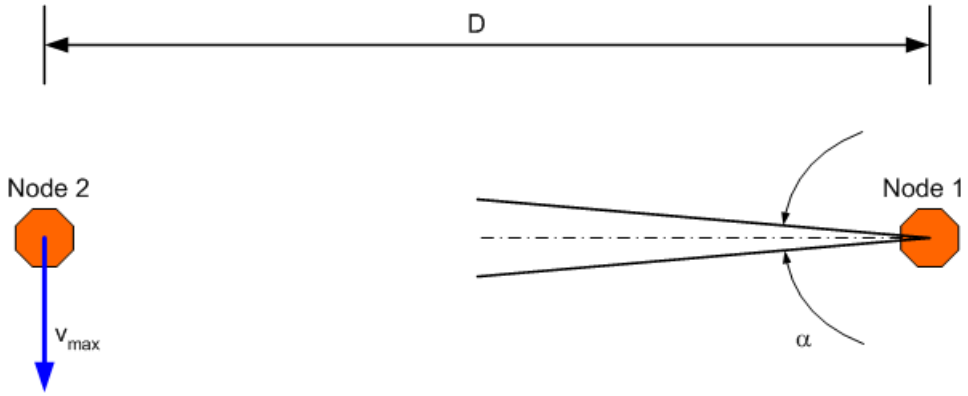

Figure 4.9 Calculation of the re-point timer t.

In Figure 4.9, D (m) represents the distance between the two nodes; v_{max} (m/s) represents the maximum velocity of Node 2 with respect to Node 1, in the perpendicular direction of the link between the two nodes; and α (rad) is the FOV of the antenna. In order to ensure that Node 2 does not escape the FOV of Node 1 before Node 1 re-points its antenna, the re-point timer t must satisfy

$$t \le \frac{D \cdot \frac{\alpha}{2}}{v_{max}} \tag{4.1}$$

In the simulation setup, D is calculated using the position information, α is set to be 1 degree, or 0.01745 rad, and v_{max} is assumed to be 100 km/hr, or about 28 m/s.

4.3.3 Simulation Results

After running the simulation, the following statistics were obtained at the receiver: bit error rate (BER), signal-to-noise ratio (SNR), and throughput. Figures 4.10 through 4.12 provide plots of these statistics.

The results shown in the figures agree with the expectations. Take the BER (Figure 4.10), for example, where in the initial stage it reached as high as 0.006 due to the waiting periods observed by all three nodes, when the receiver antenna was pointed at both tx and tx2. After tx started moving and the three nodes were no longer along a straight line, however, the BER dropped to zero and remained so until the end of the simulation. Similar justifications can be made to the graphs for SNR and throughput.

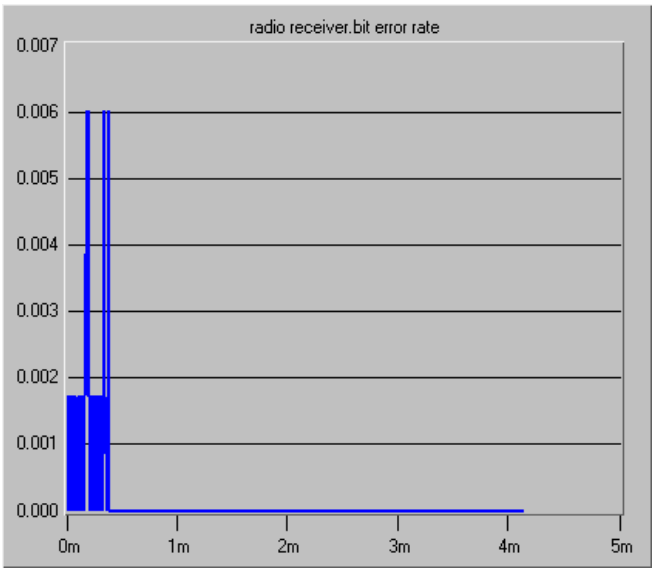

Figure 4.10 Bit error rate in the received data.

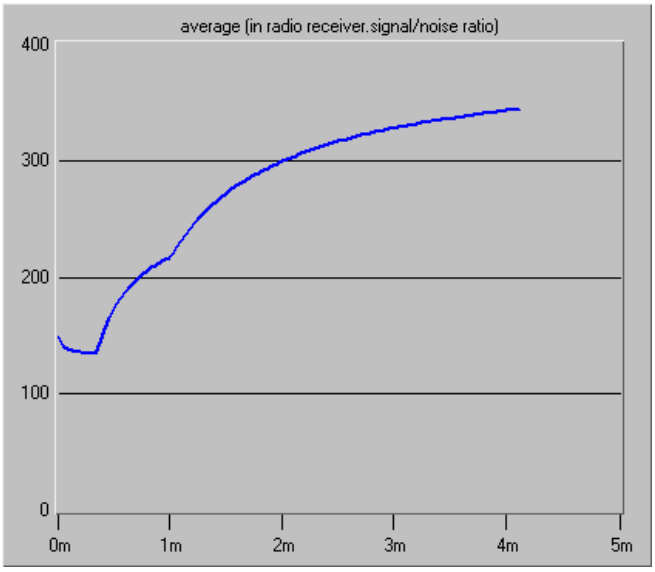

Figure 4.11 Signal-to-noise ratio of received signals.

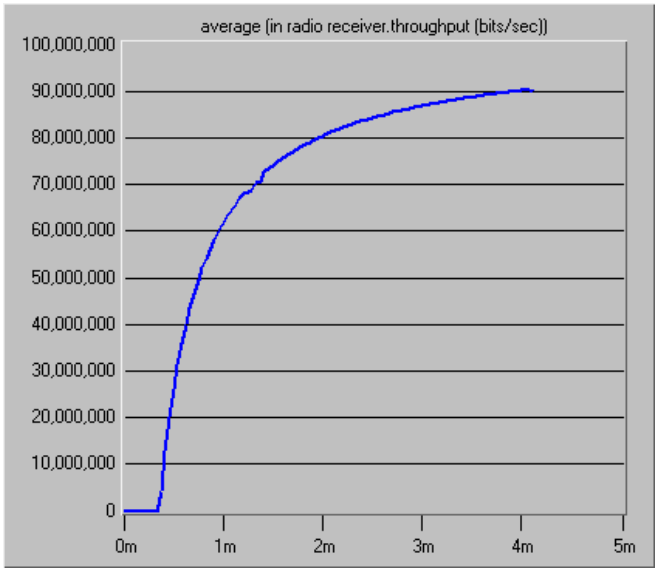

Figure 4.12 The throughput (bits/sec) of rx.

4.4 CONCLUSIONS

Based on the investigations reported in the previous sections of this chapter, the following conclusions can be drawn:

- The built-in wireless propagation environment of Modeler and directional antennas can be combined to model point-to-point FSO links;
- The automatic tracking of FSO links required by MANET operations can be modeled by dynamically pointing directional antennas;
- Modeler is a suitable software tool for the research project of this dissertation. The modeling of the proposed FSO MANET will follow the hierarchical methodology employed by Modeler.

CHAPTER 5 - A SIMPLIFIED MODEL

This chapter reports preliminary efforts on the modeling of the proposed FSO MANET.

As mentioned in the previous chapters, it is unrealistic to have a pure FSO MANET because of the point-to-point nature of FSO communications. For example, if a source node S needs to establish a data route to a destination node D, it has to have knowledge of the geographic position of D (and possibly of additional relay nodes R1, R2, etc.) so that it can steer its optical transmitter to the direction of the vicinity of D in search of D's receiver. Without the convenience of the broadcasting service offered by RF communications, the dissemination of dynamically changing position information among all the mobile nodes in a network is extremely difficult if not impossible. Nevertheless, FSO is an attractive enhancement to the existing RF MANETs because of its high bandwidth, interference-free operation, and intrinsically excellent security. Therefore, the realistic goal is to make an additional FSO module serve as an enhancement to the original RF communication nodes.

In this initial study, emphasis was put on the operation of the FSO module. The RF module was not included in the models presented in this chapter. Since Modeler offers open-source MANET models operating in the RF domain, it would not require an unreasonable amount of effort to include the RF module in later models.

5.1 ASSUMPTIONS

The following assumptions were made for the models presented in this chapter:

1. Each node has means (such as via GPS) to obtain its own position information;
2. Such information can be reliably distributed in the network via normal RF operations in a timely fashion;
3. LOS exists between any two nodes, and weather conditions are uniform and unchanging throughout the network. In other words, the only physical constraint on whether an FSO link can be established is the distance between the transmitter and the receiver.

5.2 SIMULATION MODELS

This section will discuss the architectures of the network, node, and process models involved in the simulation project presented in this chapter.

There are two node types in the network, namely “terminal” and “relay”. A terminal node is one that has full functionality and can serve as both a data source and a destination. A relay node does not generate or sink data packets. It only forwards packets at the request of their source nodes.

The architecture of a terminal node is shown in Figure 5.1.

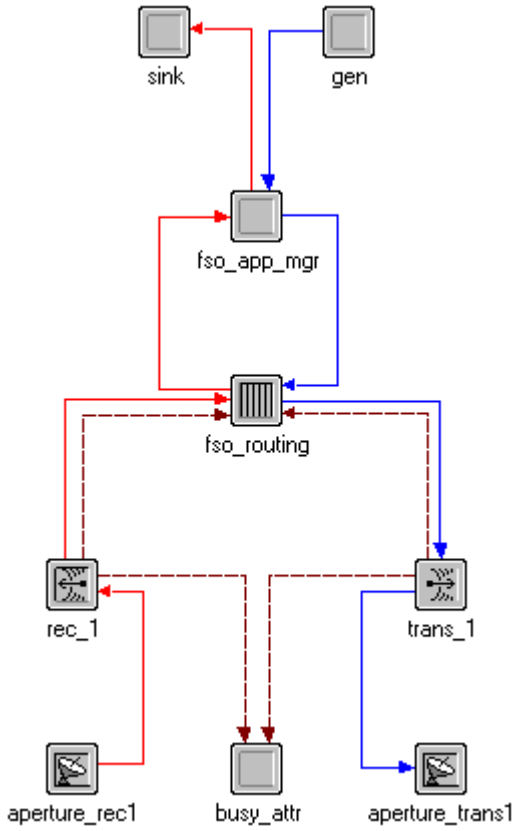

Figure 5.1Terminal node architecture.

The node consists of several modules connected by stream wires (solid lines) and statistic wires (dashed lines). The modules include: optical apertures (antennas) of the receiver and transmitter ("aperture_rec1" and "aperture_trans1", respectively); optical receiver and transmitter ("rec_1" and "trans_1", respectively); a routing module ("fso_routing"); an application manager module ("fso_app_mgr"); a signal generator ("gen"); a data sink ("sink"); and a module managing the "busy" attribute of the node's linkhead ("busy_attr").

Among the modules listed above, the antennas, the optical receiver and transmitter, the signal generator, and the data sink are built-in modules of Modeler; the others were designed specifically for this simulation project. In terms of source code openness, processors (represented by plain boxes) and queues (represented by striped boxes), i.e., the generator, the sink, the application manager, the router, and the busy-attribute manager, are fully programmable.

The functions of all modules except "fso_app_mgr", "fso_routing", and "busy_attr" are straightforward, and therefore are not explained in detail here.

The process model for the "fso_app_mgr" module is illustrated in Figure 5.2.

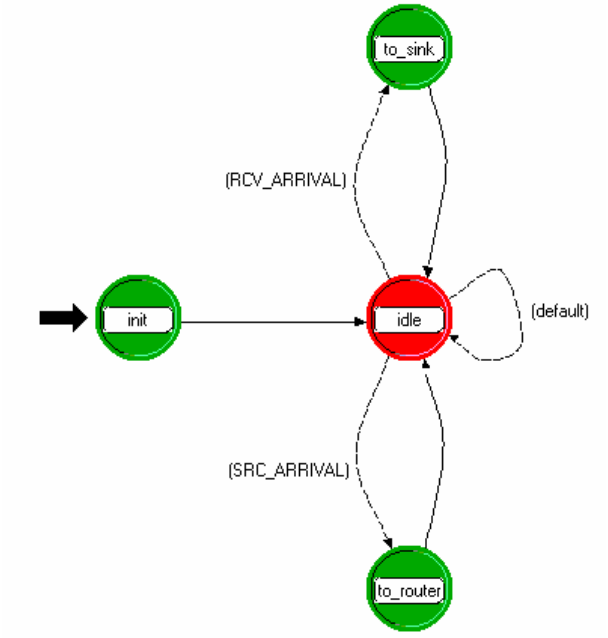

Figure 5.2 The "fso_app_mgr" process model.

The function of this module is to decide whether a packet arriving at it was from the upper layer (the signal generator), or the lower layer (the routing layer). If the former, i.e., the condition "SRC_ARRIVAL" is satisfied, the "to_router" state of this module randomly generates a destination address, writes it in the "destination address" field of the packet, and forwards the packet to the routing layer. If the latter, i.e., the condition "RCV_ARRIVAL" is satisfied, the "to_sink" state reads the content of the packet, performs computations for statistical purposes, and sends the packet to the upper layer to be sunk.

Figure 5.3 shows the process model for the "busy_attr" module.

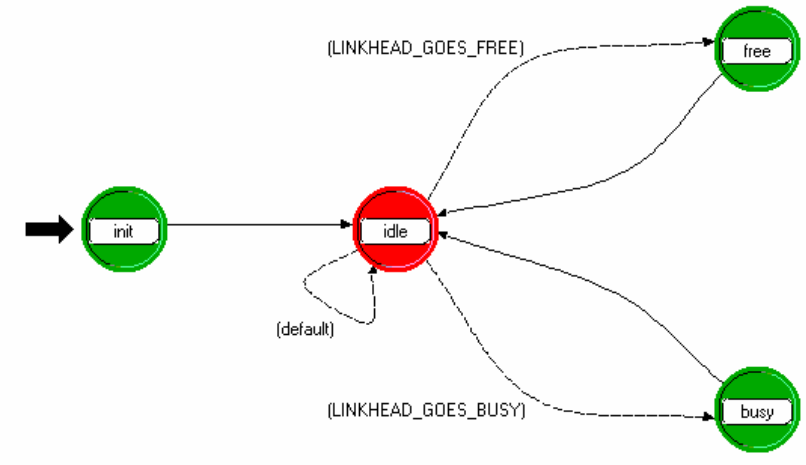

Figure 5.3 The "busy_attr" process model.

The "busy_attr" module is in charge of only one operation: it reads the "busy" status of the linkhead (the receiver and transmitter) through the statistic

wires; if the linkhead goes from “not busy” to “busy”, the module immediately sets the “busy” attribute of the node to “TRUE”. The attribute is set to “FALSE” when the linkhead goes from “busy” to “not busy”. This attribute is used by the routing module to help determine if a packet can be transmitted to its destination node (explained in detail later).

The routing module “fso_routing” is the core module of the simulation model. It performs packet-based source routing for data that is to be transmitted to another node. It also routes all received packets to the upper layer (the application manager). The process model for the routing module is shown in Figure 5.4.

The simple source routing algorithm that is implemented in this initial study works as follows:

After initialization, the module waits for packet arrivals. If a packet arrives from the upper layer, the routing module first checks if the self linkhead is busy. If yes, it queues the packet for later transmission; if no, it extracts the destination address from the content of the packet, and checks if the destination linkhead is busy. If it is busy, the algorithm queues the packet and waits a random back-off period before it checks the destination again. If the destination is not busy, the routing module then checks the distance between the self node and the destination node to see if it is within a predetermined transmission range. If yes, it steers the linkhead toward the destination and forwards the packet to the optical transmitter to be sent to the destination. If no, it checks if the dedicated common relay node

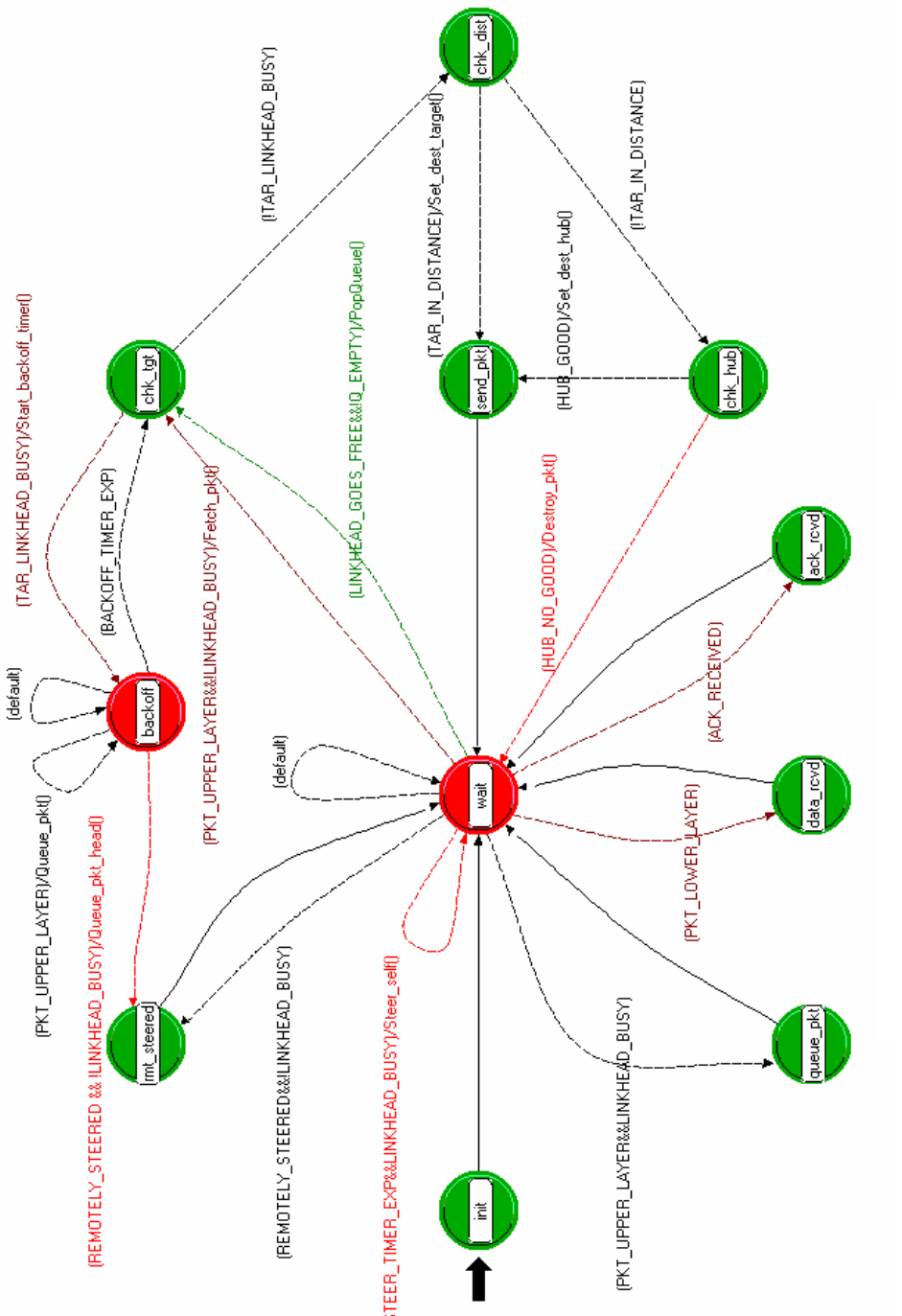

Figure 5.4 The "fso_routing" process model

in the network (“hub”) is free and if the hub is within transmission range of both the self node and the destination node. If yes, the algorithm notifies both the hub and destination, and sends the packet to the hub, which will relay it to the destination; if the answer is “no” to either question, the packet is considered undeliverable and destroyed.

If a packet arrives from the lower layer, the routing module simply sends out an acknowledgment to the data source node and forwards the packet to the upper layer.

The architecture of the relay node, which is shown in Figure 5.5, is similar to that of the terminal node, except that there is no signal generator, sink, or application manager module.

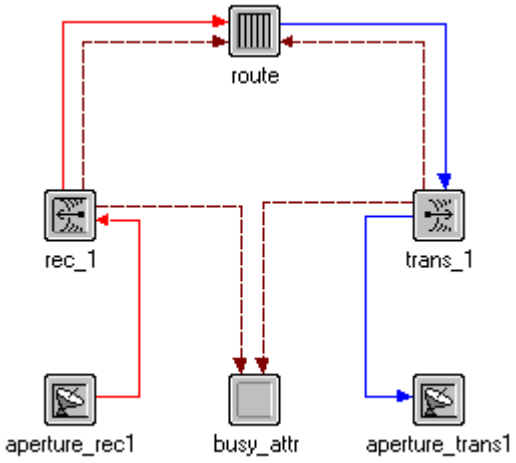

Figure 5.5 Relay node architecture.

The simple network model in which the FSO routing algorithm was simulated is shown in Figure 5.6. It consists of four (4) terminal nodes and one (1) relay node. Each node follows its own trajectory (arrowed lines). The packet inter-arrival time at the generator module of each terminal node follows a normal distribution of a 5-second mean and 3-second variance. The size of each packet is set as 100 megabits, and the optical transmission bandwidth is set as 100 Mbit/s. The simulation runs for 60 seconds, which is also the time for each node to complete its own trajectory. The initial coordinates of the nodes, in kilometers, are (1.5, 1.5), (3.5, 1.5), (3.5, 3.5), (1.5, 3.5), and (2.5, 2.5), for "node_0" through "node_3" and "relay", respectively.

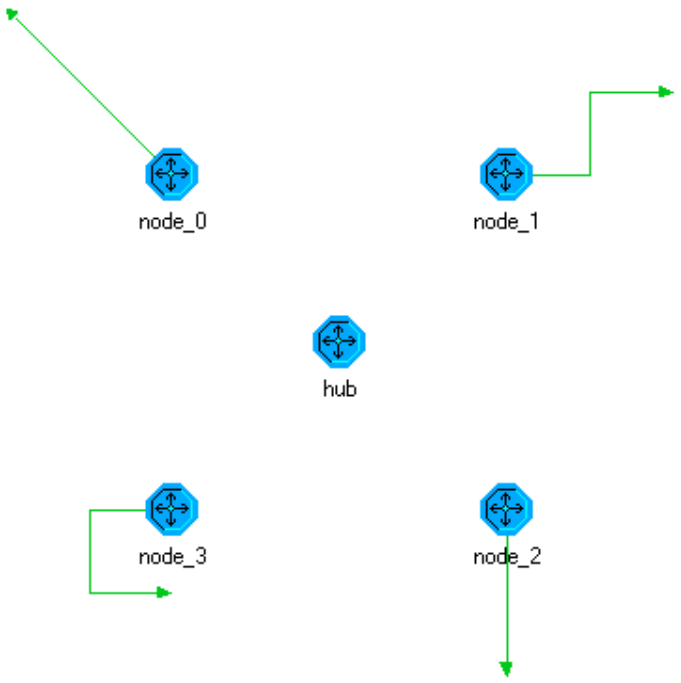

Figure 5.6 The network model.

5.3 SIMULATION RESULTS

The following results were obtained by running the simulation in Modeler:

5.3.1 End-To-End (ETE) Delay

The ETE delay of a packet is the time period between its creation at the source node and its reception at the destination node. The average ETE delay for all received packets against simulation time, in seconds, is shown in Figure 5.7. From the graph, we see that the values of ETE delay in our experimental setup fall between 1.0 second and 1.5 seconds, with a mean value of about 1.3 seconds.

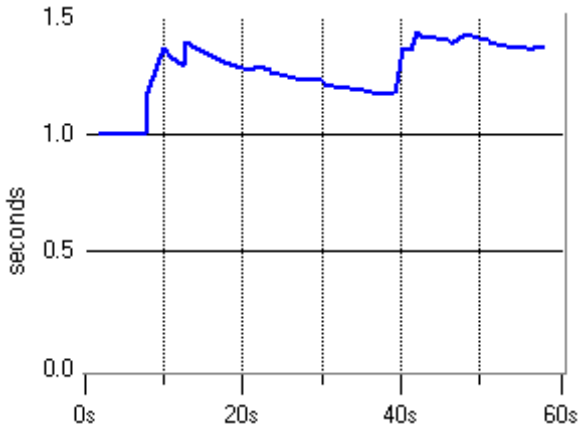

Figure 5.7 ETE delay.

5.3.2 Packets Generated vs. Packets Received

Figure 5.8 displays the number of packets generated by all the signal generators in the network. Figure 5.9 shows the number of packets received by

the receivers. The two curves are similar, thus proving that most packets successfully reached their destinations.

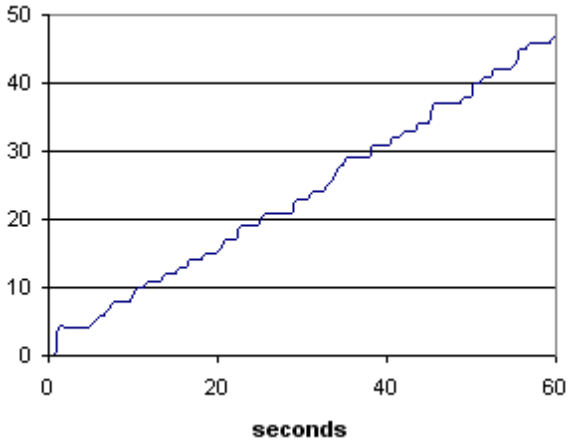

Figure 5.8 Packets generated.

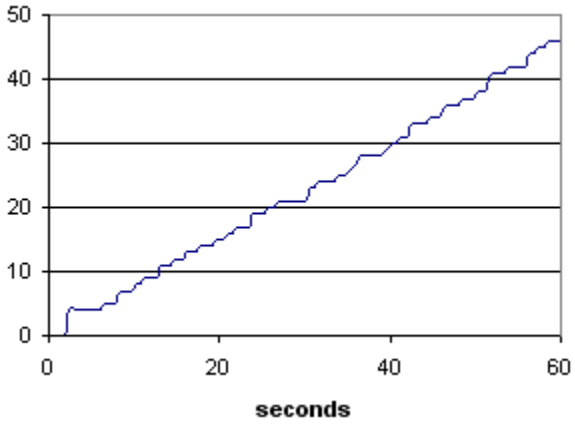

Figure 5.9 Packets received.

5.3.3 Utilization of Receivers

Figure 5.10 shows the as-is values of utilization of the optical receiver of each terminal node. The average values of the same data are shown in Figure 5.11. The converged value of the average utilization for all nodes is around 20%, which is expected as the mean value of the packet inter-arrival time at each signal generator is 5 seconds, and it takes a 100Mb/s channel one second to transmit a 100Mb packet.

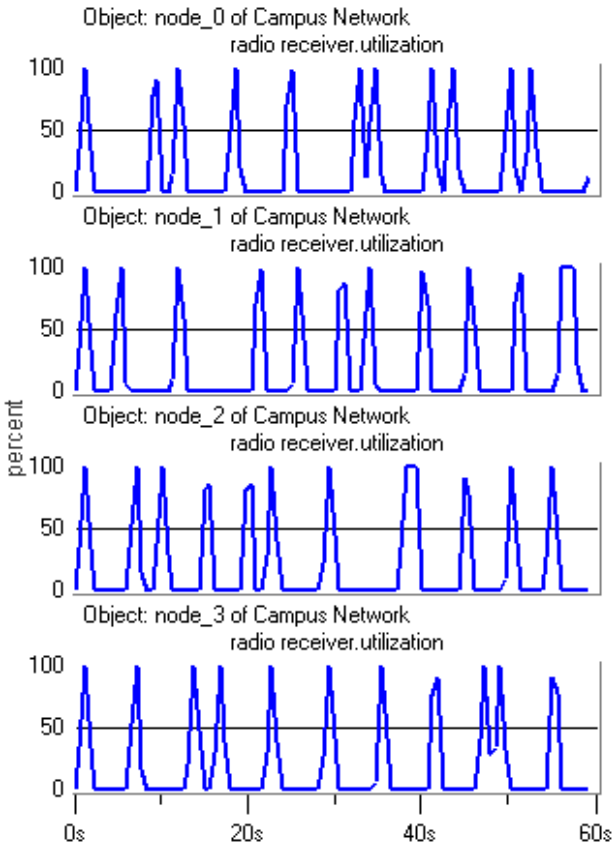

Figure 5.10 Receiver utilization (as is).

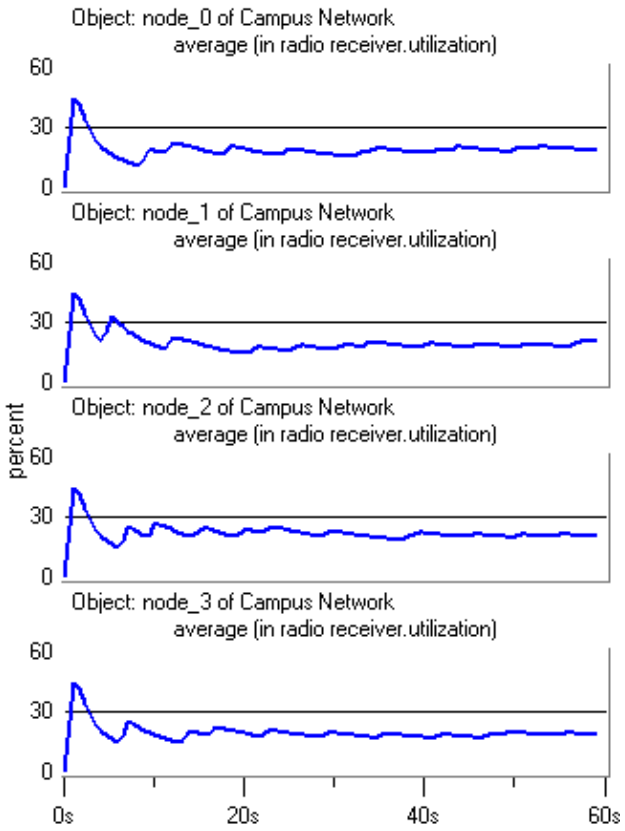

Figure 5.11 Receiver utilization (average).

5.4 CONCLUSIONS

As the preliminary simulation results have shown, Modeler is a suitable tool for the modeling and simulation of such hybrid networks. The proposed enhancement to an RF MANET by introducing an FSO module is viable, and the resulting network sustainable.

Major limitations of the simplified model presented in this chapter include:

1. Attributes of each node in the network, including position, busy status, etc., are made available to other nodes by means of the so-called "internal modal access (IMA)" tools provided by Modeler. In order to simulate the network more realistically, the attribute data should be exchanged via RF operations. An RF module will be introduced to each node in an improved model.
2. The node mobility model is very simple, in which each node follows a predefined trajectory. It needs to be re-designed to introduce random motion in order to mimic behaviors of mobile nodes in a physical network.

To address these limitations, improved models will be presented in the next two chapters. Specifically, Chapter 6 will introduce models for FSO-enhanced IEEE 802.11 ad hoc networks, where RF communications between any two nodes are single-hop only, and Chapter 7 will discuss FSO enhancement to multi-hop RF MANETs.

CHAPTER 6 - WLAN ENHANCED WITH FSO

A Wireless LAN (WLAN) is a local area network that uses RF signals to communicate between devices. Due to the increasingly prevalent demand for mobile computing, WLANs are becoming more and more popular and have been widely accepted as a good alternative to wired LANs. In a rapidly growing number of cases, WLAN is favored over wired LAN as the first choice in deploying communication networks in local area scenarios.

This chapter will begin with an overview of the WLAN technology, including its benefits and shortcomings. The modeling of a WLAN enhanced with FSO will follow. The performance of such networks will then be evaluated based on simulation results.

6.1 OVERVIEW OF WLAN [95]

The technical standards that define WLAN technologies are developed by the IEEE LAN/MAN Standards Committee (IEEE 802), working group 11. The trade group Wi-Fi Alliance [96], currently consisting of more than 250 member companies, serves to perform testing, certify interoperability of products, and promote the WLAN technology. The commonly seen "Wi-Fi" logo is carried by Wi-Fi Alliance-certified equipment. Therefore, the terms WLAN, Wi-Fi, and IEEE 802.11, or simply 802.11, are interchangeable in most cases.

The 802.11 family of standards focuses on specifications in the medium access control (MAC) and physical (PHY) layers of a wireless device, which correspond to Layers 1 and 2 of the seven-layer OSI model [97], or Layer 1 of the four-layer DoD model [98].

There are mainly three WLAN protocols in operation today, namely 802.11b, 802.11a, and 802.11g. The 802.11b protocol employs a spread-spectrum technique called direct-sequence spread spectrum (DSSS) to achieve a maximum raw data rate of 11 Mbit/s, while 802.11a and 802.11g use a modulation scheme named orthogonal frequency-division multiplexing (OFDM), and have a maximum data rate of 54 Mbit/s. The carrier frequency is 2.4 GHz for 802.11b and 802.11g, and 5 GHz for 802.11a.

In a WLAN, the set of all wireless devices ("stations") that can communicate with each other form a Basic Service Set (BSS). If a BSS contains an access point (AP), through which the stations can access network resources outside of the BSS, it is called an infrastructure BSS. If there is no AP in a BSS and the stations operate in ad hoc mode, the BSS is called an independent BSS. The acronym "IBSS" refers to the latter. With the help of a distribution system, usually in the form of wired LAN, a number of BSS can establish an Extended Service Set (ESS) to accommodate a larger network.

WLANs have many advantages over wired LANs, such as mobility support, affordability, fast and scalable deployment, and better disaster

survivability. Its major disadvantage, intrinsically determined by the physical characteristics of RF communications, is its relatively low bandwidth, which is just a fraction of the typical bandwidth offered by optical communications.

It is therefore proposed that a FSO module be added to a typical WLAN node so that the throughput of the network will be vastly improved. The next section will study the proposal in detail via the means of OPNET modeling.

6.2 SIMULATION MODELS

This section presents OPNET models developed to study the integration of a FSO module into a typical WLAN node, which already contains an RF module.

Within each node, the RF module is responsible for the network-wide dissemination of information needed by the FSO routing algorithm. Such information includes the geographic location of the node and the availability (busy status) of its FSO linkhead. Bulk data is delivered solely by the FSO module. The first and third assumption listed in Section 5.1 still hold true for models presented in this chapter.

As a starting point, the WLAN node provided by the OPNET Modeler software package ("wlan_station_adv") is presented in Figure 6.1. Its lower layer (PHY and MAC) consists of a radio transmitter ("wlan_port_tx0"), a radio receiver ("wlan_port_rx0"), and a MAC algorithm module ("wireless_lan_mac"). Its upper layer (application) is represented by a packet generator ("source") and a

data sink (“sink”). An interface module (“wlan_mac_intf”) links the upper layer and lower layer.

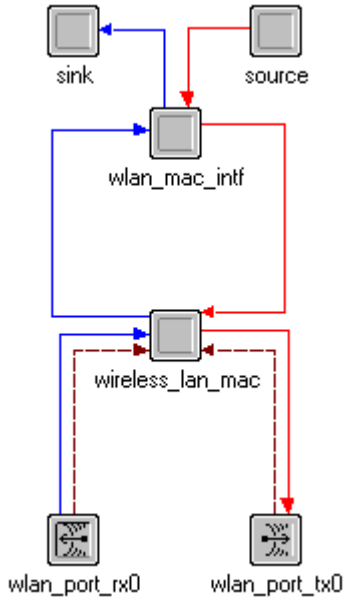

Figure 6.1 The built-in WLAN node.

The MAC module plays the most important role in defining the behaviors of the node. Detailed discussion on the module’s internal mechanism is beyond the scope of this dissertation. It suffices to note that it is developed conforming to the IEEE 802.11 standards and implements a Carrier-Sense Multiple Access with Collision Avoidance (CSMA/CA) algorithm as the protocol for medium access.

In the hybrid node model developed for this dissertation, the lower layer of the built-in WLAN node was retained, the higher layer discarded, and the interface component modified to suit the need of the added FSO module. Components similar to those introduced in Chapter 5, which comprise the FSO module, were added to the RF (WLAN) module. The architecture of the hybrid node is presented in Figure 6.2.

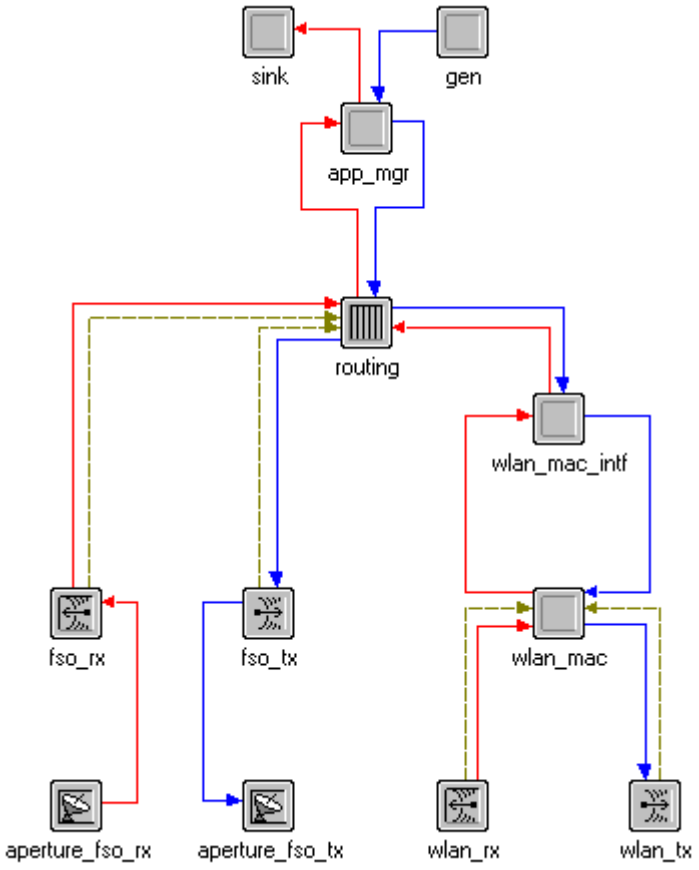

Figure 6.2 The FSO-enhanced WLAN node.

The basic work flow of the node shown above is explained as follows:

At the source node, the application manager ("app_mgr") passes down the bulk data packet generated by the packet source ("gen"). The routing algorithm ("routing") fills in the destination address, creates a probe packet with the same destination address and sends the probe packet out through the RF module, which operates in WLAN's IBSS mode. At the destination node, the RF module receives the probe and passes it up to the routing layer. If the FSO linkhead of the destination node is idle, its routing layer generates a reply packet containing the coordinates of the destination node and sends it back to the source node, via RF operations. The source node then extracts the information embedded in the RF reply packet and uses it to steer its FSO aperture and transmit the bulk data.

As their names indicate, the components of the FSO module, i.e. "gen", "sink", "app_mgr", "routing", "fso_rx", "fso_tx", "aperture_fso_rx", and "aperture_fso_tx", have similar functions to those constituting the simplified model presented in Chapter 5 (see Figure 5.1). Major changes made include:

1. In the hybrid model, the application manager "app_mgr" no longer fills the field for destination address in the FSO packet. Instead, this task is now assigned to the routing layer due to a minor technical issue (synchronization of initialization stages with the built-in WLAN models).

2. For conciseness in the layout of the node architecture, the "busy_attr" processor in the simplified model is removed, its functionality integrated into that of "routing".
3. Most importantly, the routing process is completely rewritten to coordinate the interaction between the RF module and the FSO module, which is explained in detail below.

The development of the new routing process was carried out with considerations to the following factors: interfacing between the FSO module and the built-in WLAN module, simulation of the FSO link acquisition process, and error handling.

In general, it is advisable for the development of complex process models to follow the Process Model Development Methodology, available in Modeler documentation [99]. The methodology lists seven stages of process model development:

1. Defining the system's context;
2. Process-level decomposition;
3. Enumeration of events;
4. State-level decomposition;
5. Developing the state transition diagram;
6. Specifying process actions; and
7. Selecting an initial state.

In practice, the seven stages can be roughly sorted into two phases: the phase of preparation (Stages 1~4) and the phase of actual development (Stages 5~7).

For the routing process model presented in this chapter, a Phase-1 investigation on planned system behavior suggested that the major states of the process model include the following: idle, reserved for transmission, reserved for reception, transmitting, and receiving. It is specifically worth noting that the two "reserved" states were used to put the FSO linkhead on hold in order for the RF signaling exchange to take place, and to simulate the link acquisition process by setting a delay timer.

Serving as a direct guide to Phase-2 tasks, the finished chart of event enumeration is presented in Table 6.1.

STATE	EVENT	CONDITION	ACTION	NEXT STATE
init	Power up			idle
idle	FSO packet arrival from upper layer		Parse packet; send RF probe to destination; set tx_reserve timer	tx_reserve
	FSO packet arrival from lower layer		Process packet; send packet to upper layer	idle
	RF probe received		Send RF ready reply; set acquisition timer; set rx_reserve timer	rx_reserve
	Default			idle

(Continued on next page)

STATE	EVENT	CONDITION	ACTION	NEXT STATE
tx_reserve	Destination RF ready reply received		Set acquisition timer; steer linkhead when timer expires; send FSO packet	transmitting
	Destination RF busy reply received	Queue empty	Parse packet; send RF probe to destination	tx_reserve
		Queue not empty	Queue packet; pop queue; parse popped packet; send RF probe to destination	tx_reserve
	TX_reserve timer expires (without receiving reply from destination)	Queue not empty	Queue packet; pop queue; parse popped packet; send RF probe to destination	tx_reserve
		Queue empty	Parse packet; send RF probe to destination; set tx_reserve timer;	tx_reserve
	FSO packet arrival from upper layer		Queue packet	tx_reserve
	FSO packet arrival from lower layer		Process packet;	tx_reserve
	Retry limit exceeded			idle
	Default			tx_reserve
transmitting	Steer timer expires	Linkhead busy	Re-steer linkhead	transmitting
	Linkhead goes free (which means data reception completed)	Queue not empty	Pop queue; parse packet; send RF probe to destination; set tx_reserve timer	tx_reserve
		Queue empty		idle
	RF probe received		Send RF busy reply	transmitting
	FSO packet arrival from upper layer		Queue packet	transmitting
	Default			transmitting

(Continued on next page)

STATE	EVENT	CONDITION	ACTION	NEXT STATE
rx_reserve	Acquisition timer expires (i.e. link is established)		Steer linkhead	rx_reserve
	Linkhead goes busy			receiving
	RX_reserve timer expires without receiving any FSO packets			idle
	FSO packet arrival from upper layer		Queue packet	rx_reserve
	Default			rx_reserve
receiving	Steer timer expires	Linkhead busy	Re-steer linkhead	receiving
	Linkhead goes free	Queue not empty	Pop queue; parse packet; send RF probe to destination; set tx_reserve timer	tx_reserve
		Queue empty		idle
	RF probe received		Send RF busy reply	receiving
	FSO packet arrival from upper layer		Queue packet	receiving
	FSO packet arrival from lower layer		Process packet;	receiving
	Default			receiving

Table 6.1 Routing layer event enumeration.

Based on the event enumeration chart above, the FSM implementation of the routing layer was developed, which is shown in Figure 6.3.

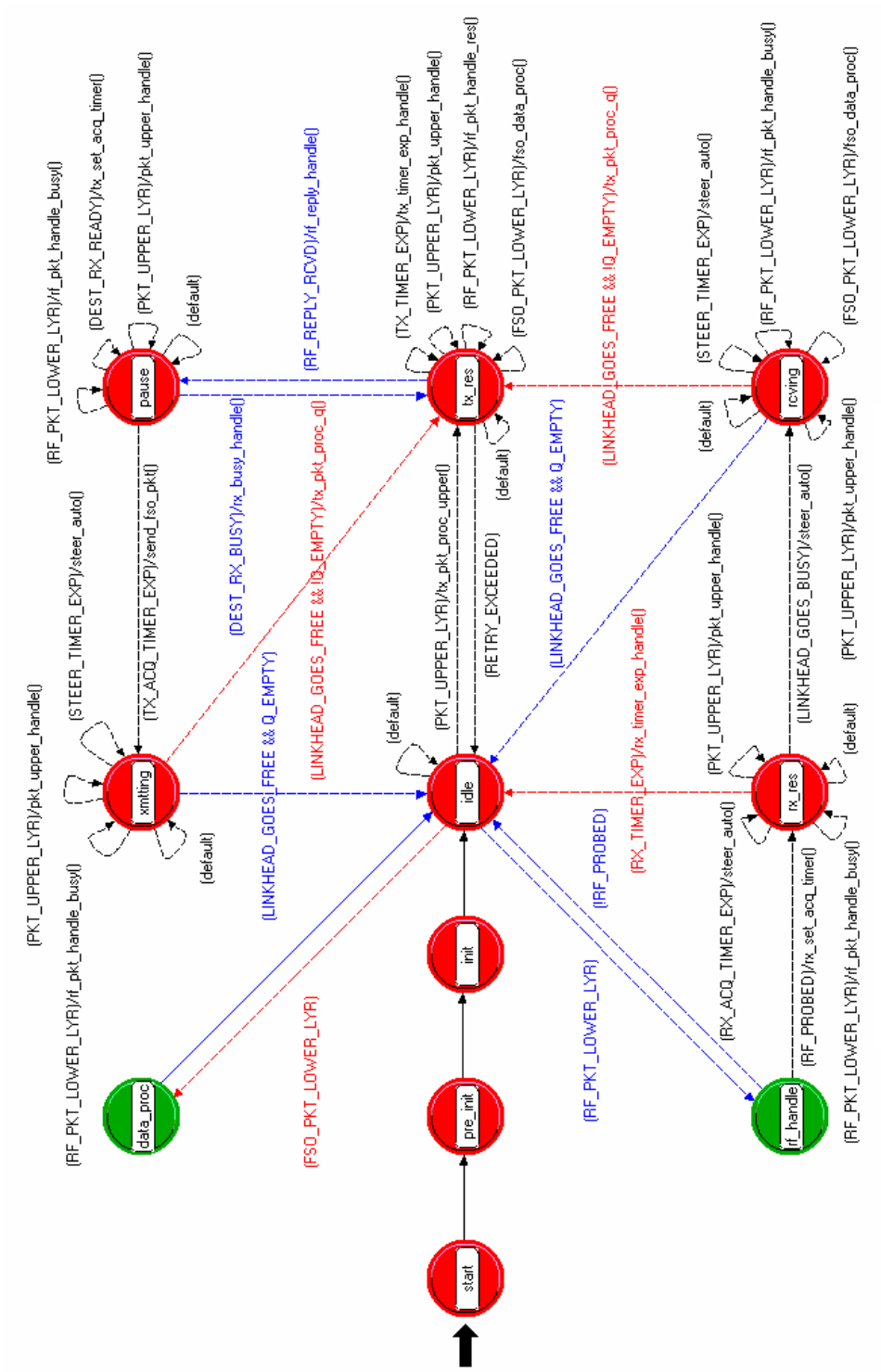

Figure 6.3 The routing process model.

Up to now, all components that make up the hybrid node shown in Figure 6.2 have been introduced. A model of a 200m×200m network consisting of several such nodes is depicted in Figure 6.4.

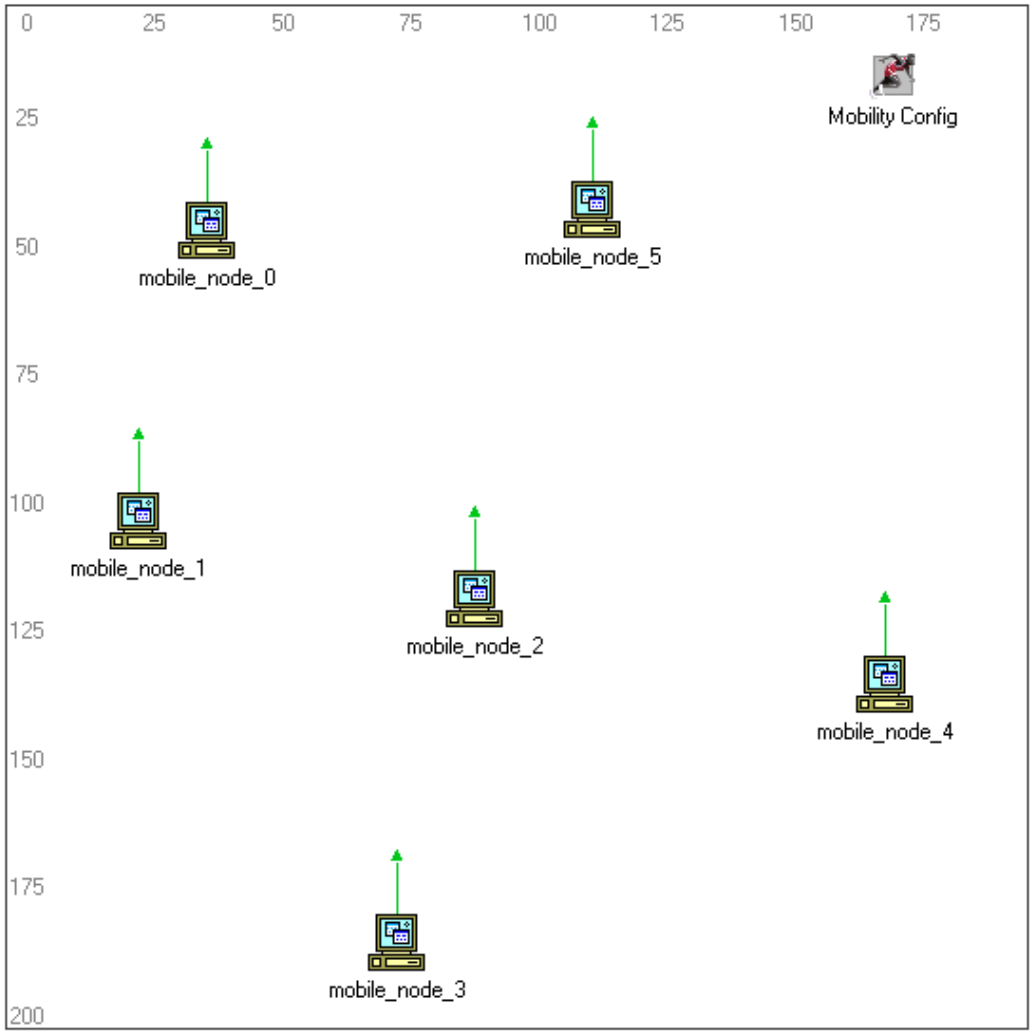

Figure 6.4 The network model.

The network contains an additional node called “Mobility Config”, which is not an actual communication node. Instead, it manages the movement of the communication nodes, which is determined by the so-called “random waypoint” mobility model. With this model present, each communication node can be randomly placed at any location within the network border without concern for its exact coordinates. During the simulation, a node with random waypoint mobility picks an arbitrary destination in the region of the network and moves towards it. When it arrives at the destination, it pauses before repeating the process by randomly selecting another destination. Parameters affecting the node movement, such as start time, speed, pause time, range, and stop time, can be configured with statistical distributions. Compared with the predefined trajectories employed by the simplified model in Chapter 5, the random waypoint model is a better representation of real-world scenarios.

6.3 SIMULATION RESULTS

For the purpose of studying the performance of the FSO-enhanced WLAN, several scenarios were created by modifying relevant parameters. This section will first present the baseline scenario, followed by perturbation scenarios.

Certain attributes have consistent values throughout all scenarios. These common settings are listed in Table 6.2.

Attribute Name		Value	Unit
Network size	X-span	200	m
	Y-span	200	m
Simulation time		400	s
FSO channel data rate		1.0E+9	bit/s
FSO carrier frequency		1.9355E+14 *	Hz
Simulated FSO link acquisition time		3.0	s
FSO receiver ECC threshold **		1.0E-7	-
FSO packet generator	Start time	Normal, μ=50.0, σ=15.0	s
	Stop time	350	s
Queue size for FSO packets		5	packets
Node mobility	Start time	10	s
	Stop time	End of simulation	-
RF operation mode		802.11b, IBSS	-

Table 6.2 Common simulation settings.

6.3.1 The Baseline Scenario

The specific settings for the baseline scenario are listed in Table 6.3.

Attribute Name	Value	Unit
Node count	6	-
Node speed	Uniform, min=5, max=10	m/s
FSO packet interarrival time	Normal, μ=100.0, σ=20.0	s
FSO packet bulk size	2.0E+8	bytes

Table 6.3 Simulation settings for the baseline scenario.

* This value corresponds to a wavelength of 1,550 nm, which is commonly used in FSO communications.

** This attribute is the highest proportion of bit errors allowed in a packet for the packet to be accepted by the receiver.

The results yielded by the simulation for the baseline scenario are discussed in detail in Section 6.3.1.1 through 6.3.1.4.

6.3.1.1 End-to-End Delay (RF)

Figure 6.5 shows the average ETE delay for all received RF probe and reply packets against simulation time.

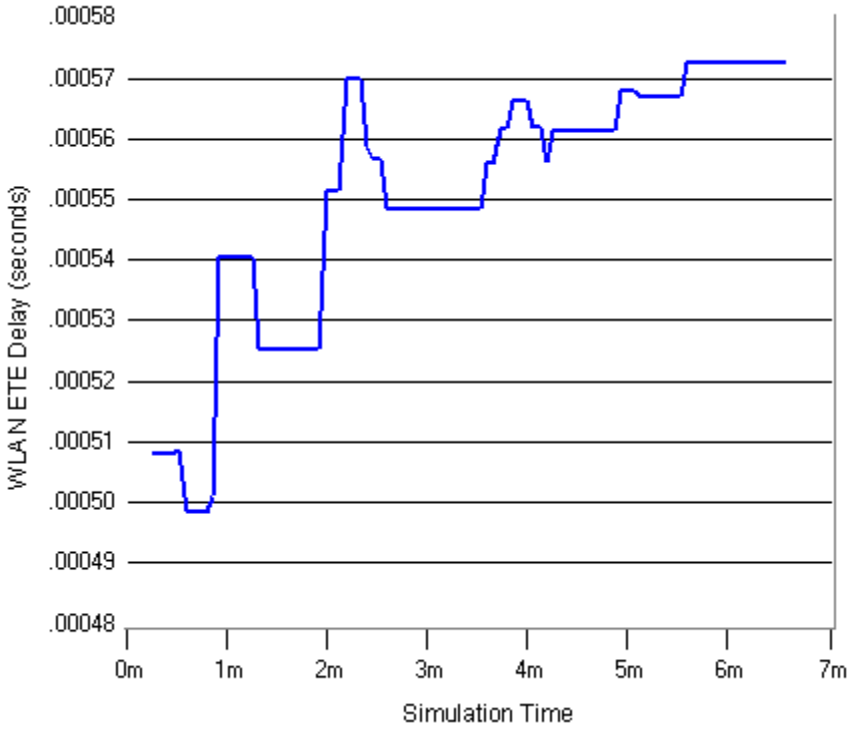

Figure 6.5 Average ETE delay for RF packets.

The values fall between 0.49 millisecond and 0.58 millisecond. Therefore, it can be concluded that the RF information exchange, which is of assistance to FSO operations, does not introduce heavy delays in FSO data transmission.

6.3.1.2 End-to-End Delay (FSO)

For an FSO packet, its ETE delay is the sum of the following: the time needed for the RF information exchange between the source node and the destination node (i.e. the RF ETE delay), queuing delay (if any), link acquisition time, transmission delay (the length of the packet divided by the channel data rate), and propagation delay (the time needed for the optical wave to traverse the link distance).

The average ETE delay for all received FSO packets is shown in Figure 6.6. The rather flat curve indicates that, for the baseline scenario, the FSO ETE delay (approximately 4.6 ~ 4.7 seconds) is dominated by link acquisition time, which is set to be 3.0 seconds, and transmission delay, which has a value of 1.6 seconds for a 200MB packet in a 1Gbit/s channel.

6.3.1.3 Packets Generated vs. Packets Received

Figure 6.7 displays the total number of FSO packets generated, in red, and received, in blue, by all nodes in the network.

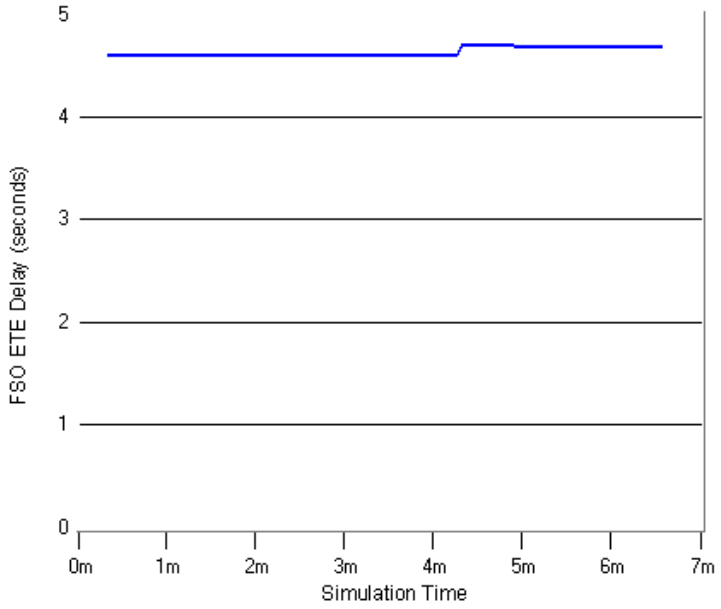

Figure 6.6 Average ETE delay for FSO packets.

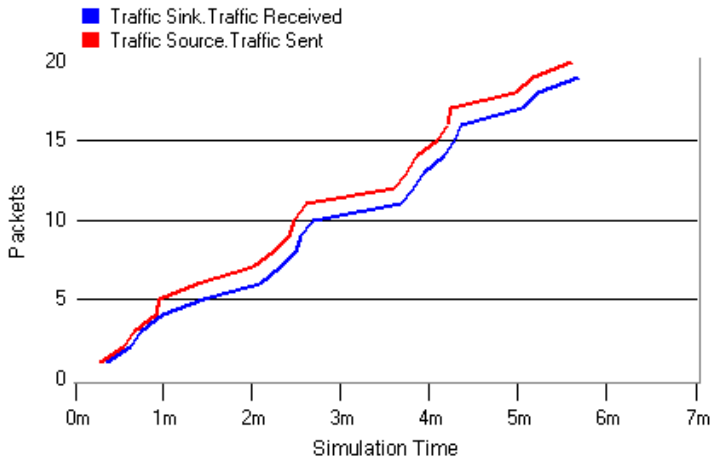

Figure 6.7 FSO packets generated and received.

The two curves are close to each other. An analysis on the data reveals that only one packet was dropped during the course of simulation. Of all FSO traffic generated, 95% was successfully received.

6.3.1.4 Throughput

The overall throughput of the network is presented in Figure 6.8. The individual throughputs of all nodes are shown in Figure 6.9, with different colors identifying different nodes.

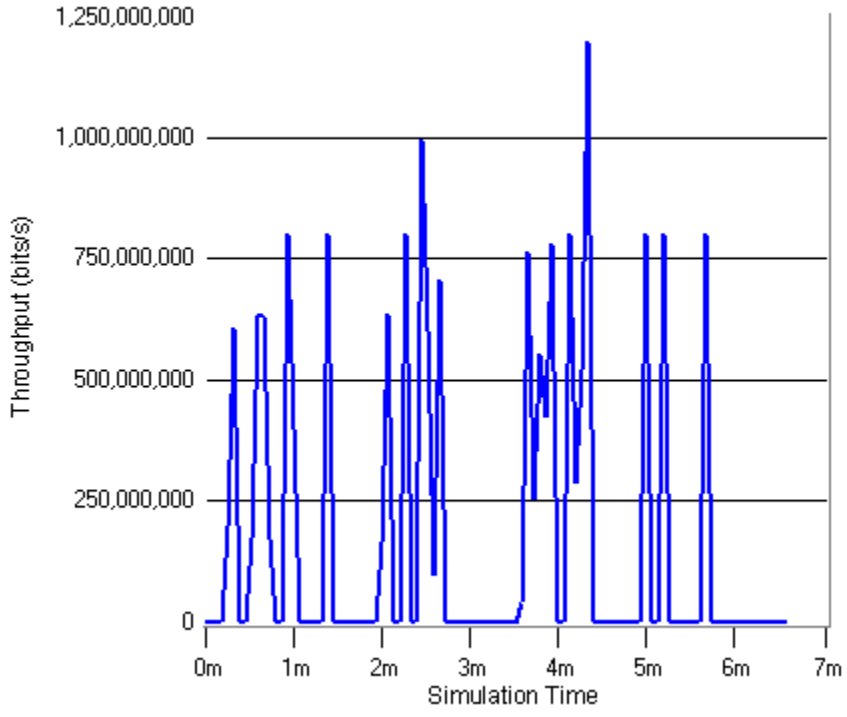

Figure 6.8 Overall throughput of the network.

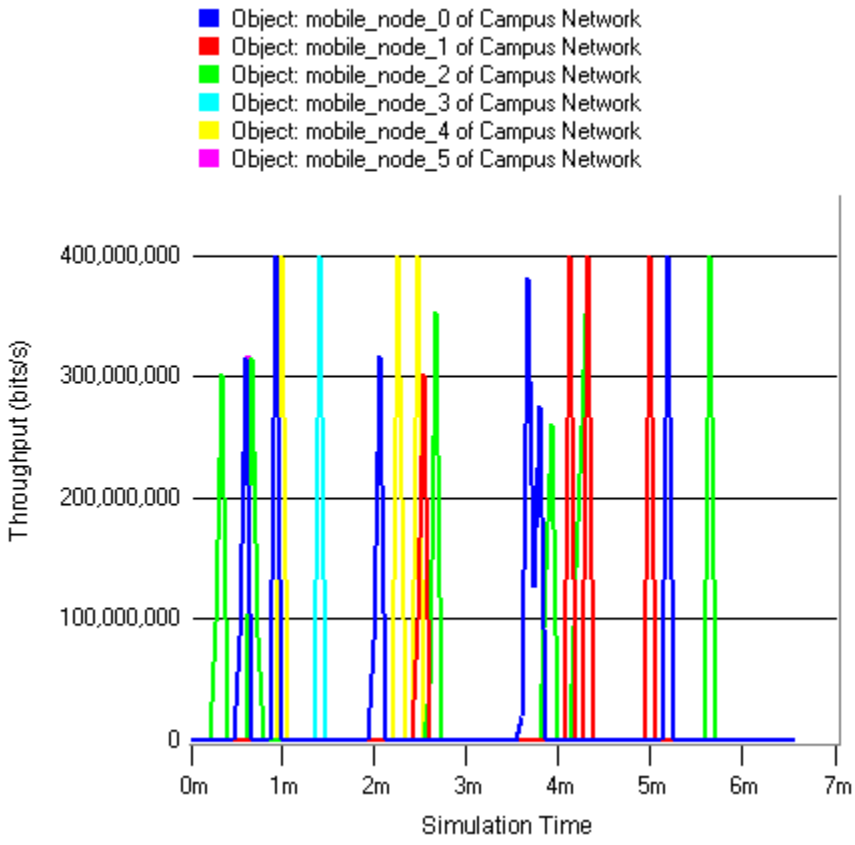

Figure 6.9 Throughputs of individual nodes.

The "bursty" nature of the throughput diagrams is intrinsically determined by the way FSO works in the mobile network. As expected, the throughput of a node reaches several hundred megabits per second during the time its FSO module is in operation, and gigabit-per-second throughput can be achieved by the overall throughput of the network. Therefore, the proposed hybrid network especially sees potential application in such scenarios where each mobile node

spends most time in collecting and assembling data and is allowed or forced to dispatch the amassed data on sparse intervals. Examples of such a scenario include scientific and military reconnaissance missions, media-rich file sharing, distributed gaming, etc.

6.3.2 Network Density Variations

In the first case, the network was made "denser" by increasing the number of communication nodes from 6 in the baseline scenario to 12. The denser network resulted in a higher packet loss ratio, as indicated by Figure 6.10.

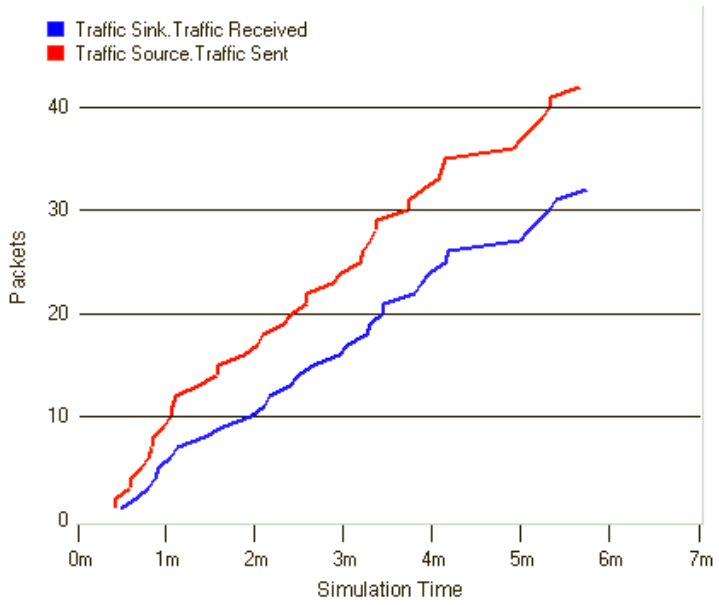

Figure 6.10 FSO packets generated and received in a denser network.

The raw data used to draw the figure shows that only 32 out of 42 packets were successfully received, yielding a 24% packet loss. If the node count is increased to 24, the packet loss ratio will reach 47%. The number of lost packets becomes greater than that of received packets when the node count reaches 44. The degradation of packet reception ratio accelerates as the node count gets even higher. (Note that due to the randomness of certain simulation aspects, the numbers presented here are for qualitative or rough quantitative analysis only; they may not be exactly reproduced by other simulation runs. This statement generally applies to all simulation results.)

In the second case, the node count was decreased to 4. The "sparser" network resulted in no packet losses, as shown in Figure 6.11.

6.3.3 Node Speed Effects

In the baseline model, the values of node speed fit a uniform distribution with a minimum of 5 m/s and a maximum of 10 m/s. If the minimum and maximum values were increased to 15 m/s and 30 m/s, respectively, the packet loss ratio resulted in an increase from 5% to 20%, as shown in Figure 6.12 (16 packets out of a total 20 were successfully received).

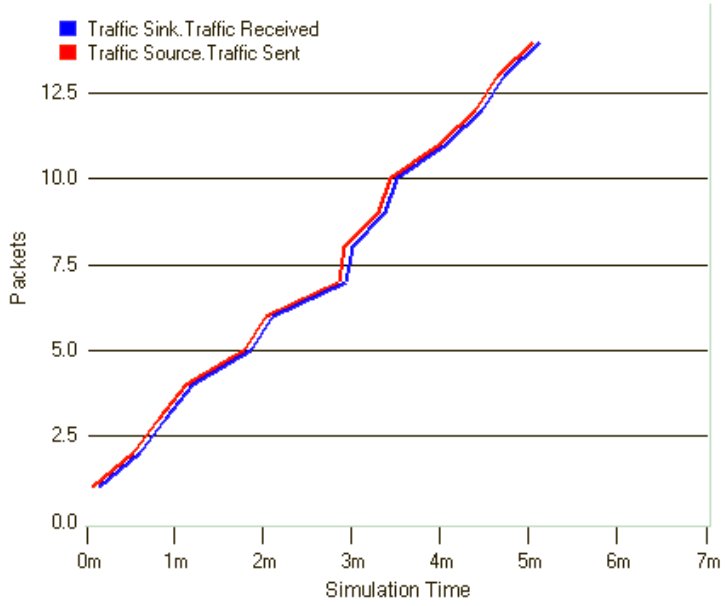

Figure 6.11 FSO packets generated and received in a sparser network.

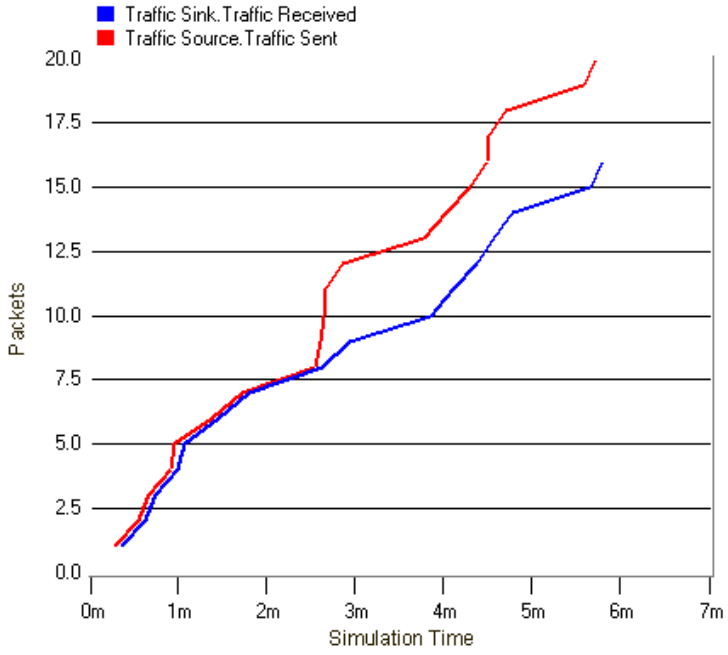

Figure 6.12 FSO packets generated and received with increased node speed.

6.3.4 Traffic Pattern Changes

Traffic pattern changes in the network were made by adjusting the settings for packet interarrival time and packet size at the FSO packet sources.

In the baseline model, the packet interarrival time at each node is defined by a normal distribution with a mean value of 100 seconds and a standard deviation of 20 seconds. If the mean was changed to 50 and all other settings kept unchanged, the packet loss ratio would increase from 5% to 25%, as shown in Figure 6.13. Moreover, the more congested traffic led to more utilization of the queuing resources on the nodes, which resulted in longer ETE delays. The new average ETE delay is shown in Figure 6.14.

Another approach to change the traffic pattern is to modify the size of the packets generated by FSO packet sources. When the packet size was changed from 200 MB in the baseline model to 400 MB, both the packet loss ratio and the average ETE delay increased as expected. Figure 6.15 shows the updated comparison between generated packets and received packets, and Figure 6.16 plots the increased ETE delay.

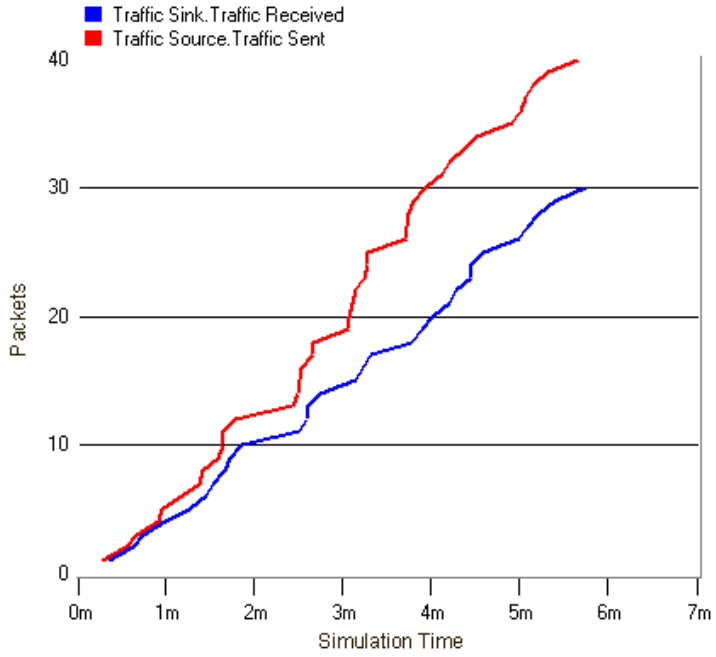

Figure 6.13 FSO packets generated and received – shorter interarrival time.

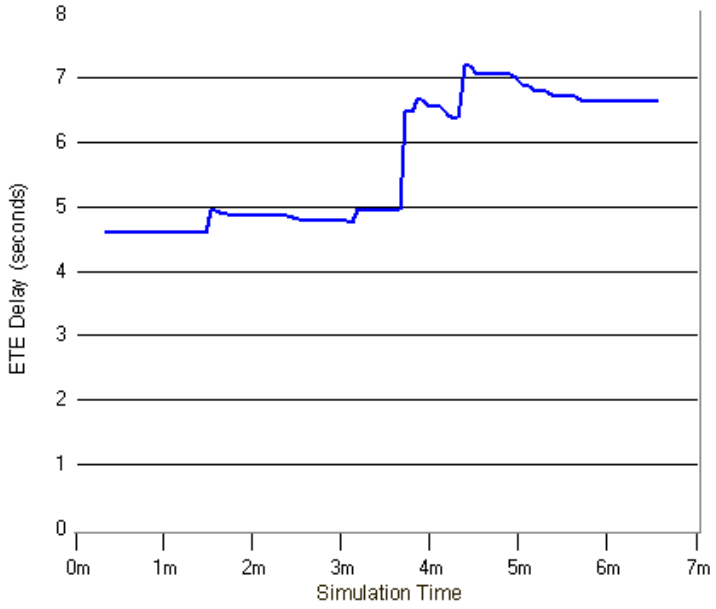

Figure 6.14 Average ETE delay – shorter interarrival time.

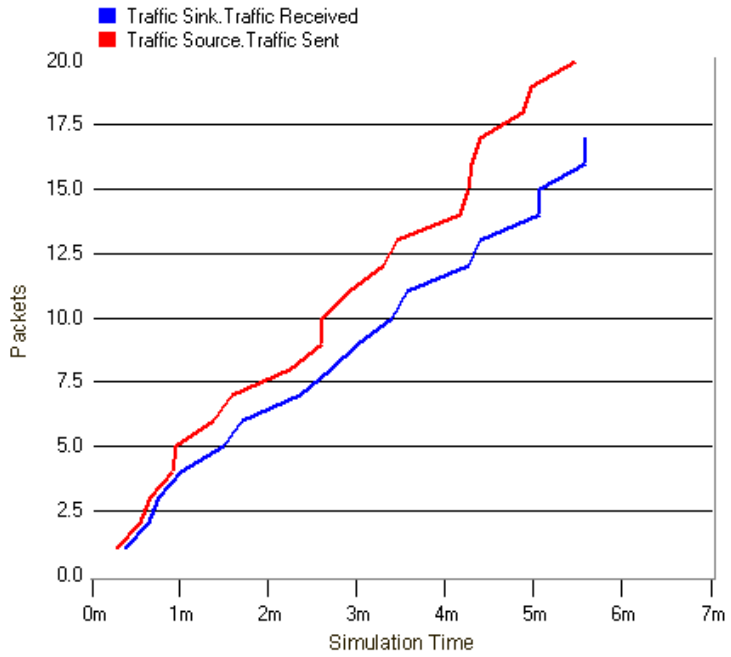

Figure 6.15 FSO packets generated and received – larger packet size.

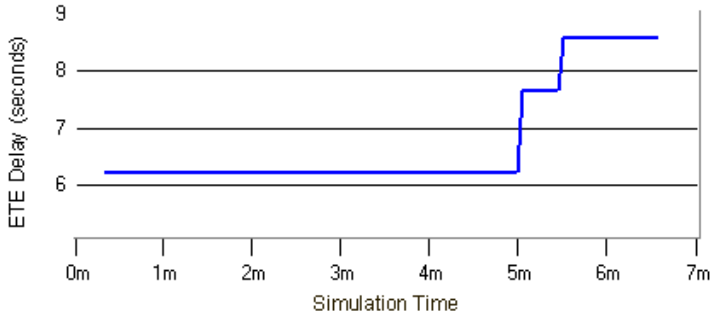

Figure 6.16 Average ETE delay – larger packet size.

6.4 CONLUSIONS

This chapter presented the development of simulation models for 802.11 networks enhanced with FSO capabilities. Such networks were proved to be sustainable, and of which the performance, mainly in the sense of throughput, were improved compared to purely RF WLANs. The coexistence of and interaction between the RF and FSO modules were demonstrated to be problem-free. Various scenarios were constructed to study the impact on network performance by different parameters. The simulation results corroborated design expectations.

One limitation of the simulation models presented in this chapter is that the network region is restricted within a 200m×200m area, thus the full potential of FSO communications, which is capable of sending data over a one- to several-kilometer distance, is not exploited. This is due to the fact that the transmission range for a WLAN node is rather limited (according to Modeler documentation, a distance beyond 300 meters would result in unreliable behaviors in the WLAN model). To overcome this limitation, multi-hop RF operations, i.e. MANET, can be implemented on top of the current WLAN PHY and MAC layers in order to support longer-range FSO data transmission. Chapter 7 will discuss the issue in detail.

CHAPTER 7 - MANET ENHANCED WITH FSO

The last chapter discussed OPNET models for FSO-enhanced IEEE 802.11 networks operating in ad hoc (IBSS) mode. In such a network, the potential of FSO communications is not fully utilized as the FSO link distance is limited by the transmission range of RF signals, which is due to the fact that an ad hoc routing protocol is not part of the 802.11 standards, i.e., the data route between any two nodes does not involve a third node.

A MANET is a different type of wireless ad hoc network. In a MANET, each node is willing to forward data for other nodes. Therefore, a communications link exists between two nodes S_0 and S_N if there exists a chain of nodes S_1, S_2, …, S_{N-1} such that the distance between S_n and S_{n+1} is within the maximum RF transmission range for all values of n satisfying $0 \leq n \leq N-1$. If FSO capabilities are added onto a MANET, the lengths of optical links will no longer be limited by the transmission properties of RF signals, thus the potential of FSO communications can be exploited to a fuller extent.

This chapter presents models developed to study such FSO-enhanced MANETs. It is organized in a similar way to Chapter 6 except that the overview of RF MANETs is omitted since such an overview was already included in Chapter 2.

7.1 SIMULATION MODELS

Similar to the FSO-enhanced WLAN node presented in Chapter 6, the RF module of the FSO-RF MANET node is only responsible for disseminating node coordinates and busy status information, while the FSO module takes charge of transmitting bulk data. The RF module is directly modified from the built-in "manet_station_adv" node in Modeler, which consists of a raw packet generator running over IP over WLAN. The architecture of the built-in MANET node is shown in Figure 7.1.

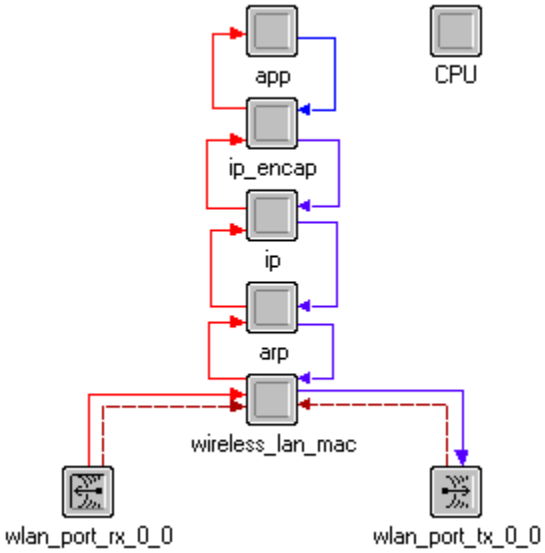

Figure 7.1 The built-in MANET node.

In the node depicted above, the application layer ("app") is the combination of a traffic source and a sink. The auxiliary module "CPU", which

simulates the utilization of hardware resources, is also part of the application layer. An IP-encapsulation process model ("ip_encap") on the layer below encapsulates packets coming from the traffic source into IP packets. It also decapsulates packets arriving from the lower layer and passes them to the application layer to be processed. The IP process model sitting further below implements fragmentation and reassembly of IP packets as well as IP routing functions. On the bottom, the PHY and MAC layers are identical to those in the WLAN node shown in Figure 6.2. Between the IP and MAC layers, the Address Resolution Protocol (ARP) translates IP addresses to MAC addresses. The process model that manages all MANET routing protocols, called "manet_mgr", is a child process of the IP process. Invoked by the IP process during simulation runs, it spawns the appropriate MANET routing protocol running on the node as specified by the user.

A modified version of the node shown in Figure 7.1 constitutes the RF portion of the FSO-RF hybrid node developed for the purposes of this dissertation. Specifically, the "app" process model is replaced by an "rf_interface" process model, which is no longer involved in generating or destroying RF packets. Instead, it converts the WLAN MAC addressing information embedded in the RF probe or response packets generated by the "routing" process into addressing information in IP format and passes the packets downward to be sent out. It also forwards all probe and response packets received by the RF module of the node to the routing layer for processing.

A major advantage of this modification approach was that in this way the FSO portion of the node, including the routing algorithm and the RF probe/reply scheme, did not have to undergo significant changes in order to operate in accord with the RF portion, which was now much different from the RF module of the node shown in Figure 6.2.

The architecture of the new hybrid node is shown in Figure 7.2.

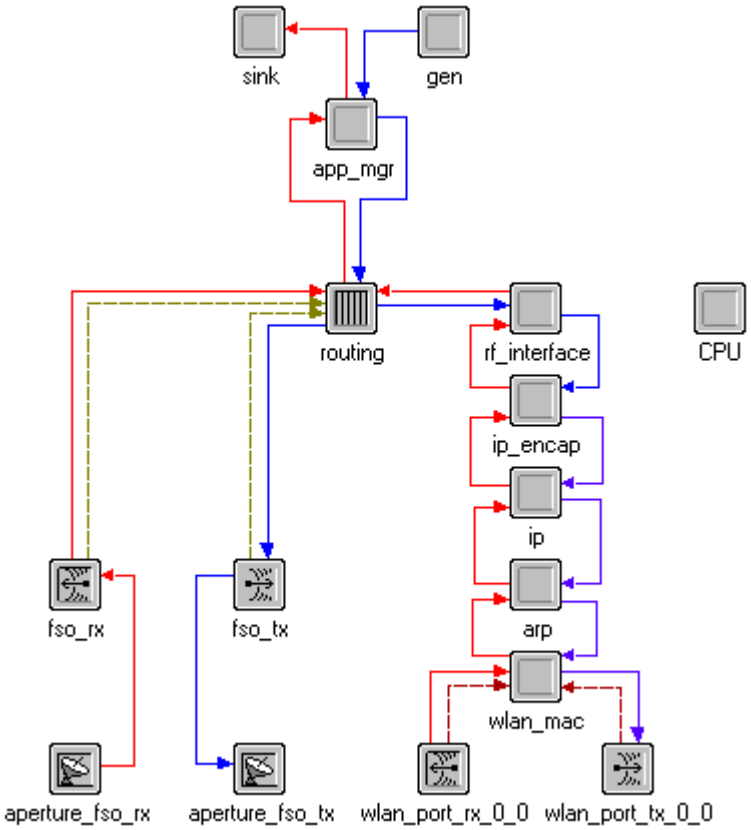

Figure 7.2 The FSO-enhanced MANET node.

In general, the principle by which the node operates remains the same as described in Section 6.2. The only difference is that the RF probe and response packets can now be passed along multi-hop links by the MANET routing process, which effectively extends the maximum distance over which two nodes can communicate.

A network model was formed by placing a number of nodes in a domain. Network models with different specifications will be presented in the next section, Simulation Results.

7.2 SIMULATION RESULTS

This section takes the same baseline-perturbation approach as described in Section 6.3.

7.2.1 The Pre-Baseline (Validation) Scenario

An exact copy, from a network-level perspective, of the baseline scenario presented in Section 6.3.1 was studied to validate the new node model. The network layout is shown in Figure 7.3, which is a replica of Figure 6.4. The simulation settings for this scenario, listed in Table 7.1, were all directly imported from the baseline scenario in Chapter 6.

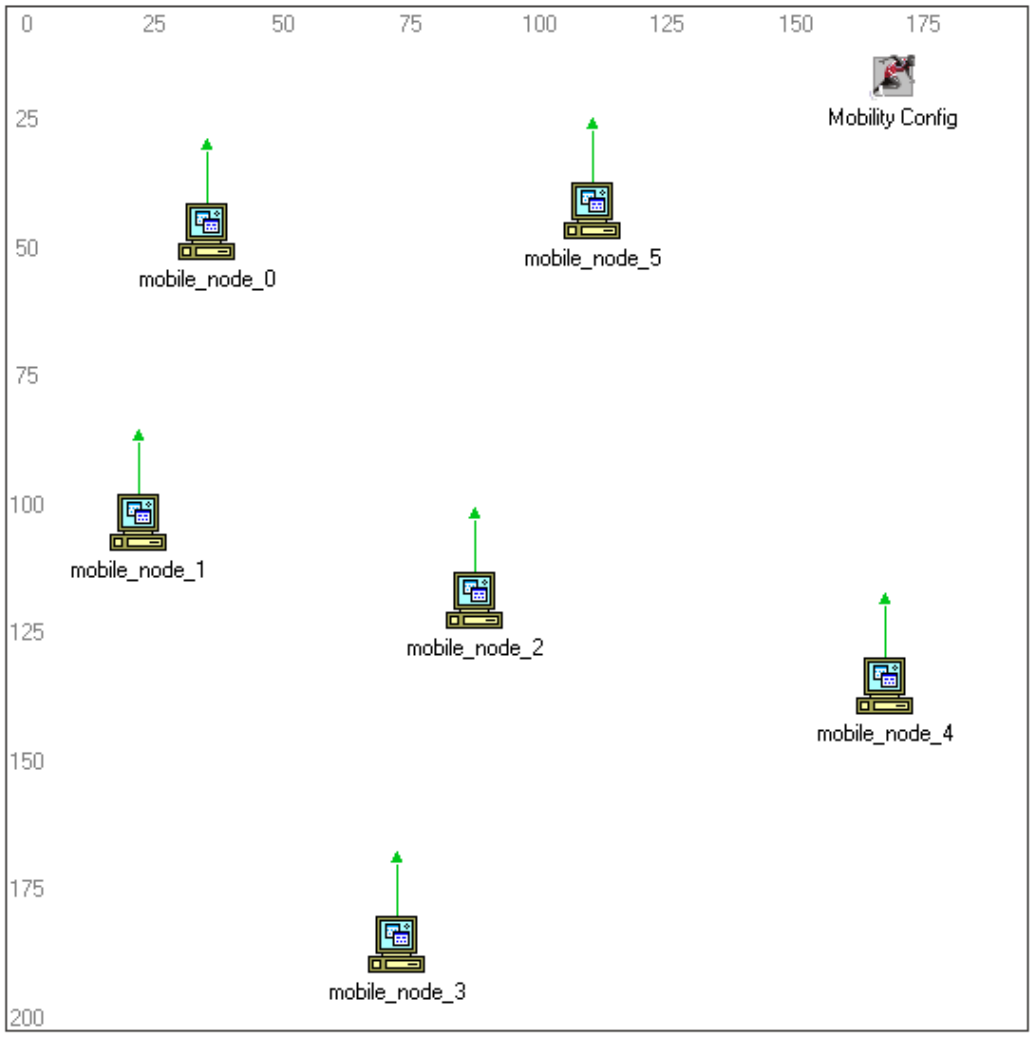

Figure 7.3 Network layout for the pre-baseline scenario.

Attribute Name		Value	Unit
Network size	X-span	200	m
	Y-span	200	m
Simulation time		400	s
Node count		6	-
Node speed		Uniform, min=5, max=10	m/s
FSO packet interarrival time		Normal, μ=100.0, σ^2=400.0	s
FSO packet bulk size		2.0E+8	bytes
FSO channel data rate		1.0E+9	bit/s
FSO carrier frequency		1.9355E+14 *	Hz
Simulated FSO link acquisition time		3.0	s
FSO receiver ECC threshold **		1.0E-7	-
FSO packet generator	Start time	Normal, μ=50.0, σ^2=225.0	s
	Stop time	350	s
Queue size for FSO packets		5	packets
Node mobility	Start time	10	s
	Stop time	End of simulation	-
RF module	WLAN mode	802.11b	-
	MANET routing protocol	Dynamic Source Routing (DSR)	-

Table 7.1 Simulation settings for the pre-baseline scenario.

7.2.1.1 End-to-End Delay (RF)

Figure 7.4 shows the average ETE delay for all received RF probe and reply packets against simulation time. The ETE delay is the sum of physical transmission delay and routing delay introduced by the DSR routing scheme. Its values fall between 0.001 and 0.008 second, which are several times longer than the WLAN ETE delay values depicted in Figure 6.5. However, they are still very

* This value corresponds to a wavelength of 1,550 nm, which is commonly used in FSO communications.

** This attribute is the highest proportion of bit errors allowed in a packet for the packet to be accepted by the receiver.

short time measurements and not expected to introduce any significant degradation to network performance.

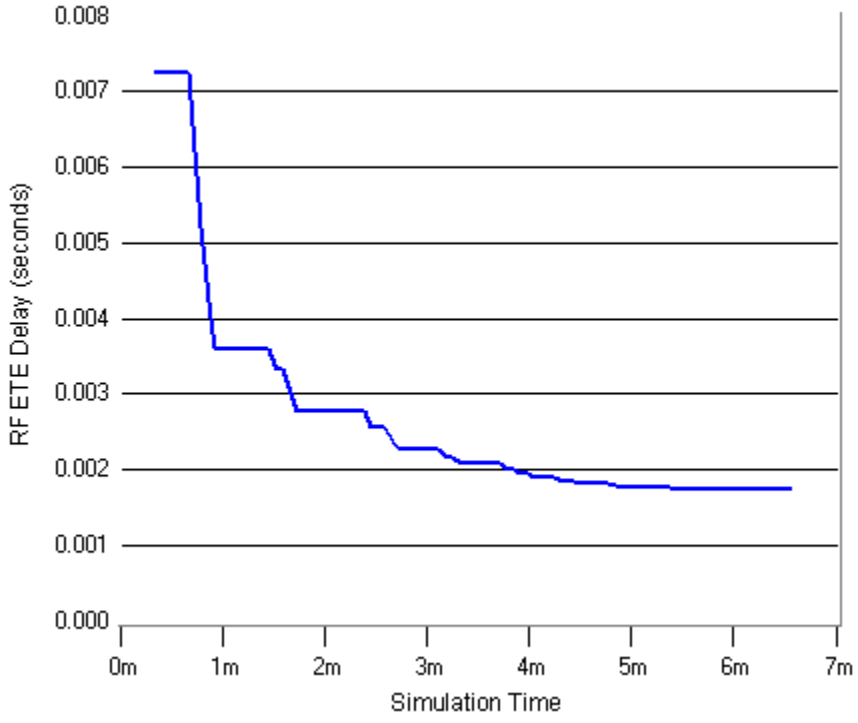

Figure 7.4 Average ETE delay for RF packets.

7.2.1.2 End-to-End Delay (FSO)

The average ETE delay for all received FSO packets is shown in Figure 7.5. The values are similar to those represented by Figure 6.6, and range between 4.6 and 5.0 seconds.

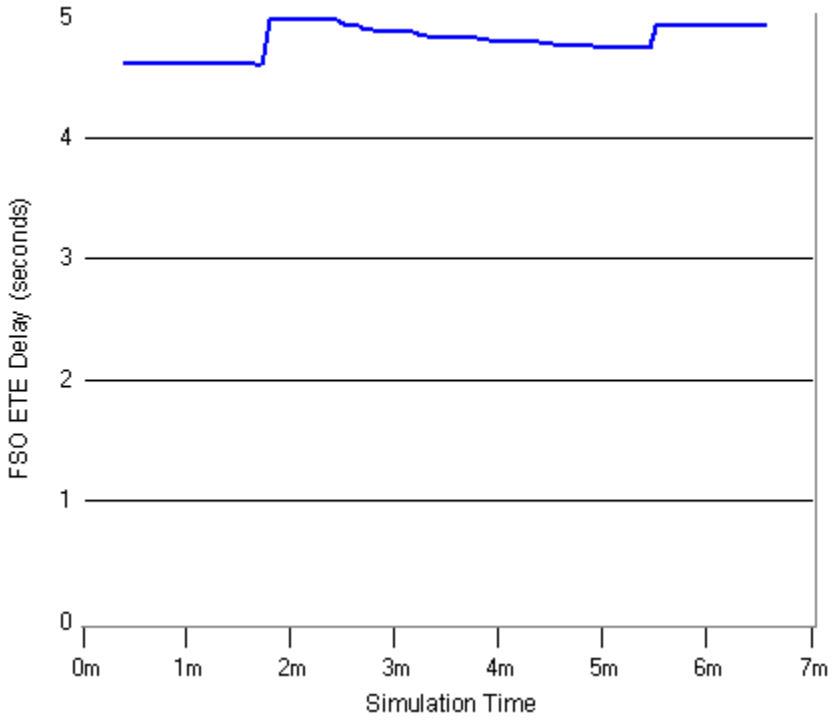

Figure 7.5 Average ETE delay for FSO packets.

7.2.1.3 Packets Generated vs. Packets Received

Figure 7.6 illustrates the total number of FSO packets generated, in red, and received, in blue, by all nodes in the network. The figure indicates that all packets generated were successfully received.

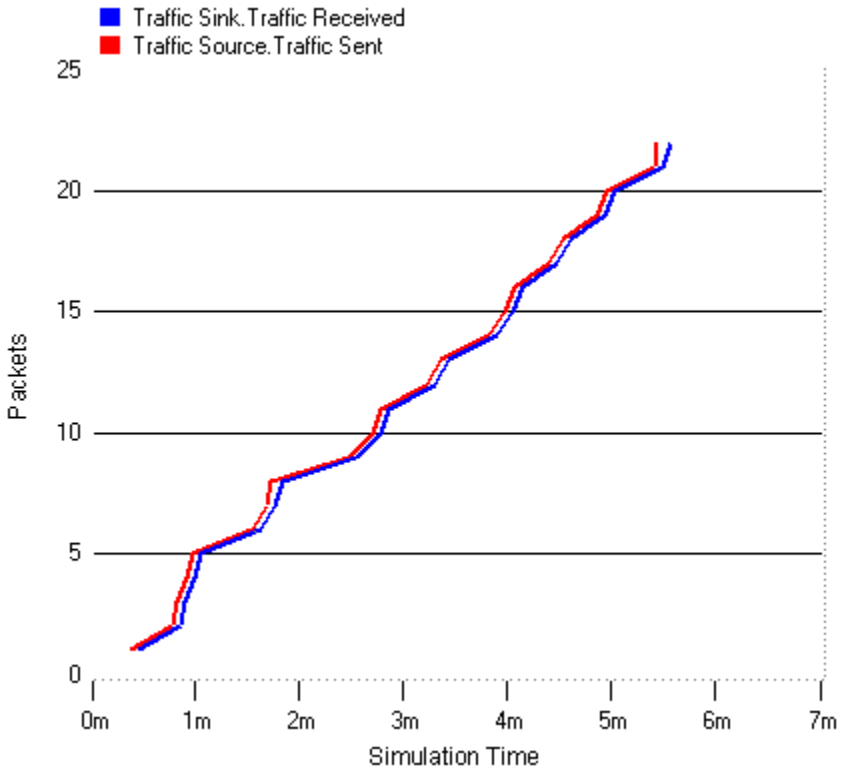

Figure 7.6 FSO packets generated and received.

7.2.1.4 Throughput

The overall throughput of the network is presented in Figure 7.7. The individual throughputs of all nodes are shown in Figure 7.8, with different colors identifying different nodes. The high data rates and the bursty nature of FSO communications can be clearly observed from the figures.

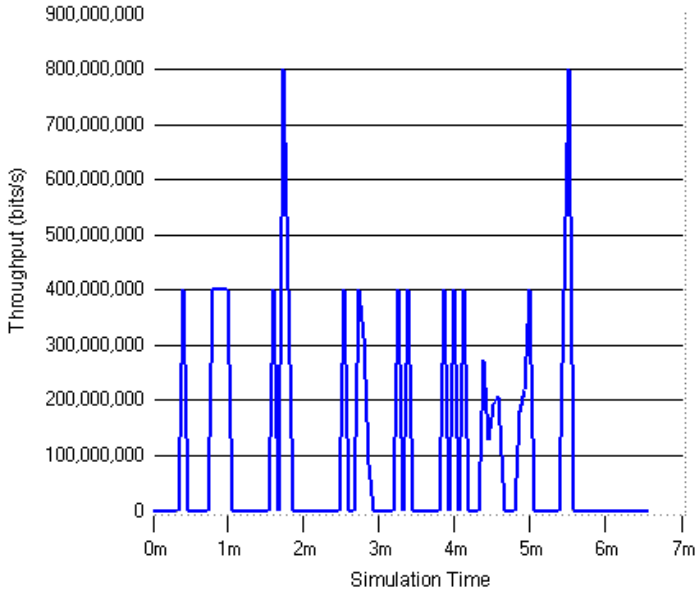

Figure 7.7 Overall throughput of the network.

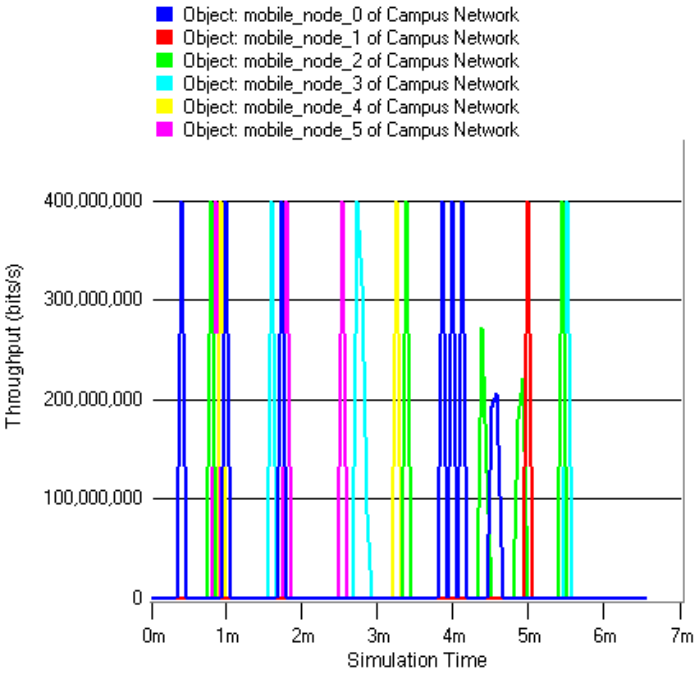

Figure 7.8 Throughputs of individual nodes.

The simulation results presented in Sections 7.2.1.1 through 7.2.1.4 are comparable to those in Sections 6.3.1.1 through 6.3.1.4, which proves the validity of the FSO-enhanced MANET node model.

7.2.2 The Baseline Scenario

As mentioned earlier, the rather small size of the network domain (200m×200m) was due to the short WLAN transmission range. It can be expanded to exploit the FSO link distance to a fuller extent with the use of the MANET module to conduct RF information exchange in the network. Therefore, the domain size was increased to 500m×500m for the baseline scenario. Other parameters were also adjusted to adapt to the size change. The new simulation settings are listed in Table 7.2 (unlisted parameters remain unchanged from Table 7.1) The new network model is depicted in Figure 7.9.

Attribute Name		Value	Unit
Network size	X-span	500	m
	Y-span	500	m
Simulation time		2000	s
Node count		20	-
FSO packet interarrival time		Normal, μ=400.0, σ^2=10000.0	s
FSO packet generator	Start time	Normal, μ=50.0, σ^2=400.0	s
	Stop time	1950	s
Queue size for FSO packets		5	packets

Table 7.2 Simulation settings for the baseline scenario.

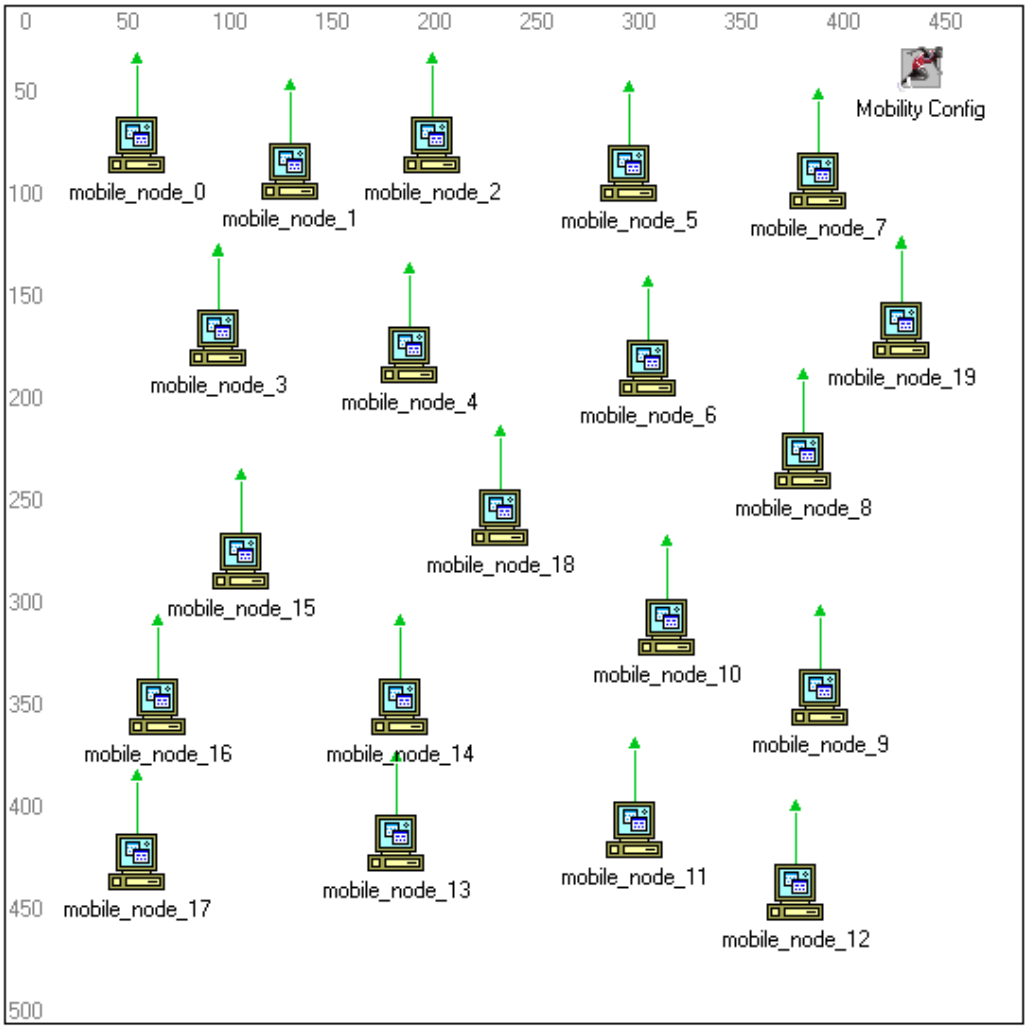

Figure 7.9 Network model.

7.2.2.1 End-to-End Delay (RF)

Figure 7.10 shows the average ETE delay for all received RF probe and reply packets against simulation time. The values fall between 0.005 and 0.025 second.

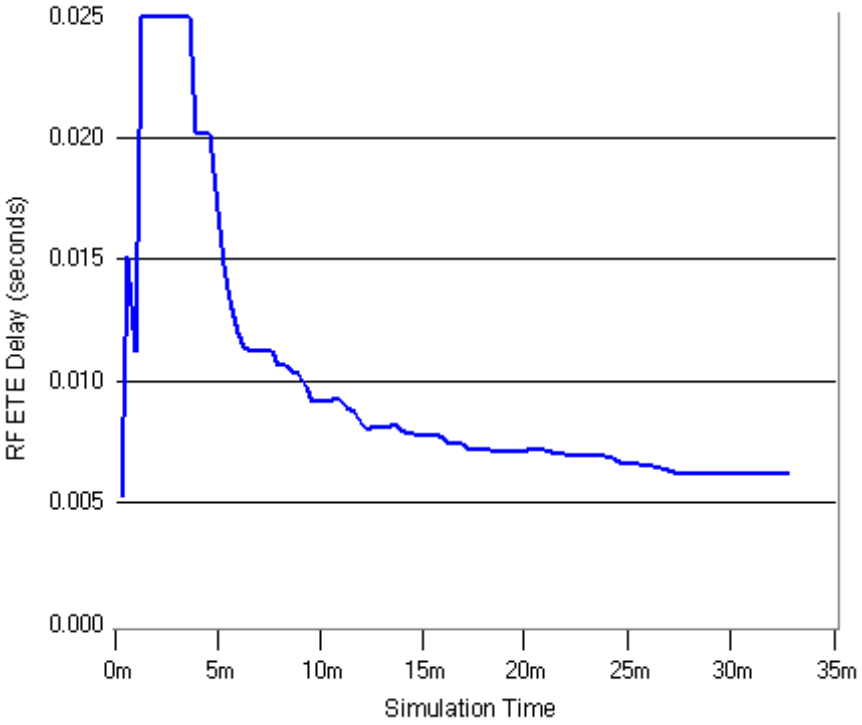

Figure 7.10 Average ETE delay for RF packets.

7.2.2.2 End-to-End Delay (FSO)

Figure 7.11 displays the average ETE delay for all received FSO packets. Similar to all scenarios discussed previously, the curve is flat with an average value of about 4.6 seconds, which indicates that the ETE delay for FSO packets is dominated by link acquisition time and transmission delay.

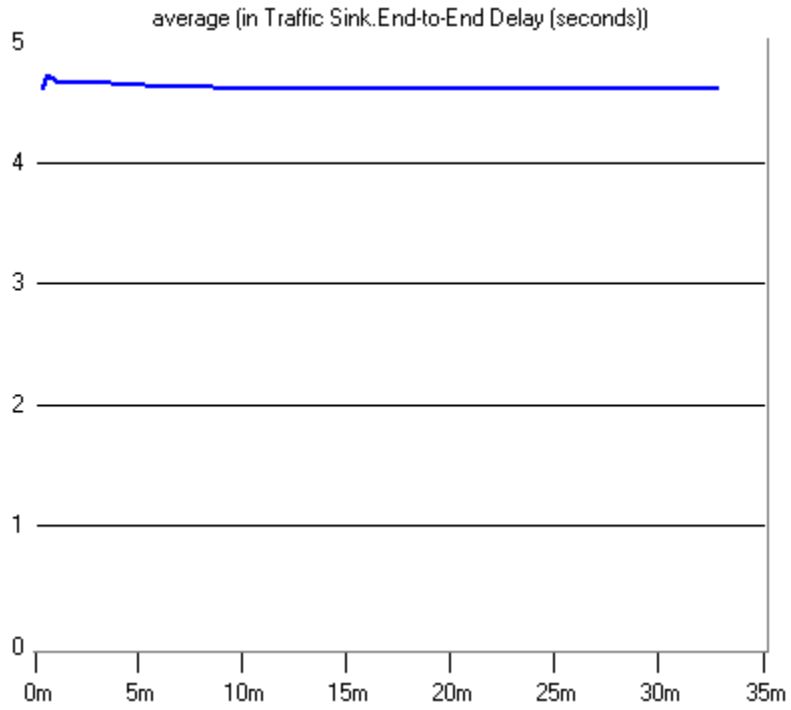

Figure 7.11 Average ETE delay for FSO packets.

7.2.2.3 Packets Generated vs. Packet Received

Figure 7.12 shows the total number of FSO packets generated, in red, and received, in blue, by all nodes in the network. At the end of the simulation, the packet loss ratio was about 13% (79 packets out of 91 were successfully received).

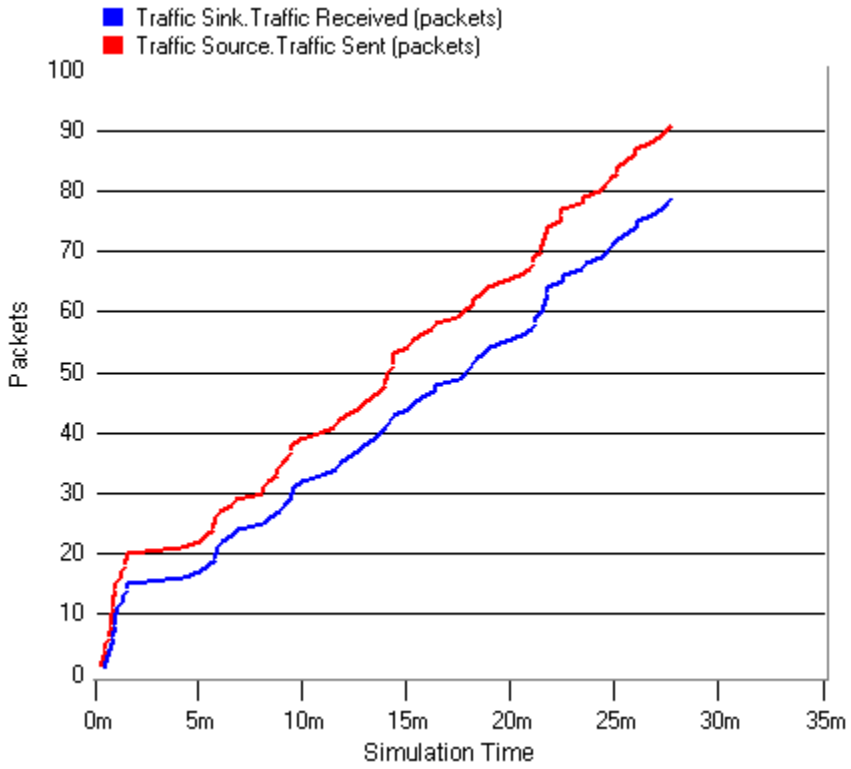

Figure 7.12 FSO packets generated and received.

7.2.2.4 Throughput

The overall throughput of the network is shown in Figure 7.13. Due to the rather large number of nodes, the graph showing the throughputs of individual nodes became congested thus is omitted here. Again, the high bandwidth and data bursts can be clearly observed.

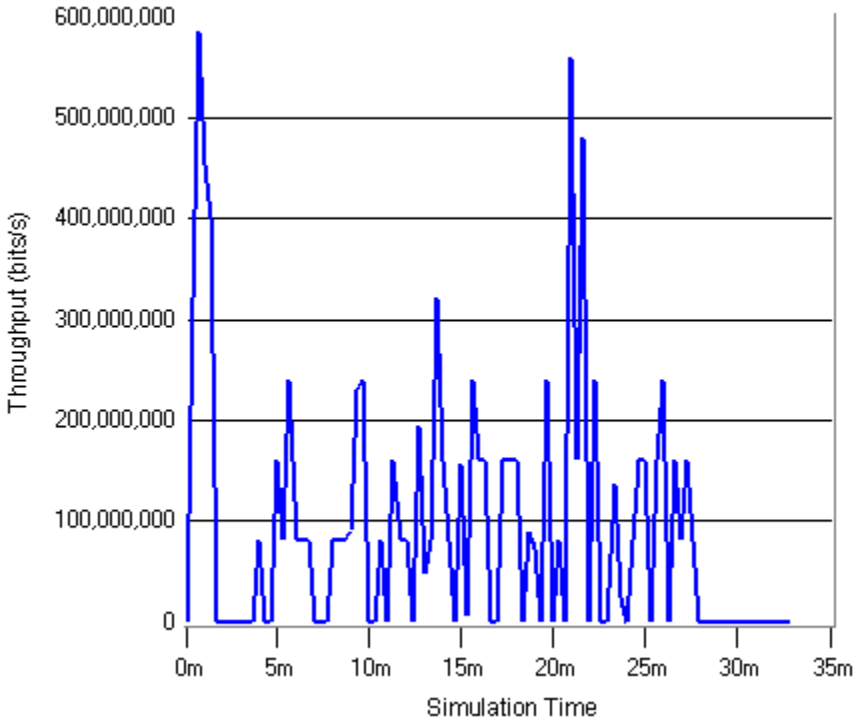

Figure 7.13 Overall throughput of the network.

7.2.2.5 DSR Routes

In contrast to the FSO-enhanced WLAN networks presented in Chapter 6, where RF traffic between two nodes took single hops and single hops only, the RF packets in the network shown in Figure 7.9 might traverse a chain of more than two nodes, as directed by the DSR routing algorithm. Two instances of such multi-hop routes are displayed in Figure 7.14. In one instance, the data link between Node 5 and Node 11 took two hops (shown in red) at simulation time 1292.86 seconds; in the other instance, the link between Node 8 and Node 0 took

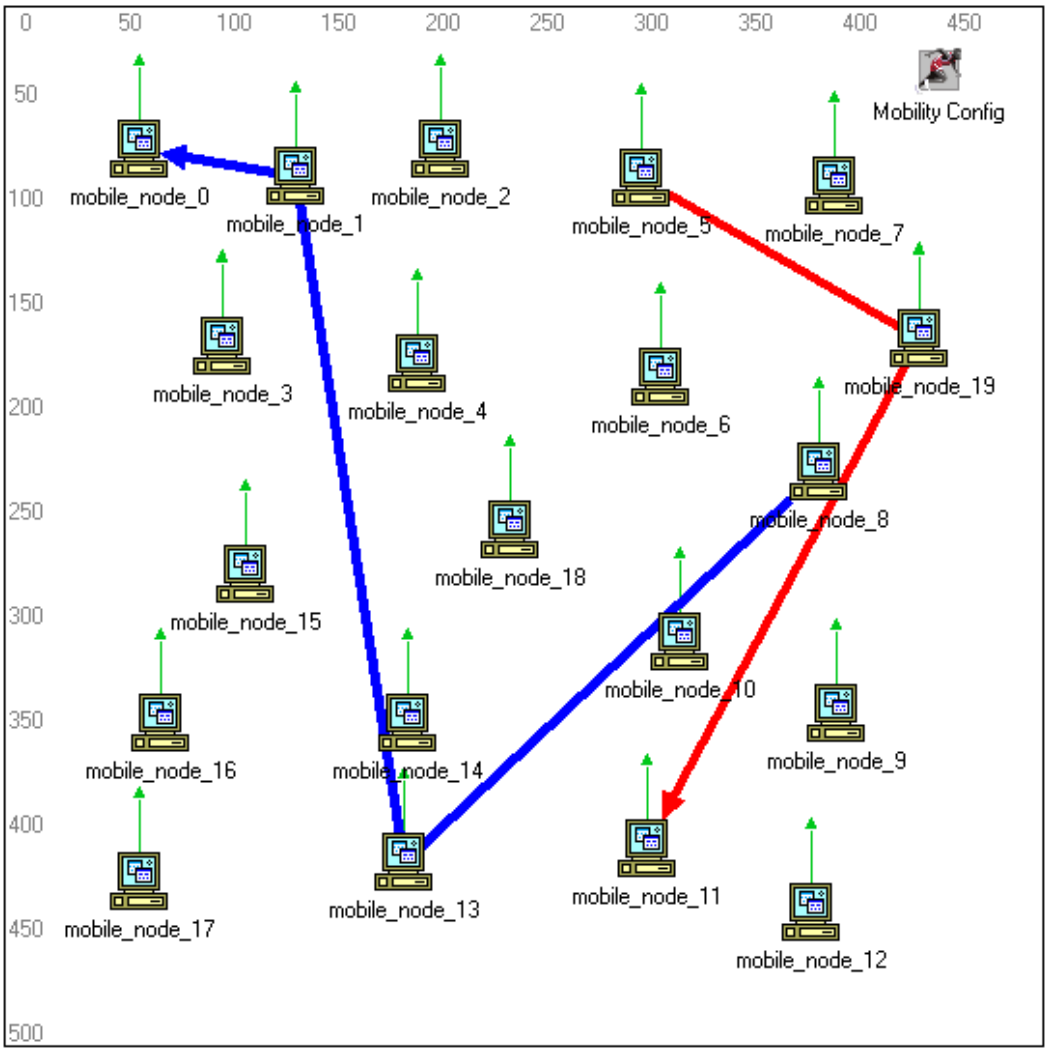

Figure 7.14 Examples of RF traffic routes.

three hops (shown in blue) at simulation time 1067.25 seconds. Note that due to Modeler functionality limitations, these routes can only be drawn over the initial network layout, i.e., the node positions in Figure 7.14 don't represent their actual coordinates when the routes took place.

Obviously, the ability of delivering an RF packet to its destination over multiple hops enables the establishment of an FSO link that may not be possible otherwise.

7.2.3 Network Density Variations

As expected, a denser network (40 nodes) produced a higher packet loss ratio (19%) than the baseline scenario (Figure 7.15).

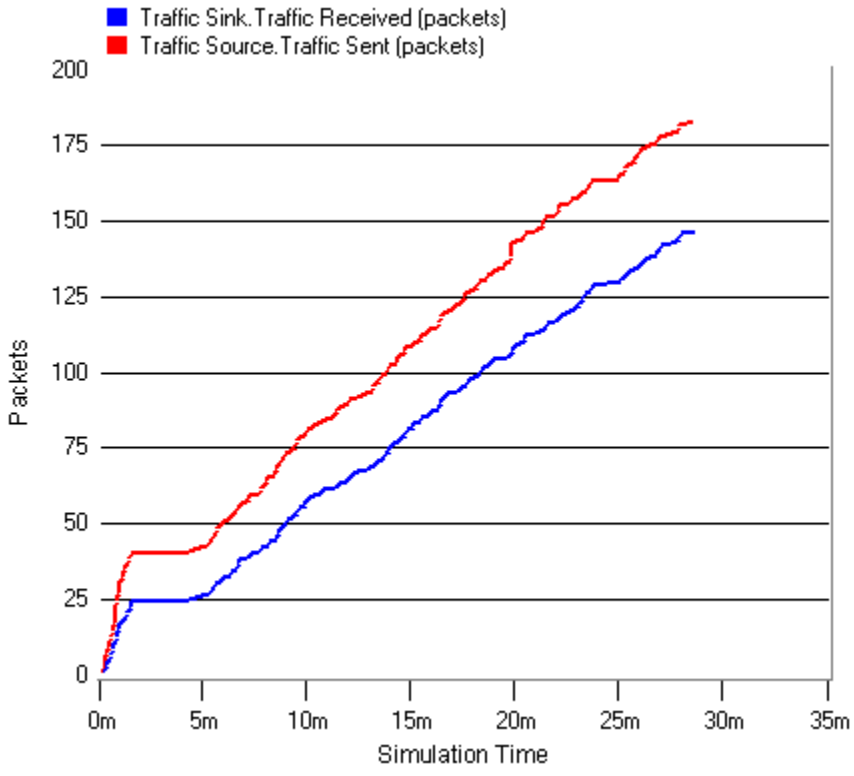

Figure 7.15 FSO packets generated and received in a denser network.

In a sparser network (12 nodes), however, the packet loss ratio (19%) also exceeded the packet loss ratio in the baseline network (Figure 7.16). This is because each hop on a MANET route still has to be within the maximum RF operational distance. Therefore, if the network is too sparse, some RF packets will fail to be delivered, resulting in failures in establishing FSO links.

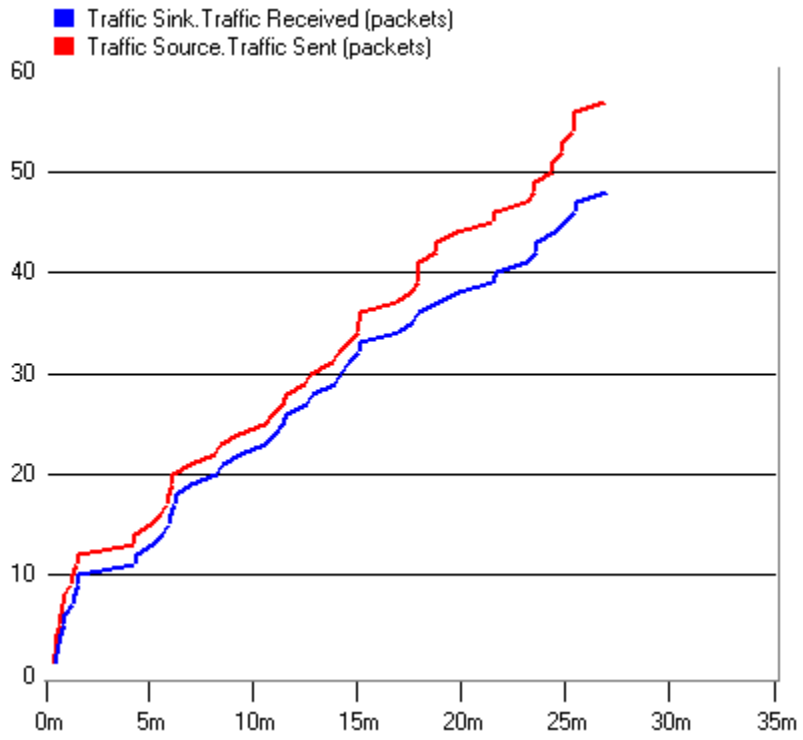

Figure 7.16 FSO packets generated and received in a sparser network.

7.2.4 Node Speed Effects

If the minimum and maximum values of node speed, which follows a uniform distribution, were increased from their baseline values 5 and 10 to 15 and 30 (unit: m/s), respectively, the packet loss ratio (13%) resulted in no significant change (Figure 7.17). This is because of the intrinsic characteristics of the DSR protocol, which was designed to provide better accommodation to node mobility than the IEEE 802.11 IBSS mode.

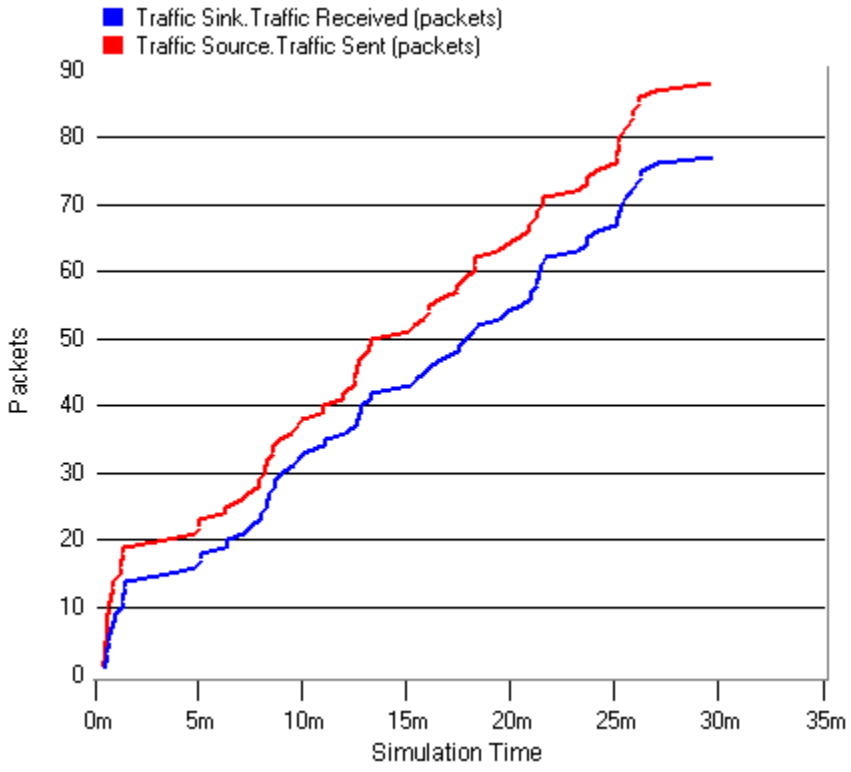

Figure 7.17 FSO packets generated and received with increased node speed.

7.2.5 Traffic Pattern Changes

As shown in Table 7.2, for the baseline model, the packet interarrival time at each node is defined by a normal distribution with a mean value of 400 seconds and a standard deviation of 100 seconds. If the mean was changed to 100 and the standard deviation 50, the packet loss ratio would increase from 13% to 22%, as shown in Figure 7.18. The shorter interarrival time also resulted in increased ETE delay due to more queuing (Figure 7.19).

In another approach, if the size of the FSO packets was changed from 200 MB to 600 MB, both the packet loss ratio and the average ETE delay again increased as expected. Figure 7.20 shows the updated comparison between generated packets and received packets, which represents a packet loss ratio of 28%. Figure 7.21 plots the increased average ETE delay.

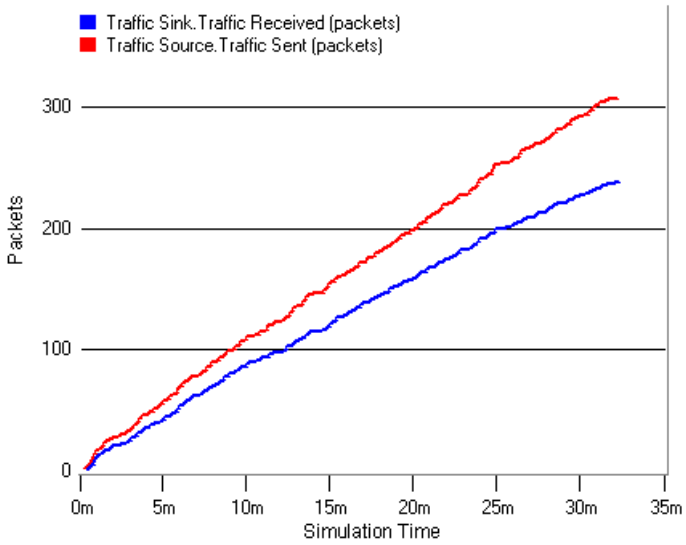

Figure 7.18 FSO packets generated and received – shorter interarrival time.

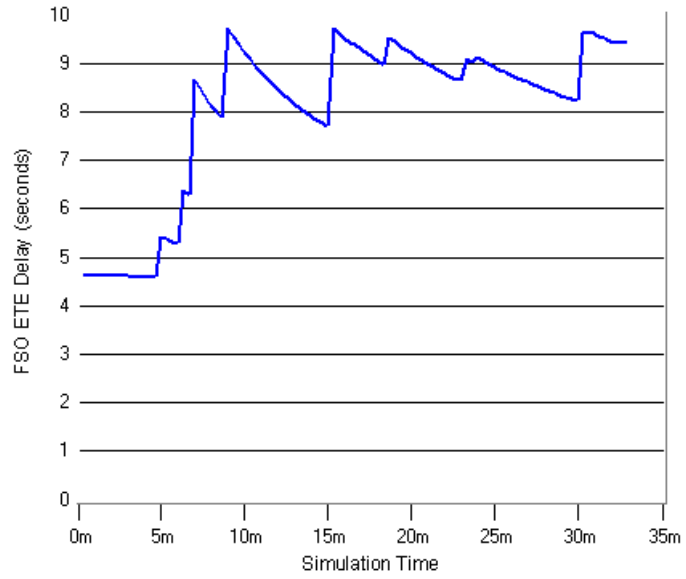

Figure 7.19 Average ETE delay – shorter interarrival time.

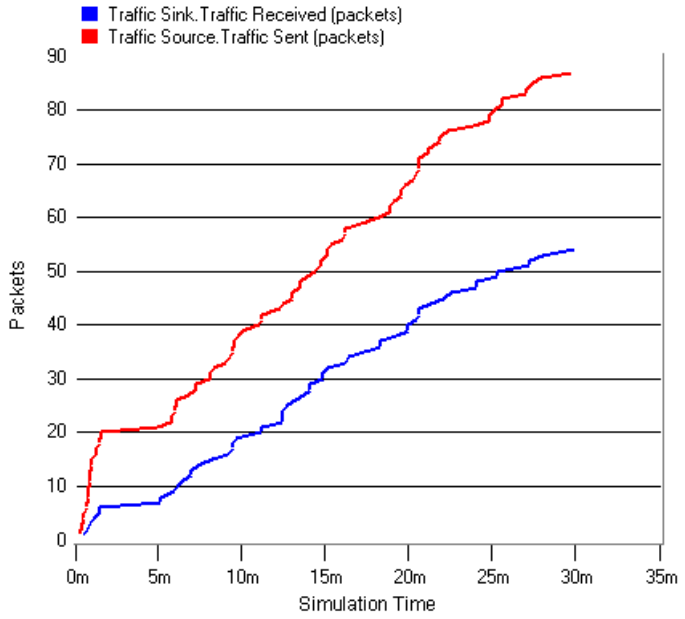

Figure 7.20 FSO packets generated and received – larger packet size.

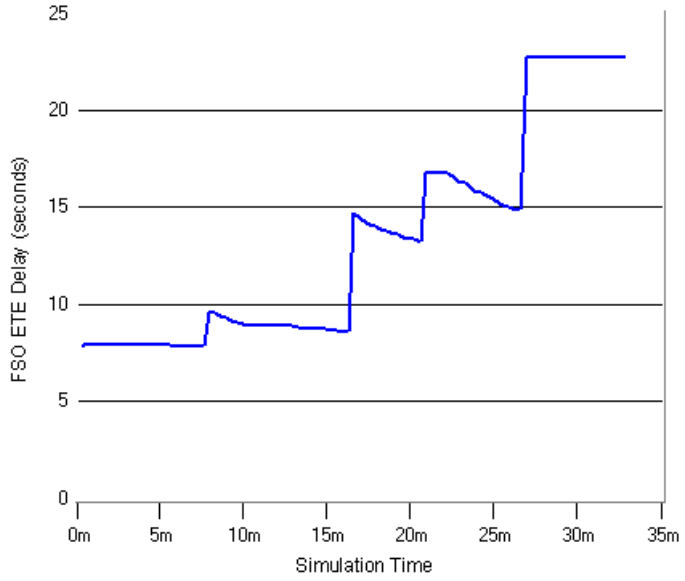

Figure 7.21 Average ETE delay – larger packet size.

7.3 CONLUSIONS

OPNET simulation models for FSO-enhanced MANETs were presented. The simulation models proved the viability of such networks and demonstrated significant improvements in throughput upon purely RF MANETs. They also showed that the limit on FSO link distances imposed by the RF transmission range in a single-hop WLAN could be overcome by employing a multi-hop MANET routing protocol. It was proved feasible for an FSO module and an RF module running a MANET routing algorithm to be integrated into one communications node; the two modules could operate in coordination to transfer large amounts of data in high-bandwidth bursts. In summary, the goals of the design were met as evidenced by the simulation results.

CHAPTER 8 – CONCLUSIONS

This dissertation is concerned with the project of using optical means of communications to improve the performance of mobile ad hoc networks.

The initial motivation of the project was followed by a literature survey regarding the background knowledge, the feasibility of the project, and published peer research in related areas. Based on the literature survey, it was determined that modeling of MANETs equipped with FSO capabilities was a suitable topic for further research leading to this dissertation.

The context of the proposed project and the methodology used to study the project were then defined. It was decided that the FSO and MANET technologies were to be utilized in combination in order to achieve high data rate yet maintain advantageous MANET features such as its ability to operate without the need for infrastructure and support for node mobility. The network simulation software package OPNET Modeler was selected as the major tool of research.

The development of simulation models for the networks to be studied was explained in detail, following a simple-to-more-complex pattern. Simulation results were presented to assess expectations for the proposed design. Various indicators, including packet loss ratio, end-to-end delay, throughput, etc., were examined in order to evaluate the performance of the network. Perturbation scenarios were constructed to further investigate effects on network performance

imposed by certain conditions, such as node speed, network density, and traffic pattern.

Based on the investigations, it was concluded that the proposal of using FSO communications to boost the data delivering capacities of MANETs was viable, the resulting networks were sustainable, and significant improvements to the original networks in the sense of increased throughputs clearly observable.

To recapitulate, this dissertation has made the following original contributions: a suitable method to study mobile networks communicating in optical means was devised and thoroughly examined; effective simulation models for such networks were developed; and the network performance was methodically evaluated by perturbation.

It is the author's hope and confidence that the investigations made throughout this dissertation will be of importance in assisting further explorations in related topics by others, both technically and methodologically. It would be a great honor for the author if the study presented in this dissertation laid the foundation for the future development of the final product that will see a great deal of exciting applications as pointed out in the opening chapter of the dissertation.

Some limitations of the research presented in this dissertation were identified. They are listed here along with suggestions on future work to overcome these limitations or improve upon the current models.

First and foremost, although the FSO routing algorithm introduced in Chapters 6 and 7 has a queue-and-retry mechanism serving as a method of protection when the node is facing difficulties in establishing an FSO link with another node, the non-zero packet loss ratios in the simulation results indicate that the delivery of FSO packets is not guaranteed in the current model. In some situations, it may be considered acceptable if the packet loss ratio is below a certain threshold; in other situations, a 100% successful delivery rate may be required. In order for the networks studied in this dissertation to suit the need of the latter, the packet delivery scheme needs to be improved to include a guaranteed delivery mechanism, which may take the form of something similar to the widely implemented Transmission Control Protocol (TCP).

Second, the FSO traffic in the networks studied was designed to be single-hop only. The decision of not developing a multi-hop FSO routing algorithm was based on the following observations: the distance over which an FSO link can be established is relatively long by itself; the dominating factor in the ETE delay of an FSO packet is the link acquisition time (it takes several seconds to establish a link), therefore, it would greatly reduce the efficiency of the network if even more such delays were introduced; the large sizes of the FSO packets (several hundred

MB each) would impose heavy extra burdens on the queuing and processing resources on the relay nodes, which are also source and destination nodes by themselves according to the requirements of an ad hoc network. Nevertheless, whether or not the added complexity of multi-hop routing would be advantageous can only be confirmed by experiment.

Last but not least, the ultimate goal of this research is to build a working product. During the course of research for this dissertation, the availability of critical hardware components was verified, the validity of the software algorithm demonstrated. However, to actually put together a physical product based on the investigations in this dissertation will surely pose a whole new set of challenges. This task is left to anyone who has the inspiration to do so with his/her ingenuity, creativity, and hard work.

REFERENCES

[1] Bloom S, Korevaar E, Schuster J, and Willebrand H, "Understanding the performance of free-space optics", *Opt. Soc. Am. J. Opt. Networking,* Vol. 2, No. 6, pp. 178-200, June 2003

[2] Willebrand H and Ghuman S, "Fiber optics without fiber", *IEEE Spectrum*, August 2001, pp. 40-45

[3] Killinger D, "Free space optics for laser communication through the air", *Opt. & Phot. News*, October 2002, pp. 36-42

[4] Jeong, M-C, Lee J-S, Kim S-Y, Namgung S-W, Lee J-H, Cho M-Y, Hum S-W, Ahn Y-S, Cho J-W and Lee J-S, "8×10 Gb/s terrestrial optical free-space transmission over 3.4 km using an optical repeater", *IEEE Phot. Tech. Lett.,* Vol. 15, No. 1, January 2003

[5] Willebrand H and Ghuman B S, *Free-space optics: enabling optical connectivity in today's networks*, Sams Publishing, Indianapolis, IN, 2002

[6] Kalashnikova O V, Willebrand H A, and Mayhew L M, "Wavelength and altitude dependence of laser beam propagation in dense fog", *Free-Space Laser Communication Technologies XIV*: *Proc. SPIE 4635*, pp. 278-287, 2002

[7] Johnson G W, Cornish J P, Wilburn J W, Young R A and Ruggiero A J, "Characterization of gigabit Ethernet over highly turbulent optical wireless links", *Free-Space Laser Communication and Laser Imaging II*: *Proc. SPIE 4821*, pp. 283-290, 2002

[8] Davis C C, Smolyaninov I I and Milner S D, "Flexible optical wireless links and networks", *IEEE Comm. Mag*., Vol. 41, Iss. 3, pp. 51-57, March 2003

[9] MODTRAN and PcModWin, Ontar Corporation (http://www.ontar.com)

[10] Kaneko S, Oba K and Hamai T, "Evaluation of free space optical link availability in metropolitan Tokyo area", *Free-Space Laser Communication Technologies XIV*: *Proc. SPIE 4635*, pp. 262-271, 2002

[11] Korevaar E, Kim I I and McArthur B, “Atmospheric propagation characteristics of highest importance to commercial free space optics”, *MRV Communications Inc. White Paper*, January 2001

[12] Hatcher M, ““Free-space data links: time for a reality check”, *Opto & Laser Europe*, June 2002

[13] Kim I I and Korevaar E J, “Availability of free space optics (FSO) and hybrid FSO/RF systems”, *Proc. SPIE,* vol. 4530, pp. 84-95, 2001

[14] *ANSI Z136 Series of Laser Safety Standards,* Laser Institute of America (http://www.laserinstitute.org and http://www.z136.org)

[15] Achour M, “Simulating atmospheric free-space optical propagation: part I, rainfall attenuation”, *Free-Space Laser Communication Technologies XIV*: *Proc. SPIE 4635*, pp. 192-201, 2002

[16] Kiasaleh K, “Performance analysis of free-space, on-off-keying optical communication systems impaired by turbulence”, *Free-Space Laser Communication Technologies XIV*: *Proc. SPIE 4635*, pp. 150-161, 2002

[17] Piazzolla S and Slobin S D, “Statistics of link blockage due to cloud cover for free-space optical communications using NCDC surface weather observation data”, *Free-Space Laser Communication Technologies XIV*: *Proc. SPIE 4635*, pp. 138-149, 2002

[18] Vilcheck M J, Reed A E, Burris H R, Scharpf W J, Moore C and Suite M R, “Multiple methods for measuring atmospheric turbulence”, *Free-Space Laser Communication and Laser Imaging II*: *Proc. SPIE 4821*, pp. 300-309, 2002

[19] Young C Y, “Broadening of ultra-short optical pulses in moderate to strong turbulence”, *Free-Space Laser Communication and Laser Imaging II*: *Proc. SPIE 4821*, pp. 74-81, 2002

[20] Kalashnikova O V and Willebrand H A, “Free-space optics system operation in Asian cities under heavy dust loading conditions”, *Free-Space Laser Communication and Laser Imaging II*: *Proc. SPIE 4821*, pp. 310-319, 2002

[21] Johnson G W, Cornish J P, Wilburn J W, Young R A and Ruggiero A J,

"Characterization of gigabit Ethernet over highly turbulent optical wireless links", *Free-Space Laser Communication and Laser Imaging II*: *Proc. SPIE 4821*, pp. 283-290, 2002

[22] Al-Habash M A, Nash J, Baars J, Witiw M, Fischer K and Desmet K, "Visibility in low clouds and its impact on FSO links", *Free-Space Laser Communication and Laser Imaging II*: *Proc. SPIE 4821*, pp. 11-20, 2002

[23] Kukshya V, Rappaport T S, Izadpanah H, Tangonan G, Guerrero R A, Mendoza J K and Lee B, "Free-space optics and high-speed RF for next generation networks – propagation measurements", *Proc. Veh. Tech. Conf. 2002,* IEEE 56th, Vol. 1, pp. 616 -620

[24] Comeron A, Bara J, Belmonte A, Ruiz D and Czichy R, "Inter-islands optical link tests", *IEEE Phot. Tech. Lett.,* Vol. 2, No. 5, May 1990

[25] Zhu X and Kahn J M, "Free-space optical communication through atmospheric turbulence channels", *IEEE Trans. Comm.,* Vol. 50, No. 8, August 2002

[26] Rollins D, Baars J, Cashion A, Herbert J, Narigon M, Plett M and Wiltsey T, "Installation environments for free-space optical terrestrial communications links: terminal base motion", *Free-Space Laser Communication Technologies XIV*: *Proc. SPIE 4635*, pp. 236-247, 2002

[27] Nykolak G, Szajowski P F, Jacques J, Presby H M, Abate J A, Tourgee G E and Auborn J J, "4×2.5 Gb/s 4.4 km WDM free-space optical link at 1550 nm", *Tech. Dig. OFC/IOOC '99*, Vol. Supplement, 1999

[28] ElBatt T and Izadpanah H, "Design aspects of hybrid RF/free space optical wireless networks", *Dig. IEEE Emerging Tech. Symp. Broadband Comm. for the Internet Era***,** 2001

[29] Clark G, Willebrand H and Achour M, "Hybrid free space optical/microwave communication networks: a unique solution for ultra high-speed local loop connectivity", *Proc. SPIE,* vol. 4214, pp. 46-54, 2001

[30] Moore C I, Burris H R, Suite M R, Stell M F, Vilcheck M J, Davis M A, Smith R, Mahon R, Rabinovich W S, Koplow J, Moore S W, Scharpf W

J and Reed A E, “Free-space high-speed laser communication link across the Chesapeake Bay”, *Free-Space Laser Communication and Laser Imaging II*: *Proc. SPIE 4821*, pp. 474-485, 2002

[31] Comeron A, Bara J, Belmonte A, Ruiz D and Czichy R, “Inter-islands optical link tests”, *IEEE Phot. Tech. Lett.,* Vol. 2, No. 5, May 1990

[32] Kedar D and Arnon S, “Adaptive field-of-view receiver design for optical wireless communication through fog”, *Free-Space Laser Communication and Laser Imaging II*: *Proc. SPIE 4821*, pp. 110-116, 2002

[33] Goetz P G, Mahon R, Stievater T H, Rabinovich W S, and Binari S C, “High-speed large-area surface-normal multiple quantum well modulators”, *Free-Space Laser Communication and Active Laser Illumination III*: *Proc. SPIE 5160,* pp. 346-354, January 2004

[34] Capasso F, Paiella R, Martini R, Colombelli R, Gmachl C, Myers T L, Taubman M S, Williams R M, Bethea C G, Unterrainer K, Hwang H Y, Sivco D L, Cho A Y, Sergent A M, Liu H C, and Whittaker E A, “Quantum cascade lasers: ultrahigh-speed operation, optical wireless communication, narrow linewidth, and far-infrared emission”, *IEEE J. Quantum Electron.,* Vol. 38, Iss. 6, pp. 511-532, June 2002

[35] Sergienko A V, Atatüre M, Di Giuseppe G, Jaeger G, Saleh B E A and Teich M C, “Hyper-entangled states and free-space quantum cryptography”, *Free-Space Laser Communication and Laser Imaging II*: *Proc. SPIE 4821*, pp. 352-362, 2002

[36] Barbosa G A, Corndorf E, Kumar P and Yuen H P, “Quantum cryptography in free space with coherent-state light”, *Free-Space Laser Communication and Laser Imaging II*: *Proc. SPIE 4821*, pp. 409-420, 2002

[37] Williams C J, Tang X, Heikkero M, Rouzaud J, Lu R, Goedecke A, Migdall A L, Mink A, Nakassis A, Pibida L S, Wen J, Hagley E and Clark C W, “High-speed quantum communication testbed”, *Proc. SPIE,* vol. 4821, pp. 421-426, 2002

[38] Yaqoob Z and Riza N A, “Smart free-space optical interconnects and communication links using agile WDM transmitters”, *Advanced*

Semiconductor Lasers and Applications/Ultraviolet and Blue Lasers and Their Applications/Ultralong Haul DWDM Transmission and Networking/WDM Components, 2001 Digest of the LEOS Summer Topical Meetings, 2001

[39] Milner S D, Ho T H, Smolyaninov I I, Trisno S and Davis C C, "Free-space optical wireless links with topology control", *Free-Space Laser Communication and Laser Imaging II*: *Proc. SPIE 4821*, pp. 175-180, 2002

[40] Krishnamurthy S V and Acampora A S, "Capacity of a multihop mesh arrangement of radio cells connected by free-space optical links", *12th IEEE Int'l Symp. Personal, Indoor and Mobile Radio Comm.,* Vol. 2, September/October 2001

[41] fSONA Systems Corp. (http://www.fsona.com)

[42] LightPointe Inc. (http://www.lightpointe.com)

[43] Terabeam Wireless (http://www.terabeam.com)

[44] Piccinin D, Boffi P, Cabas A and Martinelli M, "Free-space system for metropolitan optical network transparent link", *Free-Space Laser Communication Technologies XIV*: *Proc. SPIE 4635*, pp. 50-56, 2002

[45] Izadpanah H, Dolezal F and Tangonan G, "Hybrid access technology applications to the Next Generation Internet (NGI) network extension", *Proc. 27th Euro. Conf. Opt. Comm. (ECOC) '01,* Amsterdam, 2001

[46] Willebrand H A and Clark G R, "Free space optics: a viable last-mile alternative", *Wireless and Mobile Communications*, *Proc. SPIE*, Vol. 4586, pp. 11-21, 2001

[47] Hemmati H, "Status of free-space optical communications program at JPL", *IEEE Aerospace Conf. Proc,* Vol. 3, pp. 101-105, 2000

[48] Boroson D M, Biswas A and Edwards B L, "MLCD: overview of NASA's Mars laser communications demonstration system", *Free-Space Laser Communication Technologies XVI*, *Proc. SPIE,* Vol. 5338, pp. 16-28, 2004

[49] Lambert S and Casey W, *Laser Communications in Space*, Artech House, Boston,
MA, 1995

[50] Toh C-K, *Ad Hoc Mobile Wireless Networks: Protocols and Systems*, Prentice Hall, Upper Saddle River, New Jersey, 2002

[51] MANET Charter, the Internet Engineering Task Force (IETF) (http://www.ietf.org/html.charters/manet-charter.html)

[52] Karn P, "MACA – a new channel access method for packet radio", *ARRL/CRRL Amateur Radio 9th Computer Networking Conference*, pp. 134-140, 1990

[53] Talucci F and Gerla M, "MACA-BI (MACA by invitation) – a wireless MAC protocol for high speed ad hoc networking", *IEEE 6th Int'l Conf. on Universal Personal Communications Record*, Vol. 2, pp. 913-917, 1997

[54] Singh S and Raghavendra CS, "PAMAS – power aware multi-access protocol with signaling for ad hoc networks", *ACM SIGCOMM Computer Communication Review*, Vol. 28, Iss. 3, pp. 5-26, 1998

[55] Haas ZJ and Deng J, "Dual busy tone multiple access (DBTMA) – a multiple access control scheme for ad hoc networks", *IEEE Trans. Communications*, Vol. 50, Iss. 6, pp. 975-985, 2002

[56] Garcia-Luna-Aceves JJ and Fullmer CL, "Floor acquisition multiple access (FAMA) in single-channel wireless networks", *ACM Mobile Networks and Applications*, Vol. 4, Iss. 3, pp. 157-174, 1999

[57] Huang Z and Shen C-C, "A comparison study of omnidirectional and directional MAC protocols for ad hoc networks", *Proc. IEEE GLOBECOM '02*, Vol.1, pp. 57-61, November 2002

[58] IETF RFC3561, "Ad hoc On-Demand Distance Vector (AODV) routing" (http://www.ietf.org/rfc/rfc3561.txt), July 2003

[59] IETF Internet Draft, "The Dynamic Source Routing protocol for mobile ad hoc networks (DSR)" (http://www.ietf.org/internet-drafts/draft-ietf-manet-dsr-10.txt), July 2004

[60] University of Maryland, Center for Networking of Infrastructure Sensors (http://www.cnis.umd.edu/index.htm)

[61] Rensselaer Polytechnic Institute, Networks Lab, Free Space Optical Networks Project (http://poisson.ecse.rpi.edu/~sri/fso_webpage/)

[62] Lehigh University, Department of Computer Science and Engineering, Hybrid FSO/RF Mobile Ad-hoc Networks Project (http://www.cse.lehigh.edu/~jcd6/fso)

[63] Milner S D, Ho T H, Smolyaninov I I, Trisno S and Davis C C, "Free-space optical wireless links with topology control", *Free-Space Laser Communication and Laser Imaging II*: *Proc. SPIE 4821*, pp. 175-180, 2002

[64] Akella J, Yuksel M and Kalyanaraman S, "Multi-element array antennas for free-space-optical communication", *Proc. IFIP/IEEE International Conference on Wireless and Optical Communications Networks (WOCN),* Dubai, United Arab Emirates, March 2005

[65] Akella J, Liu C, Partyka D, Yuksel M, Kalyanaraman S and Dutta P, "Building blocks for mobile free-space-optical networks", Proc. *IFIP/IEEE International Conference on Wireless and Optical Communications Networks (WOCN)*, Dubai, United Arab Emirates, March 2005

[66] Derenick J, Thorne C and Spletzer J, "Hybrid free-space optics/radio frequency networks for mobile robot teams", *Multi-robot Systems: From Swarms to Intelligent Automata*, Schultz AC and Parker LE (eds.), Springer, March 2005

[67] Derenick J, Thorne C and Spletzer J, "On the deployment of a Hybrid FSO/RF mobile ad hoc network", *IEEE/RSJ Int'l Conf. on Intelligent Robots and Systems*, Edmonton, August 2005

[68] NASA, gimbal illustration in the Apollo Lunar Surface Journal (http://www.hq.nasa.gov/office/pao/History/alsj/4gimb.jpg)

[69] Sagebrush Technology, Inc., Model-20 Servo pan & tilt gimbal (http://www.sagebrushtech.com/products/gimbals/Model-20s/specifications.html)

[70] Newmark Systems, Inc., Gimbal: GM-12E (http://www.newmarksystems.com/gimbal-gm12e.html)

[71] Merchele G S, "Active pointing for terrestrial free space optics", *LEOS 2002. The 15th Annual Meeting of the IEEE,* Vol.2, pp. 451-452, Nov. 2002

[72] Vasey F, Reinhart F K, Houdre R and Stauffer J M, "Spatial optical beam steering with an AlGaAs integrated phased array", *Applied Optics,* Vol. 32, No. 18, 1993

[73] Meyer R A, "Optical beam steering using a multichannel lithium tantalate crystal", *Applied Optics,* Vol. 11, pp. 613–616, 1972

[74] Love G D, Major J V and Purvis A, "Liquid-crystal prisms for tip-tilt adaptive optics", *Optics Letters,* Vol. 19**,** pp. 1170–1172, 1994

[75] Song Q W, Wang X-M, Bussjager R and Osman J, "Electro-optic beam-steering device based on a lanthanum-modified lead zirconate titanate ceramic wafer" *Applied Optics,* Vol. 35, No. 17, 1996

[76] Bulmer C H, Burns W K and Giallorenzi T G, "Performance criteria and limitations of electro-optic waveguide array deflectors", *Applied Optics*, Vol. 18, No. 19, 1979

[77] Chen C, Shi S, Prather D W and Sharkawy A, "Beam steering with photonic crystal horn radiators", *Optical Engineering,* Vol. 43, No.1, 2004

[78] Nikulin V V, Bouzoubaa M, Skormin V A and Busch T E, "Modeling of an acousto-optic laser beam steering system intended for satellite communication", *Optical Engineering,* Vol. 40, No.10, 2001

[79] Chang I C, "Acousto-optic devices and applications", *IEEE Trans. Sonics and Ultrasonics,* Vol. su-23, No. 1, 1976

[80] Newport Corp., Fast Steering Mirrors (http://www.newport.com/store/product.aspx?lone=Optics&ltwo=Optical+Systems&id=3881&lang=1)

[81] Physik Instrumente. S-334 Piezo tip/tilt platform.

(http://www.physikinstrumente.de/products/prdetail.php?secid=3-19)

[82] Melles Griot Inc. (http://205.214.33.28/glossary/imagesDir/Quadrant.gif)

[83] Wang J, Kahn J M and Lau K Y, "Minimization of acquisition time in short-range free-space optical communication", *Applied Optics,* Vol. 41, No. 36, 2002

[84] Melles Griot Inc. (http://205.214.33.28/glossary/imagesDir/CCD.gif)

[85] Herring TA, "The Global Positioning System", *Scientific America*, February 1996, pp. 44-50

[86] The University of Colorado (http://lasp.colorado.edu/snoe/graphics/GPS_orbits.GIF)

[87] Grewal MS, Weill LR and Andrews AP, *Global Positioning Systems, Inertial Navigation, and Integration*, John Wiley & Sons, New York, 2001

[88] US Marine Corps, AN/PSN-11 Precision Lightweight GPS Receiver (http://www.hqmc.usmc.mil/factfile.nsf/0/7c93296961c94c378525627a006b173a/$FILE/GPS.JPG)

[89] Texas A&M University (http://reveg-catalog.tamu.edu/images/03-GPS/02-GPS%20Unit-A.JPG)

[90] Russian Federation Ministry of Defense, GLONASS (http://www.glonass-center.ru)

[91] European Union, GALILEO (http://europa.eu.int/comm/dgs/energy_transport/galileo/index_en.htm)

[92] The University of Southern California, Information Sciences Institute (http://www.isi.edu/nsnam/ns/index.html)

[93] The University of California – Los Angeles, Parallel Computing Laboratory (http://pcl.cs.ucla.edu/projects/glomosim/)

[94] OPNET Technologies, Inc. (http://www.opnet.com)

[95] IEEE Standards, 802.11 Series. (http://ieeexplore.ieee.org/xpl/standards.jsp?findtitle=802.11&letter=802.11)

[96] The Wi-Fi Alliance (http://wi-fi.org/)

[97] Zimmermann H, "OSI reference model – the ISO model of architecture for open system interconnection", *IEEE Trans. Comm.,* Vol. 28, No. 4, April 1980

[98] Internet resource – Wikipedia (according to it, no official document defines the DoD model) (http://en.wikipedia.org/wiki/DoD_model)

[99] OPNET Technologies, Inc., Modeler documentation, Release 10.5, "Modeling concepts reference manual", MC-5-51.